UFZ-Bericht

UFZ - Umweltforschungszentrum Leipzig-Halle GmbH

Nr. 23/1998

Third Workshop on Physical Processes in Natural Waters

31.8. - 3.9.1998 in Magdeburg

Bertram Boehrer und Michael Schimmele (eds.)

Third Workshop on
Physical Processes in Natural Waters

31.8. - 3.9.1998
at the
UFZ Centre for Environmental Research Leipzig-Halle
Department of Inland Water Research Magdeburg

Collection of Written Contributions

Bertram Boehrer and Michael Schimmele (eds.)

Contents

INTERNAL WAVES

MICROSTRUCTURE AND TURBULENCE

NUMERICAL LIMNOLOGY

PHYSICAL PROPERTIES OF WATER

BOUNDARY INTERACTION

MEROMIXIS

CONVECTION

Preface

The written contributions contained in this report originate from the *Third Workshop on Physical Processes in Natural Waters* (PPNW3) held in Magdeburg, Germany in the time 30th August to 3rd September 1998 in the Umweltforschungszentrum UFZ-Sektion Gewässerforschung in Magdeburg. This workshop was the third in a sequence initiated in 1996 by the EAWAG in Kastanienbaum, Switzerland and continued in 1997 by the CEC Joint Research Center in Ispra, Italy. The meetings have been held to bring into contact the scientists working on physical limnology who mostly find themselves in small working groups. To stimulate collaboration and to provide a platform for continuous scientific exchange in Europe, the meetings have been held at annual intervals.

The participants felt that a collection of the workshop contributions would be a useful reference for the on-going work in limnophysics within Europe, and most of the oral presentations were submitted as written contributions for this volume by their authors. The division in seven sections – internal waves, microstructure and turbulence, numerical limnology, physical properties of water boundary interaction, meromixis, convection – reflects the break-up into workshop sessions. We thank the UFZ for offering editing the collection as a UFZ-report and for bearing the costs involved in printing it. The written contributions ahould serve as a reference to the wider literature and enable scientist who were not able to participate this time to keep up with the development and get into contact with the participants of the workshop.

In the concluding discussion of the workshop, the participants expressed their opinion that the *Workshop on Physical Processes in Natural Waters* should continue in the style of Kastanienbaum, CEC and Magdeburg, of some 30 contributions, and enough space for discussion after each presentation and after each session. The workshop was felt to be an important platform to concentrate on and discuss the physical features in limnic waters, which are covered neither in oceanic conferences nor limnological conferences to a satisfactory extend. Preferably the workshop should continue at annual intervals to keep the communication between the scientists alive. The participants indicated they would be happy with the continuation of the workshop in Estonia in 1999. Unfortunately by the time of printing this collection, the exact date and location of the 1999-workshop was not yet decided. However we encourage the reader to contact Madis-Jaak Lilover (madis@phys.sea.ee) about details.

We would like to thank the people who helped to organize and run this workshop. Special thanks to Prof. W. Geller for his support and for offering the facilities of the UFZ-Sektion Gewässerforschung in the Brückstraße in Magdeburg. S. Degener, U. Kiwel, K. Lerche, B. Rätzel, K. Rahn and J. Schrader helped in many ways beyond their usual job. We also thank the authors for their presentations and written contributions and for the lifely discussions during the workshop.

Magdeburg, in October 1998

Bertram Boehrer and Michael Schimmele

Erratum in the contribution Hollan, p. 71-75:

The correct condition of mass continuity, $M_b + N_b = M_c.$, results into the change of two signs in equation (5), whence

$$(5) \quad g\eta_x = F - \cfrac{F}{\cfrac{2\gamma\tilde{N}}{D_H}\left(\delta - \cfrac{L_\delta}{\gamma * \tilde{N} *}\right) + \cfrac{S_H \cdot S_\delta}{D_H \cdot \tilde{N} *} + \cfrac{C_\delta}{\tilde{N} *}}$$

The Fourth Workshop on Physical Processes in Natural Waters will be held in Estonia in the time 13 to 16th of September 1999, please check with madis@phys.sea.ee

On the linearity of internal seiches

E. Bäuerle
Limnologisches Institut, Universität Konstanz, 78457 Konstanz, Germany

Most investigations on internal seiches are done as if the underlying processes were prescribable by linear theory. Although the observed vertical displacements of the isotherms in the thermocline region (and below) sometimes approach (and exceed) the depth of the mixed layer. And although (due to the Coriolis forces of the Earth's rotation) the horizontal shear of the currents may be considerable (thus making the advective terms in the governing equations large) it is possible to interpret and reproduce many of the observations by applying tools from linear theory.

Taking recent observations from Upper Lake Constance, I will discuss how far simple linear models may help to understand the ongoing processes. Special attention will be given to the time series of temperature and velocity measured at 3 stations near the Isle of Mainau (see Fig. 1). Whereas the period of the quasi-periodic hypolimnetic in- and outflow across the sill is readily matched by the Merian formula (extended for two-layer systems), both temperature and current speed and direction indicate that non-linear processes are of importance (at least locally).
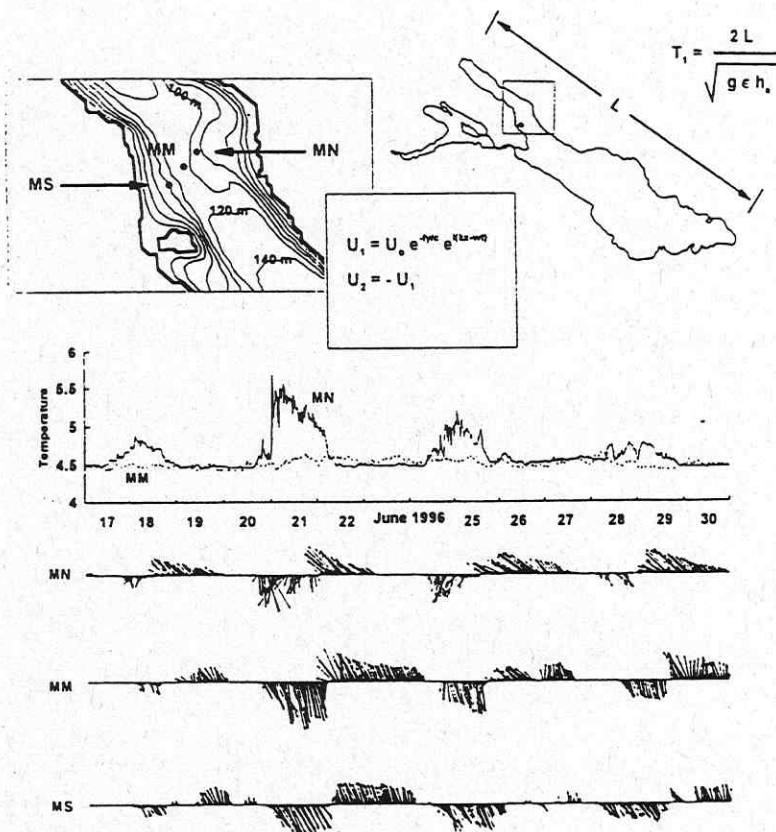

Figure 1: *Currents and temperatures measured at 3 moorings at the sill of Mainau (Upper Lake Constance) from 17th to 30th June 1996. The depths of the instruments are 84 m (MS), 78 m (MM) and 73 m (MN). Temperatures at MS (not shown) are similar to those at MM. Maximum current velocity is 12 cms^{-1}.*

However, some of the features observed at station MN (see Fig. 1) (velocity components perpendicular to the isobaths and augmented vertical displacements of the isotherms, respectively) can be understood by means of linear theory.

The linearized equations of motion in a rotating, incompressible, inviscid, stratified Boussinesq fluid on the f-plane are adopted as a starting point. All variables are assumed to be periodic with frequency ω. The equations then read

$$i\omega u - fv = -\frac{1}{\rho_0}\frac{\partial P}{\partial x} \ , \tag{1}$$

$$i\omega v + fu = -\frac{1}{\rho_0}\frac{\partial P}{\partial y} \ , \tag{2}$$

$$N^2 w = -\frac{i\omega}{\rho_0}\frac{\partial P}{\partial z} \ , \tag{3}$$

$$\frac{\partial u}{\partial x} + \frac{\partial v}{\partial y} + \frac{\partial w}{\partial z} = 0, \tag{4}$$

where u, v, w are the offshore (x), alongshore (y) and vertical (z) velocities, respectively, P is the pressure pertubation, $N^2(z) = -(g/\rho_0)(d\rho_0/dz)$ the squared buoyancy frequency, and $\rho_0(z)$ the undisturbed density.

Alongshore internal waves in a channel

Assuming all motions to travel along a straight shoreline with frequency ω and alongshore wavenumber l (i.e., $\sim e^{i\omega t + ily}$), and combining the modified equations (1) - (4) into a single equation for the pressure results in the equation for the conservation of potential vorticity

$$\frac{\partial^2 P}{\partial x^2} + (f^2 - \omega^2)\frac{\partial}{\partial z}\left(\frac{1}{N^2}\frac{\partial P}{\partial z}\right) - l^2 P = 0 \ . \tag{5}$$

Rewriting the boundary conditions in terms of pressure yields

$$\frac{\partial P}{\partial x} + f\frac{l}{\omega}P = 0 \quad \text{at} \quad x = 0 \text{ and } x = B \ , \qquad \frac{\partial P}{\partial z} = 0 \quad \text{at} \quad z = 0 \ , \tag{6}$$

$$\frac{f^2 - \omega^2}{N^2}\frac{\partial P}{\partial z} = -\frac{dH}{dx}\left[\frac{\partial P}{\partial x} + l\frac{f}{\omega}P\right] \quad \text{at} \quad z = -H(x) \ . \tag{7}$$

Eqs. (5) - (7) form an eigenvalue problem, which, for a fixed wavenumber l, has discrete eigenvalues. In solving this problem it is possible to understand the combined effects of stratification and sloping bottom.

In a homogeneous model with variable depth, topographic (rotational) waves which are trapped over the slopes of the boundary are induced by the constraint of potential vorticity conservation for a water column moving over the sloping bottom. Only for relatively long wavelengths it is justified to assign insensitivity against stratification to these waves. From Fig. 2 it is obvious that in a stratified channel of width $B = 20$ km and parabolic bottom, for waves with a wavelength of $\lambda = 10$ km dispersion curves are far from being horizontal. Following the respective curves of the individual modes we could notice that the character of the waves changes from barotropic (for weak stratification) to baroclinic (for strong stratification).
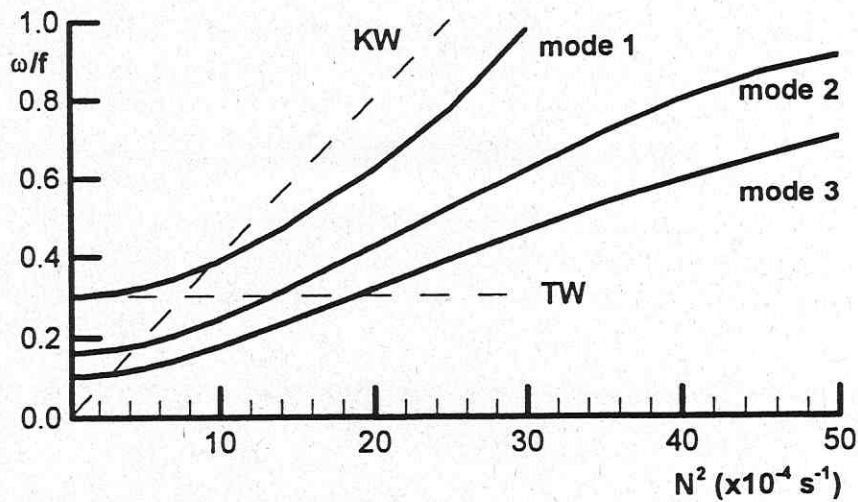
Figure 2: *Dispersion curves for modes 1 - 3 in a parabolic channel with $h_r = 5$ m, $dh = 280$ m, $B = 20$ km and $\lambda = 10$ km. Stratification is uniform. For comparison, the lowest Kelvin wave for flat bottom and the topographic wave without stratification are also shown.*

In Fig. 3 we see the pressure field with different steepness of the bottom. In the right picture the bottom is parabolic and, obviously, the pure Kelvin wave of the flat-bottomed case (left picture) has changed its appearance. The most important feature of this wave (not shown here) is, that we get a non-vanishing velocity component normal to the shoreline, a feature which is characteristic for topographic waves.
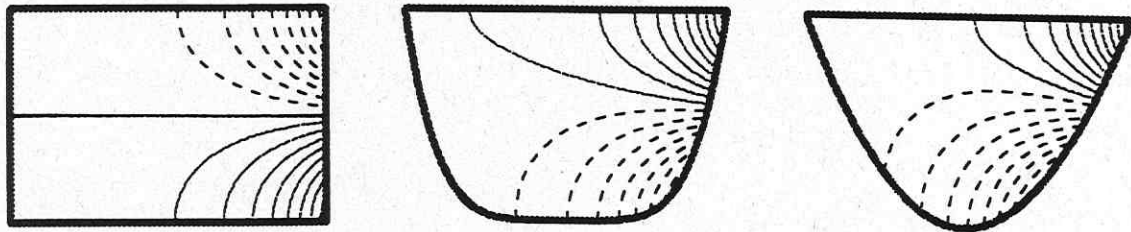
Figure 3: *Cross-channel distributions of the perturbation pressure of the lowest mode for different steepness of the topography. Stratification is uniform.*

Without going into the details of the interplay of sloping bottom and density stratification in channel models, it should be emphasized that a) waves in stratified fluids over sloping bottom exhibit rotating velocity vectors, and b) the vertical structure of the waves varies from place to place.

Surely, if we want to compare the results of the model with observations, we are confronted with the fact, that in real lakes the shoreline normally is not well approximated by a straight line, thus making the assumption of a fixed wavelength in longitudinal direction rather dubious.

Normal modes in a multilayer rectangular basin with non-flat bottom

In order to isolate the influence of topographic disturbances of an otherwise regular shoreline, we ignore most of the factors which influence the real near-shore hydrodynamics. To this purpose, we use a 4-layer rectangular basin with depth configuration of the lowest layer parabolic both in longitudinal and in transverse direction, disturbed by a local hump (see Fig. 4). The basin has vertical sidewalls down to the depth of 35 m. Maximum depth is 130 m at the center of the basin. Density distribution is given by a polygon approximating a stratification typical in early summer.
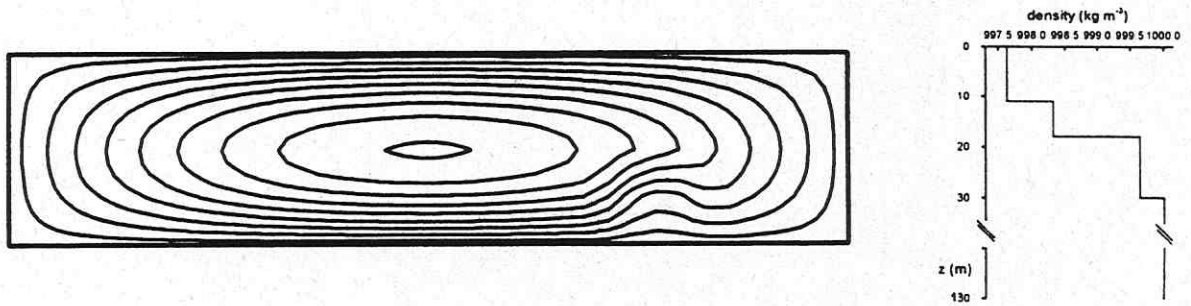
Figure 4: *Depth configuration (left) and density stratification (right) of a 4-layer basin with vertical sidewalls down to 35 m.*

If we had flat bottom we could even solve the continuous problem in separating the vertical and the horizontal dependencies, resulting in a two-dimensional eigenvalue problem for the frequencies of free internal basin-wide modes with corresponding horizontal structures of the horizontal velocities and the vertical displacements at any depth. With non-flat bottom, the vertical structure varies from place to place and the concept of vertical modes is invalid.

We concentrate here on the near-hump current field of the fundamental mode in the lowest layer (Fig. 5). In the region of the hump, the snapshots at 1/8 of the cycle exhibit a) the intensification of the flow, b) the (anti-cyclonic) rotation of the current vectors, and c) a significant offshore component of the currents, most pronounced during the phases ($t = T_1/4, 3T_1/4$), when the "gravitational part" of the mode is vanishing. Notice that the hump is only of local influence.

For real lakes, we conclude that the nearshore velocity field of internal Kelvin waves and internal seiches may offer a complicated structure both in vertical and horizontal direction.
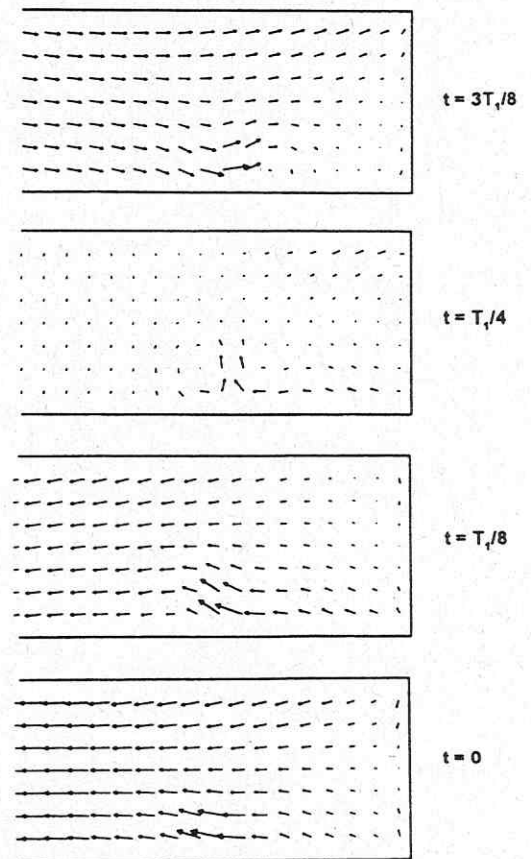
Figure 5: *The current field of the fundamental horizontal mode in the lowest layer near the hump (right half of the basin, see Fig. 4) at different phases of 1/2 cycle (from bottom to top; the second half of the cycle with opposite directions of the current vectors).*

Internal wave – shear flow resonance in the shelf zone

Vyacheslav V.Voronovich, Victor I.Shrira*

P.P.Shirshov Institute of Oceanology RAN,
36 Nakhimovsky prosp., 117851 Moscow
e-mail: vvv@wave.sio.rssi.ru; shrira@glasnet.ru

1 Introduction

Permanent progress in the remote sensing of the ocean surface makes the studies of links between the processes in the water interior and their surface signatures one of the 'hottest' topics of today's physical oceanography. Internal gravity waves being widespread in all natural basins remain the only 'internal' process having numerous and well documented surface manifestations supported by the *in situ* measurements. Recently a new mechanism of the amplification of this manifestations due to resonance with a subsurface shear current was considered in [1].

Internal waves are actively studied themselves, especially their dynamics in the shelf zone. By now its basic features are well established by numerous field experiments: waves are long in comparison to typical water depth; in-shore propagating waves are, as a rule, much more pronounced; they exhibit essentially nonlinear behaviour: solitary waves are typical, while bore-like structures occur as well. The basic theoretical model is KdV equation with variable due to bottom topography coefficients and a number of modifications taking into account Earth's rotation or cubic nonlinearity has been developed. On the contrary the influence of shear currents, often present in natural waters, is usually neglected or taken into account as a secondary effect: coefficients of KdV depend on the current's velocity profile, i.e. buyoancy is usually considered to be the main driving force of the wave motion while effect of vorticity created by the currents is assumed to be weak.

In reality subsurface drift currents, which are almost always present in the natural waters, often create quite strong vorticity field, the effect of which is comparable to that of buyoancy and can change internal wave dynamics *qualitatively*. Moreover, drift currents greatly enhance horizontal velocity component of the wave field and thus amplify internal wave signatures on the surface. This effect is particularly strong in case of *resonance*, i.e. matching of the celerity of the wave with the flow speed at the surface, as a so-called 'critical layer' is formed and one should speak about 'wave-current interaction'. A vast body of literature devoted to critical layer dynamics is almost entirely confined to the harmonic or, at best, quasimonochromatic waves, whereas internal waves in shallow water are usually far from being monochromatic.

Fortunately, this problem can be successfully treated if the currents vertical size h is much smaller than the typical wavelength L. Under this assumption an arbitrary current perturbations can be described as *vorticity waves* owing their existence to the inhomogeneous vorticity field of the shear flow and weakly influenced by the buyoancy forces [2]. Thus an untractable *wave – current* interaction can be successfully treated as a *wave – wave* interaction. The present work develops its nonlinear description and, in particular, shows its importance not only in the context of surface signatures, but for internal wave dynamics in shallow water itself.

---

*Present address: Department of Applied Mathematics, University College Cork, Cork, Ireland

2 Asymptotic analysis of basic equations

We assume the fluid to be inviscid, incompressible, uniform in horizontal direction, but vertically stratified. The shear current is assumed to occupy a thin subsurface layer of typical width h much smaller than the total depth H, its velocity profile $U(z)$ having no inflection points. In Boussinesq approximation the governing equation then are

$$\mathbf{u}_t + (\mathbf{u} \cdot \nabla)\mathbf{u} + \nabla \frac{p}{\rho_0} + \frac{\rho}{\rho_0}\mathbf{z} = 0$$
$$\rho_t + wN^2 + (\mathbf{u} \cdot \nabla)\rho = 0 \tag{1}$$
$$\nabla \cdot \mathbf{u} = 0$$

where $\rho_0(z)$ is an equilibrium density distribution and the fluid velocity contains both the mean current and perturbations[1]

$$\mathbf{u}(x, y, z, t) = \{U(z) + u, v, w\}$$

The system (1) with the proper boundary conditions

$$w = 0, \quad \text{at} \ \ z = -H, \quad z = 0 \tag{2}$$

constitutes a boundary value problem to solve.

The problem is characterized by two independent small parameters

$$\epsilon = h/H, \qquad \mu = (H/L)^2 \tag{3}$$

which we hereinafter assume to be in balance: $\epsilon = \mu^2$. The perturbation field therefore depends on slow 'evolutional' variables

$$X = \sqrt{\mu}(x - ct), \qquad Y = \mu y, \qquad T = \mu^{3/2}t. \tag{4}$$

while scales of vertical motion are different in subsurface shear layer and a still core. In result we have to introduce in the shear layer an 'inner' vertical variable

$$\zeta = \frac{z}{\epsilon}$$

to solve (1) in still core and moving shear layer separately and then match solutions at the border. Typical scales of perturbation amplitudes are also different in the core

$$u, w, p = O\left(\mu^2\right), \qquad v = O\left(\mu^{5/2}\right) \tag{5}$$

and in the shear layer

$$u = O(\mu), \qquad v = O\left(\mu^{5/2}\right), \qquad w = O\left(\mu^{7/2}\right), \quad p = O\left(\mu^2\right), \tag{6}$$

internal wave being the dominant type of motion in the core while vorticity wave – in the shear layer. Solutions are sought as asymptotic series in powers of μ^2 (see details in [3]).

---

[1]Equations are made nondimensional by using typical values of the total depth H_0 and of Brunt–Väisälä frequency $N(z)$ as the length and frequency scales.

3 Plane waves

Asymptotic analysis results in a system of coupled evolution equations for the wave amplitudes, which by means of a scaling transformation reduces to

$$\left. \begin{array}{c} (a_t + \Delta a_x + a_{xxx} - b_x)_x + a_{yy} = 0 \\[2mm] b_t + 2bb_x - a_x = 0 \end{array} \right\} \tag{7}$$

where a, b are internal and vorticity wave amplitudes and Δ describes a small mismatch of mode celerities (resonance is exact at $\Delta = 0$). For simplicity we confine ourselves by the analysis of a one-dimensional version, i.e. set $a_{yy} = 0$.

Two nontrivial conservation laws were found, the conserving quantaties being the momentum and the energy of some abstract field.

$$P[a,b] = \frac{1}{2} \int\limits_{-\infty}^{+\infty} (a^2 + b^2)\, dx, \qquad H[a,b] = \frac{1}{2} \int\limits_{-\infty}^{+\infty} \left(a_x^2 - \Delta a^2 + 2ab - \frac{2}{3} b^3 \right)\, dx$$

Though even 1D version of (7) is not completely integrable a bulk of information about its properties can be extracted by studying stationary solutions $a, b = a_s, b_s(x - vt)$. System (7) can then be integrated to result

$$a_s = b_s^2 - vb_s$$

$$(v - 2b_s)^2 \left(\frac{db_s}{dx} \right)^2 = b_s^2 \left[(v - \Delta) b_s^2 + 2 \left(\frac{2}{3} - v(v - \Delta) \right) b_s + v^2 (v - \Delta) - v \right] \tag{8}$$

and both localised and periodic solutions can be found in closed form [3].

3.1 Solitary waves

System (7) posesses two families of plane solitary waves, their speed confined to the intervals

$$\left. \begin{array}{ll} \text{"fast"} & v \in (c_+, v_+) \\[2mm] \text{"slow"} & v \in (c_-, \min{(0, \Delta)}) \end{array} \right\} \tag{9}$$

with borders dependent only on Δ

$$c_{\pm} = \frac{1}{2} \left[\Delta \pm \left(4 + \Delta^2 \right)^{\frac{1}{2}} \right] \qquad v_+ = \frac{1}{2} \left[\Delta + \left(\frac{16}{3} + \Delta^2 \right)^{\frac{1}{2}} \right]$$

Whereas "slow" solitary waves do not exhibit any peculiar features, the amplitude of "fast" ones is limited from above by a so-called "peaked" solitons: in the limit $v \to v_+$ we get

$$b_s \simeq \frac{v_+}{2} \exp \left\{ -(3v_+)^{-1/2} |x| \right\}$$

The sigularity at the crest is due to the fact that the speed of a particle in the wave can not exceed the speed of the wave itself. It is worth noting that according to (8) the internal wave amplitude a remains smooth up to the limiting configuration.

To study an initial localised pulse temporal evolution numerical simulations of (7) has been conducted. The results are dependent on how large is the initial amplitude in comparison with a certain "threshold": while "subcritical" perturbations evolve into solitary waves, "supercritical" ones develop a vertical slope in finite time, which probably leads to breaking.

4 Solitary wave transformation in the shelf zone

Up to now we implicitly assumed the depth to be constant. Yet the depth changes in the offshore directions is one of the main factors determining solitary wave transformation in the shelf zone especially important when the wave amplitude is limited from above. Indeed, initially smooth wave running onshore can reach limiting amplitude and even break due to depth changes.

To make the problem tractable we assume the depth variations to be comparativly small and smooth, i.e. put

$$H = -h_0 + \mu^2 \hat{h}(\nu x) \qquad (10)$$

An asymtotic analysis of (1)–(2) then results in a system similar to (7), but with $\Delta \sim \hat{h}$ dependent on x, t. Under additional assumption $\nu \ll \mu^{3/2}$, corresponding to smallness of the typical wave size in comparison with depth variability scale, one can study stationary wave transformation by means of Whitham's method This approximation corresponds to neglect of any reflections from the bottom and the wave assumed to be *locally* close to a stationary one, with its parameters changing with time due to depth changes.

System (7) could be derived from the variational principle $\delta L = 0$ with a lagrangian

$$L = -\frac{1}{2}(E_x F_t + F_x E_t) - \frac{1}{3}F_x^3 - \frac{1}{2}\Delta E_x^2 + \frac{1}{2}E_{xx}^2 + E_x F_x \qquad (11)$$

where the potential representaion is used: $a = E_x, b = F_x$. We look for solution in the form of a periodic wavetrain

$$E = Ax - Ct + f(\theta), \qquad F = Bx + Dt + g(\theta) \qquad (12)$$

where A and B are slowly evolving pedestals and $\theta = k(x - vt)$ – the phase. One must substitute (12) into lagrangian, average it over the period γ, variate the result with respect to $\phi = Ax - Ct, \psi = Bx - Dt, \theta$ and add the correspondent compatibility conditions. In result we get transport equation for pedestals

$$A_t + (\Delta A)_x - B_x = 0$$
$$B_t + BB_x - A_x = 0 \qquad (13)$$

which are just (7) without dispersion term. From these one can see for example that if pedestals were zero initially they remain zero in the course of evolution.

For solitary waves (in the limit $\gamma \to \infty$) after some algebra we get another equation

$$\left(\frac{\partial \Omega}{\partial v}\right)_T + v\left(\frac{\partial \Omega}{\partial v}\right)_X + 2\frac{\partial \Omega}{\partial v}\frac{\partial v}{\partial X} = 0 \qquad (14)$$

for the averaged action function

$$\Omega \simeq \sqrt{\frac{(v - 2B)(v - \Delta) - 1}{(v - 2B)}} \int_0^{u_m} (v - 2B - 2u)u\sqrt{(v - \Delta)(u - v + 2B)^2 + \frac{4}{3}u - v + 2B}\, du \qquad (15)$$

Equation (15) was studied numerically in assumption: $B = 0, \Delta = \Delta(t)$ (main influence of the changing depth is due to motion of the frame of reference with the linear wave speed, rather than to evolution on the "slow" timescale). On the figure the "fast" solitary wave speed and amplitude are pictured vias Δ (depth) changes. Dashed lines correspond to local c_+, v_+ – limits of solitary waves speeds at the given depth. One can easily see that any onshore running wave inevitably reach the critical amplitude and is going to break, though breaking itself can not, of course, be described within the frames of proposed model.
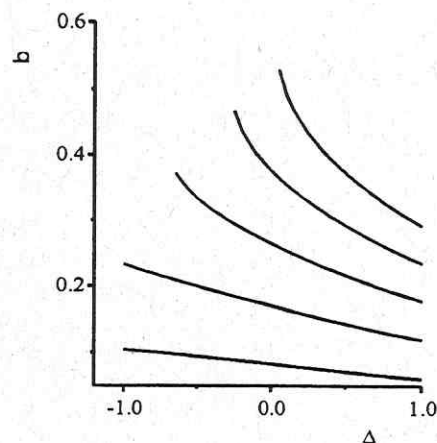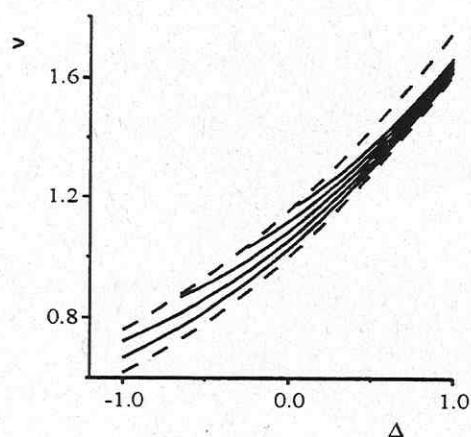
5 Conclusion

The presented results demonstrate that the subsurface shear current changes drastically, provided the resonance conditions met, an internal wave dynamics. First of all, the scaling (5) describes an internal wave of much smaller amplitude than that presumed by the traditional KdV theories. The main nonlinear effect then is due to interaction with the current, rather than the wave's own nonlinearity, which is corroborated by (7). Therefore a completely new model comprising two coupled equations was derived, possesing solitary wave solutions of two classes essentially distinct from KdV-like solitons. A peculiar property of the model is the existence of limiting solutions with a sharp corner at the crest, which do not exist in traditional models. Solitary waves are stable up to the critical amplitude and, according to numerical simulation, can be formed from an initial pulses of subcritical amplitude. The localised pulses of larger, supercritical, amplitude develop vertical slopes in finite time which indicates breaking.

An influence of depth variations analysed within the frames of adiabatic approximation results in solitary wave parameter dependence on the depth, all onshore moving waves inevitably reaching the critical amplitude and, thus breaking. Breaking waves are expected to contribute greatly into mixing processes in the upper layer. The enhanced mixing, in turn, effects heat and momentum exchange at the air/sea interface and surface transport.

Acknoledgements

References

[1] Voronovich V. V. & Shrira V. I. On the amplification of internal-wave surface manifestations due to subsurface shear current. *Okeanologia* **36**, 173–177 (1996).

[2] Voronovich V.V., Shrira V.I. & Stepanyants Yu.A. Two-dimensional models for nonlinear vorticity waves in shear flows. *Stud. Appl. Math.* **100**, 1–32 (1998).

[3] Voronovich V.V., Pelinovsky D.E. & Shrira V.I. On the internal wave – shear flow resonance in shallow water. *J. Fluid Mech.* **354**, 209–232 (1998).

EXPERIMENTAL STUDY OF STATIONARY AND NONSTATIONARY INTERNAL WAVE PATTERN INDUCED BY DRIFTING ICEBERG

Olga D. Shishkina

Institute of Applied Physics, Russian Academy of Sciences
46 Uljanov st., Nizhny Novgorod, 603600, Russia
E-mail: ols@hydro.appl.sci-nnov.ru

Natural conditions of iceberg drift - stratification parameters ($\Delta\rho$ = 1-3 kg/m^3 at the depth of 20-100 m), iceberg dimensions (the draught of 40-250 m) and drifting velocities (0.1-0.5 m/s) - provide physical conditions for intensive internal waves generation [1].

Results of experimental modelling of internal waves induced by an iceberg drifting in stratified finite-depth fluid obtained in the thermally stratified tank with the overall dimensions $L*B*H$=18*4*2 m^3 in the Institute of Applied Physics are presented. In laboratory conditions the horizontally homogeneous stratification with the thermocline of the thickness h = 0.17H was created in the fresh water, so providing a scale model (K_L = 1:100) of the seasonal thermocline ($\Delta\rho$ = 2 kg/m^3).

The vertical cylinder of the diameter D = 0.4 m had different draughts close to the thermocline's depth of h' = 0.3H. Towing velocities U were in the range of limiting phase velocities of the first and the second internal wave modes ($C_{1,2}$), which corresponds to typical natural velocities of icebergs drift, taking into account the velocity number $K_U = K_L^{1/2}$.

Indications of a vertical chain of six sensors, arranged in the thermocline, allow to distinguish temperature oscillations related to different internal wave modes. A spatial pattern of internal wave fronts was reconstructed using indications of the horizontal chain of eight sensors arranged at the depth of the thermocline's center normally to the cylinder's trajectory.

Both stationary and nonstationary (after body stopped) phase pictures for the mentioned velocity range were reconstructed. In case of stationary body motion the wave pattern was almost plane with the divergence angles $60° < \beta < 90°$ (see Figs. 1, 2). The transverse amplitude decrease observed was of about *30 %* at the distance *3D*.
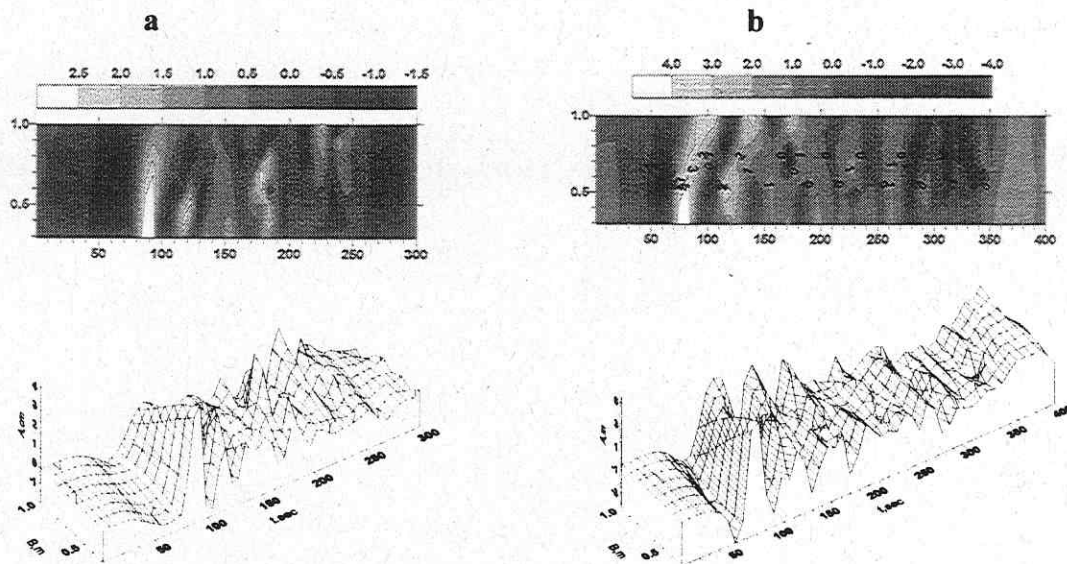
Fig. 1. Stationary internal wave pattern for $T/h' = 1$: **a** - $U/C_1=1$, **b** - $U/C_1=2$.
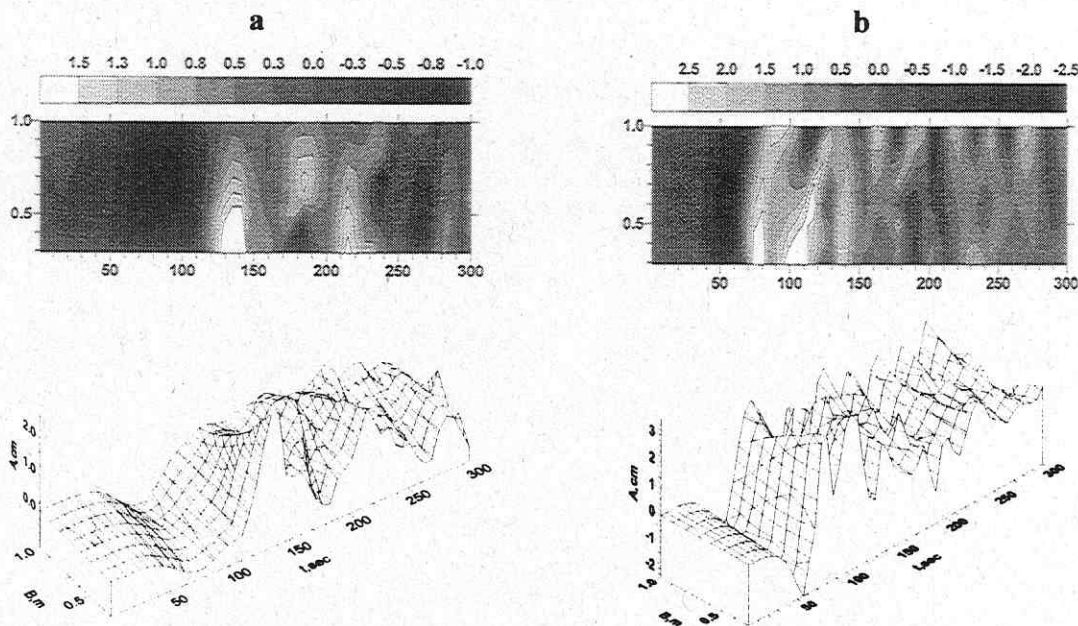
Fig. 2. Stationary internal wave pattern for $T/h' = 1.44$: **a** - $U/C_1=1$, **b** - $U/C_1=1.5$.

Propagation of nonstationary internal waves after the body stopped was studied for two relative cylinder draughts $T/h' = 0.83$ and 1.44 . For $C_2 \leq U < C_1$ the nonstationary wave system decays in time (Fig. 3a). The most intensive nonstationary waves were observed in case of the first-mode internal waves generation $U \geq C_1$ (Figs. 3b, 4). The amplitude of nonstationary internal waves grows up to *50%* towards tank side walls at the distance *3D*.
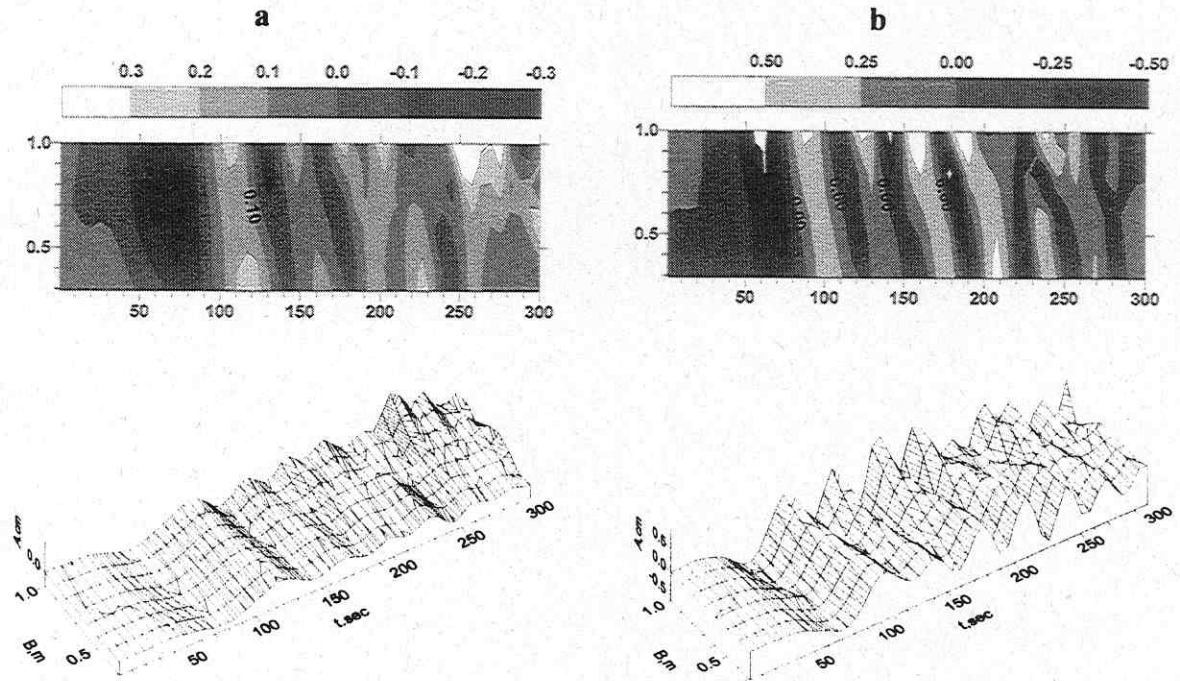
Fig. 3. Nonstationary internal wave pattern for $T/h' = 0.83$: **a** - $U/C_1 = 0.75$, **b** - $U/C_1 = 1$.
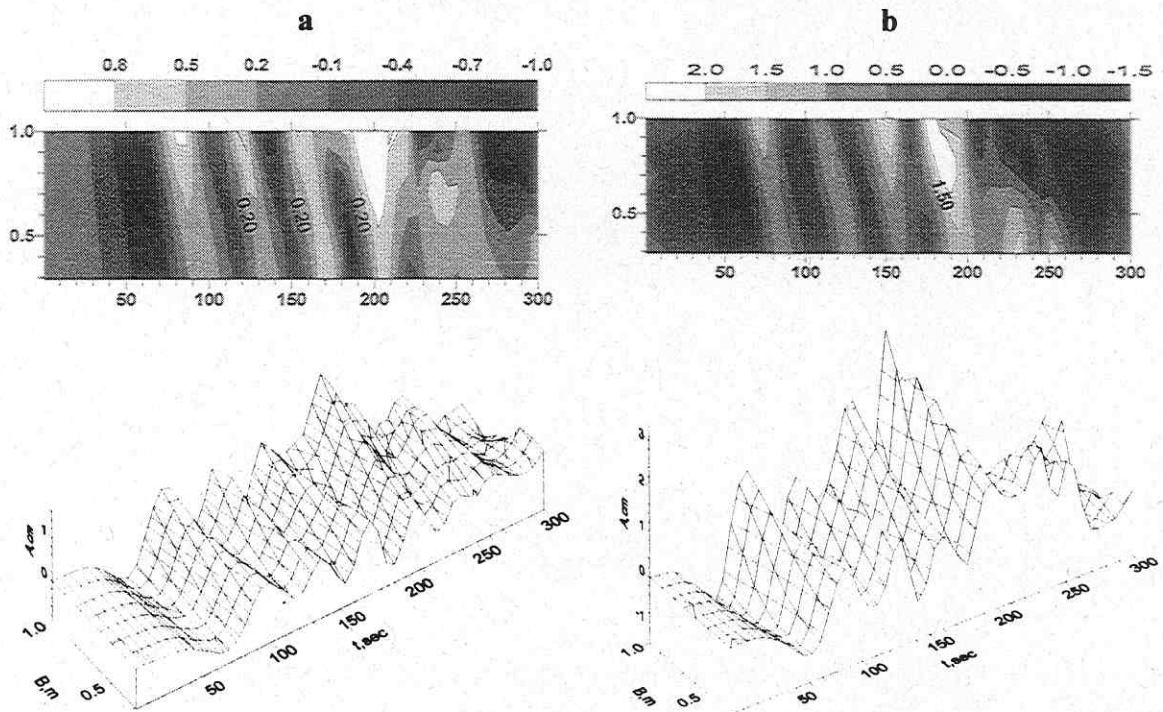
Fig. 4. Nonstationary internal wave pattern for $T/h' = 1.44$: **a** - $U/C_1 = 1.25$, **b** - $U/C_1 = 2$.

Independent propagation of each wave mode was observed (Fig. 5): the leading wave represents the first internal wave mode and the second-mode motions were observed later in accordance with the ratio of maximum mode phase velocities.
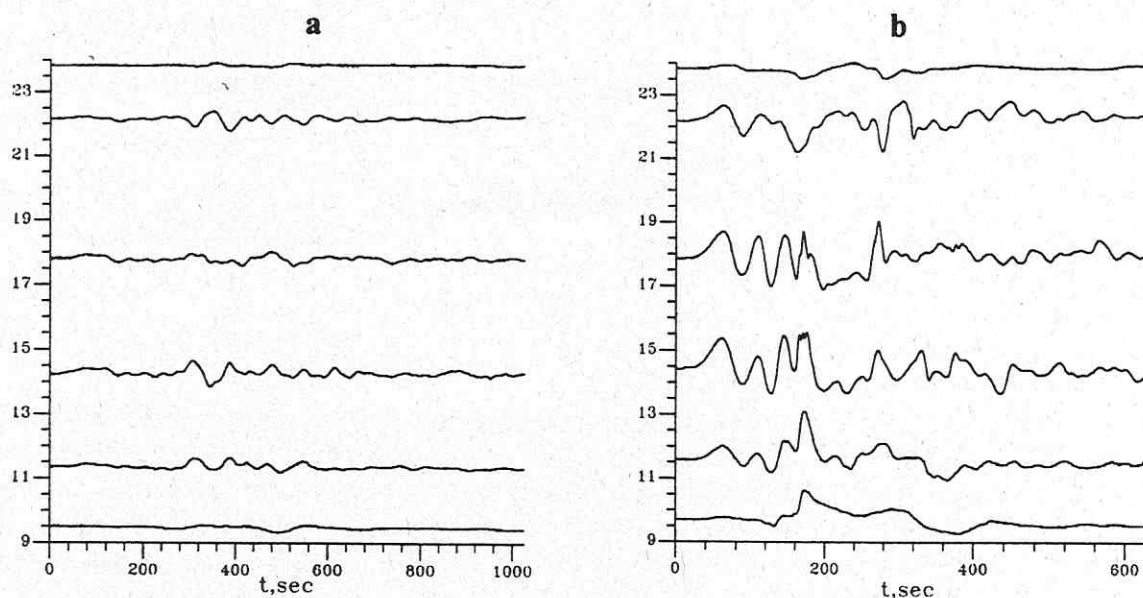
Fig. 5. Nonstationary internal wave pattern (the vertical chain) : **a** - $T/h' = 0.83$, **b** - $T/h' = 1.44$.

The vertical profile of attached second-mode internal waves depends on the body's draught (it represents a pycnocline "bulge" for $T/h' < 1$ and a local narrowing for $T/h' > 1$). After body stopped the second-mode fluid motion, governed by the stratification profile only, represents the local "bulge" for both draughts.

The phase wave picture formed after body stopped had the divergence angles $\beta > 90°$ for both draughts and in the whole velocity range.

REFERENCES

1. Vasil'yeva V. V., Pisarevskaya L. G., Shishkina O. D. Generation of internal waves by a drifting iceberg. Izvestiya Academii Nauk. Physics of Atmosphere and Ocean, 1995, v. 31, No. 6, pp. 842-851.

Statistics and scaling of turbulent kinetic energy dissipation rates in a shallow lake

Andreas Lorke

Institute of Freshwater Ecology and Inland Fisheries Berlin, Germany

Introduction

A microstructure profiler was used to investigate the statistics and scaling of turbulent kinetic energy dissipation rates ε in a shallow lake. The free rising profiler is equipped with a fast response thermistor for temperature microstructure and an airfoil shear probe for current shear microstructure measurements. Kinetic energy dissipation rates can be calculated from both signals independently. Four data sets, consisting of 11 up to 31 microstructure profiles are used to compare the different dissipation rate estimates, to investigate the statistical distribution of individual samples and means and to compare the scaling and depth dependency of the estimated dissipation rates with the law of the wall scaling of wind energy input at the lake surface.

Methods and materials

Instrumentation

The microstructure profiler was developed for use in shallow lakes. Since most investigations focus on processes in the surface mixed layer a rising profiler is used. The profiler can be employed using a special designed weight which can be released at a certain depth. The weight forces the profiler to glide down at an angel of about 45° to the vertical. Therefore the subsequent profiled water column is neither disturbed by the deployment nor by the boat.

The profiler is equipped with in *FP07* thermistor and an *PNS93* airfoil shear probe. The shear probe use a piezoceramic beam to sense a lift force on an axisymmetric foil by a turbulent velocity fluctuation perpendicular to the mean uprising speed of the profiler as it moves vertically trough the water column. Both microstructure signals are low pass filtered with a cut off frequency of 500 Hz and sampled with 1565 Hz. In addition to the microstructure signals the profiler depth and inclination to the vertical are sampled with 156 Hz.

Data processing

Individual profiles were divided into half overlapping sections of 2048 data points. Depth values were corrected to the actual surface level, which was detected from the temperature profile. The mean speed of the profiler was estimated for each section.

Turbulent kinetic energy dissipation rates ε can be estimated from the two, physically different, microstructure signals. Both methods, the dissipation method for current shear and the Batchelor method for temperature microstructure, are using the spectrum of the signals, so additional filtering of the signals is not necessary.

Temperature microstructure

The high wave number end of the reduced 1-dimesional spectrum of turbulent temperature fluctuations in isotropic and homogenous turbulence Φ_T can be described by:

$$\Phi_T = \sqrt{\frac{q}{2}} \frac{\chi_T}{k_B D} x \left(e^{-\frac{1}{2}x^2} - x \int_x^\infty e^{-\frac{1}{2}x'^2} dx' \right) \tag{1}$$

where x is the non-dimensional wave number $x=(2q)^{1/2}k/k_B$, with the wave number k, a universal constant q (set to $q=3.4$) and the Batchelor wave number k_B. D is the molecular
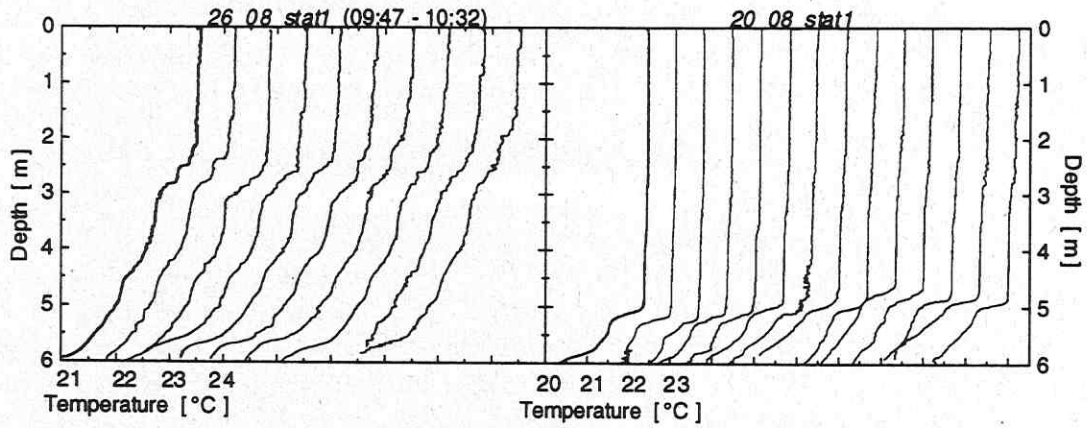
Figure 1: 10 subsequent temperature microstructure profiles from two data sets (temperature offset plot).

diffusivity of heat and χ_T the dissipation rate of temperature fluctuations, defined as the integral of the spectrum of temperature gradient fluctuations.

The Batchelor wave number k_B describes the smallest scales of temperature fluctuations, where molecular diffusion tends to overwhelm the production of fluctuations by turbulent motions.

The spectrum of temperature fluctuations according to equation 1 is universal and depends on the dissipation rate of mechanical energy ε and that of temperature fluctuations χ_T. By fitting a measured fluctuation spectrum to the theoretical Batchelor spectrum these two quantities can be determined from temperature microstructure measurements. The measured temperature spectrum for each segment was estimated using Welch's method. This spectrum was corrected for the thermistor response. ε and χ_T were used as the free parameters for a nonlinear least square fit of the measured spectrum to the Batchelor form.

Current shear microstructure

The output voltage of the shear probe is proportional to one component of the horizontal current shear and inverse proportional to the square of the uprising speed of the profiler. Under the assumption of isotropic turbulence the dissipation rate of mechanical energy ε can be estimated by

$$\varepsilon = \frac{15}{2}\nu\overline{\left(\frac{\partial u'}{\partial z}\right)^2} \qquad (2)$$

Beside the non provable assumption of isotropy the difficulty is to distinguish the real turbulent shear signal from high frequency vibrations or electronic noise and low frequency disturbances due to profiler movement or temperature changes. Therefore the averaging process in equation 2 is performed in the wave number domain. Nasmyth, 1970 found an universal shape of the spectrum of turbulent velocity fluctuations from measurements in a tidal channel. Generally, measured shear spectra using airfoil probes fit well to the empirical Nathmyth spectrum. For each section of the measured current shear microstructure profiles the power spectrum was estimated using Welchs method. The shear variance for the dissipation rate calculation according to equation 2 was estimated by integrating the spectrum from a fixed lower wave number up to the Kolmogorov wave number k_k. Since k_k itself depends on the dissipation rate an iterativ process was used. The dissipation rate estimate was used to calculate the empirical Nasmyth spectrum, which was compared visually with the measured shear spectrum. For further analysis only those dissipation rates were included, for which this comparison showed a good agreement.

Study site

Müggelsee is a shallow polymictic lake with an area of 7.3 km² in NE Germany, near Berlin. The maximum depth is 8 m. The measurements were carried out in the eastern part of the lake, where the depth was 7 m.

Data sets

Four data sets are used for the discussion of the dissipation statistics. Each data set consists of 11 to 31 microstructure profiles, measured at a fixed location in Müggelsee using a measuring interval of 5 minutes. Three of these four data sets were measured at one day so that the discussion should proof, if these may be treated as one data set. Figure 1 shows some temperature microstructure profiles from these data sets. Although the wind conditions were comparable (3 to 4 ms⁻¹), the stratification differs between the dates of measurements. Individual temperature profiles show a remarkable variability in time. This is also true for the stratified regions underneath the diurnal thermocline.

Results

Comparison of dissipation rate estimates

Turbulent kinetic energy dissipation rates were estimated using both methods. The dissipation method for current shear microstructure was successful for 1370 and the Batchelor method for temperature microstructure only for 470 data segments. The two estimates are strongly correlated in the measured range between $5 \cdot 10^{-9}$ and $5 \cdot 10^{-7}$ m² s⁻³ but individual samples can differ by more than an order of magnitude. A Kolmogorov Smirnov test found no significant difference between the frequency distributions of both estimates with 95% confidence. Also the mean and the median are not significant different.

A direct comparison of these individual estimates is not straightforward, since the two probes are mounted about 7 cm apart at the profiler. This distance is large compared to the length scales from which the dissipation rates are calculated. Therefore the comparison is only useful in a statistical sense. The individual estimates from both methods in the four data sets were found to be log-normally distributed within 1 m depth intervals. In this case the maximum likelihood estimator *mle* can be a more efficient estimator of the expected value of a
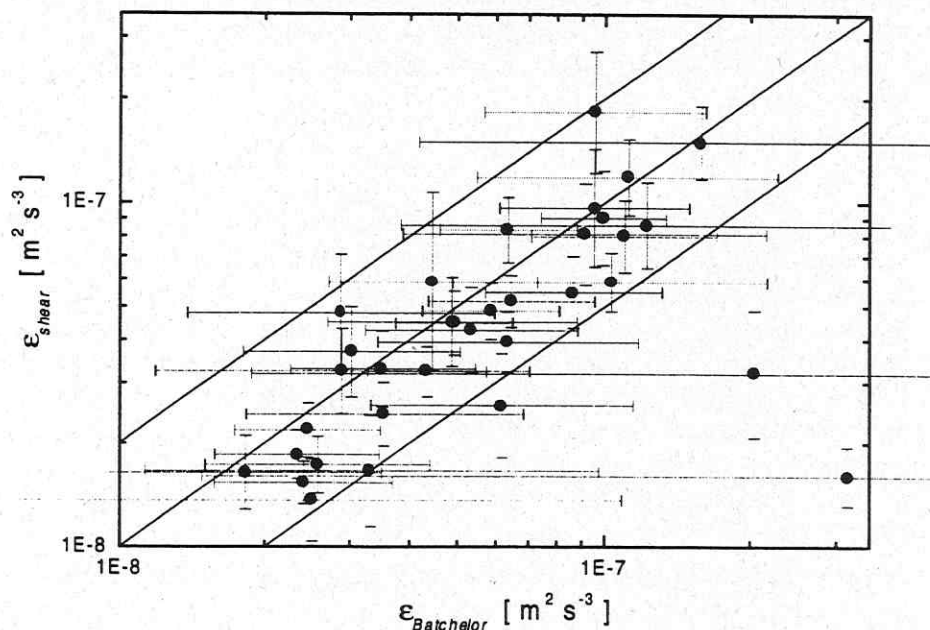
Fig. 2: Comparison of dissipation rates estimated by the Batchelor method $\varepsilon_{Batchelor}$ and by the dissipation method ε_{shear}. The graph shows the maximum likelihood estimates and the 95% confidence limits as error bars. The lines represent the equality and differences of a factor of 2.

lognormal distribution as the arithmetic mean. Fig. 2 shows the comparison of the maximum likelihood estimators for temperature and current shear based dissipation rate estimates. The figure shows that almost all estimates overlap each other within the 95% confidence interval of the maximum likelihood estimator, which are also shown. The two estimates agree within a factor of 2, a uncertainty which was also found by other authors for comparisons between different microstructure profilers or by error analysis. The good agreement between both dissipation rates and the large confidence limits especially for the Batchelor method show, that the statistical error due to the intermittent nature of turbulence is the limiting factor for the accuracy of both measurements.

Scaling

The mean dissipation rates of the four data sets are used to compare the dissipation profiles with the boundary layer prediction for an non-stratified wind-mixed layer:

$$\varepsilon_{wind} = \frac{u_*^3}{\kappa z}$$

κ is the von Kármán constant, z the depth and u_* the friction velocity, which depends on the wind speed W and the drag coefficient C_D ($u_*=(C_D \cdot \rho_d / \rho_w)^{1/2} W$). The results are shown in figure 3. The correlation between the measured dissipation rates and the predictions is good ($r^2=0.9$). At lower dissipation rates the measured values become smaller than the predictions because of the increasing influence of stratification. In spite of the good correlation the predicted values differ from the measured values by a factor of 2. This difference can be eliminated by using a drag coefficient C_D of 0.6×10^{-3} instead of the literature value of 1×10^{-3}.

A smaller drag coefficient is plausible for the study site with a limited fetch of 1 km. On the other hand, extended measurements have shown, that this factor of 2 can vary diurnaly and is a function of the time history of wind energy input.
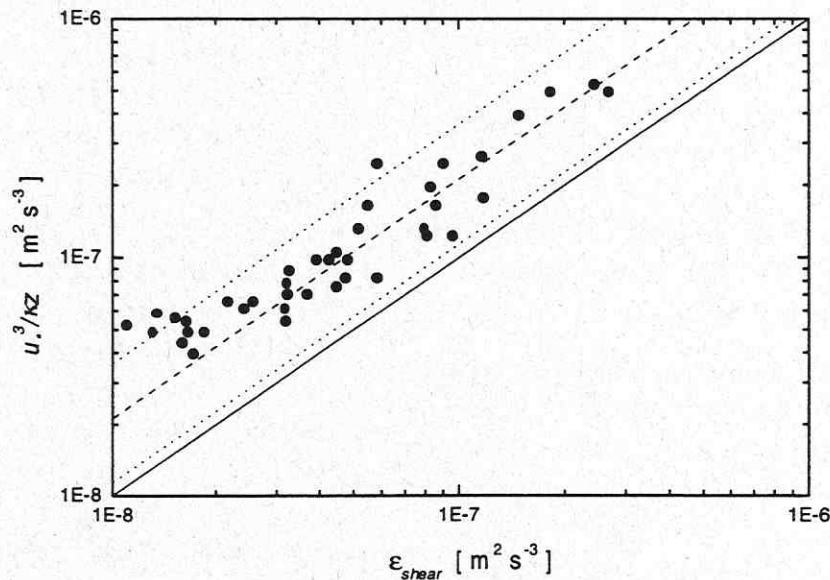
Fig. 3: Mean dissipation rates ε_{shear} compared to the boundary layer prediction of the scaling of viscous dissipation. The solid line represents equality, the dashed line a linear fit with a slope of 2.1 and the dotted lines differences according to a factor of two to this fit.

Comparison of temperature microstructure observations and large eddy simulations of turbulence in natural waters

T. Jonas[*], J. Sander[#], A. Simon[*], A. Wüest[*]

[*] Swiss Federal Institute of Environmental Science and Technology (EAWAG),
CH-8600 Dübendorf, Switzerland

[#] Physics Institute, University of Bern, Switzerland

ABSTRACT

Turbulence related properties have been estimated from temperature microstructure measurements in the upper layer of lakes affected by convection. For corresponding boundary conditions large eddy simulations (LES) have been performed and compared to observations. The time averaged vertical profile for the rate of dissipation of the turbulent kinetic energy (ε) can be reproduced very well by the simulations, while the model seem to underestimate the rate of dissipative smoothing of temperature (χ). We can show, that part of the deviation derive from lateral intrusions of fine scale fluctuations, which cannot be represented by the model.

1. INTRODUCTION

Vertical mixing is an important process for the turbulent transport of all kind of chemical and physical tracers, such as temperature. Turbulence is agitated by energy input from wind as well as by heat flux through the water atmosphere interface.

Field experiments have been carried out, in order to investigate turbulence related properties from temperature microstructure measurements for different atmospheric boundary conditions. For this presentation, we selected a convective regime, due to strong heat flux through the surface into the atmosphere, while the wind was low.

The experiment has been performed during a night in October 1994 at Lake Lucerne, Switzerland. A temperature microstructure probe was taking profiles rising from close to the bottom at 24m towards the lake surface every 10 minutes. From meteo measurements the net heat flux and the eddy momentum flux by wind have been derived.

Putting in these driving conditions large eddy simulations have been performed upon a three dimensional domain of 26m*26m*24m with an equidistant gridspacing of 25cm. The first vertical temperature profile within the investigated period of time was deviated with random noise of less than 0.001K to implement as an three dimensional initialization of the model. Furthermore, the model was started 1 hour earlier with wind forcing but without heat flux in order to obtain a realistic turbulence level at the begin.

The model's equation for continuity, momentum conservation and temperature evolution are standard assuming

incompressible fluid, applying Reynolds's averaged equations and Boussinesq's approximation. Turbulent kinetic energy (e) and temperature's autocorrelation (<T'T'>), as well as ε and χ upon the subgrid scale are being described according to *Schemm and Lipps* [1976] and *Schmidt and Schumann* [1989].

2. ESTIMATION OF ε AND χ

ε and χ are estimated by fitting Batchelor model spectra to the temperature spectra of the temperature microstructure profiles, e.g. see *Gloor et al.* [1995]. The one dimensional form of the model spectra are based upon the assumption of isotropic and stationary turbulence for small scale fluctuations and can be written as

$$\Phi_T(k) = \frac{\chi}{2}\sqrt{\frac{\kappa}{\gamma^3}}\left(\frac{\exp(-x^2)}{x} - \sqrt{\pi}(1 - \mathrm{erf}(x))\right)$$

with $\quad x = k\sqrt{\frac{\kappa}{\gamma}}, \quad \gamma = \sqrt[4]{\frac{\kappa^2}{\varepsilon k_B}}, \quad k_B = \sqrt[4]{\frac{\varepsilon}{\nu\kappa^2}},$

with molecular viscosity ν, thermal diffusivity κ and vertical wavenumber k.

As for the reliability of the fit estimations simultaneous temperature and shear microstructure profiles have been used to demonstrate, that ε obtained by the two corresponding independent methods agree very well, see *Kocsis et al.* [1998]. Furthermore fit estimations of χ have been found consistent comparing to χ via direct integration of the temperature gradient spectra from observations, corrected accounting for cutting of the noise spectra at the highest wavenumbers.

3. AVERAGING TECHNIQUE

Observational results for ε and χ are estimated within sections of 25 cm length, averaging fit results from at least 4 subsections. This windowing has been found as best compromise between statistical reliability and vertical resolution still resolving fine scale structures. The profiles have been averaged with time, in order to compensate the lack of horizontal resolution.

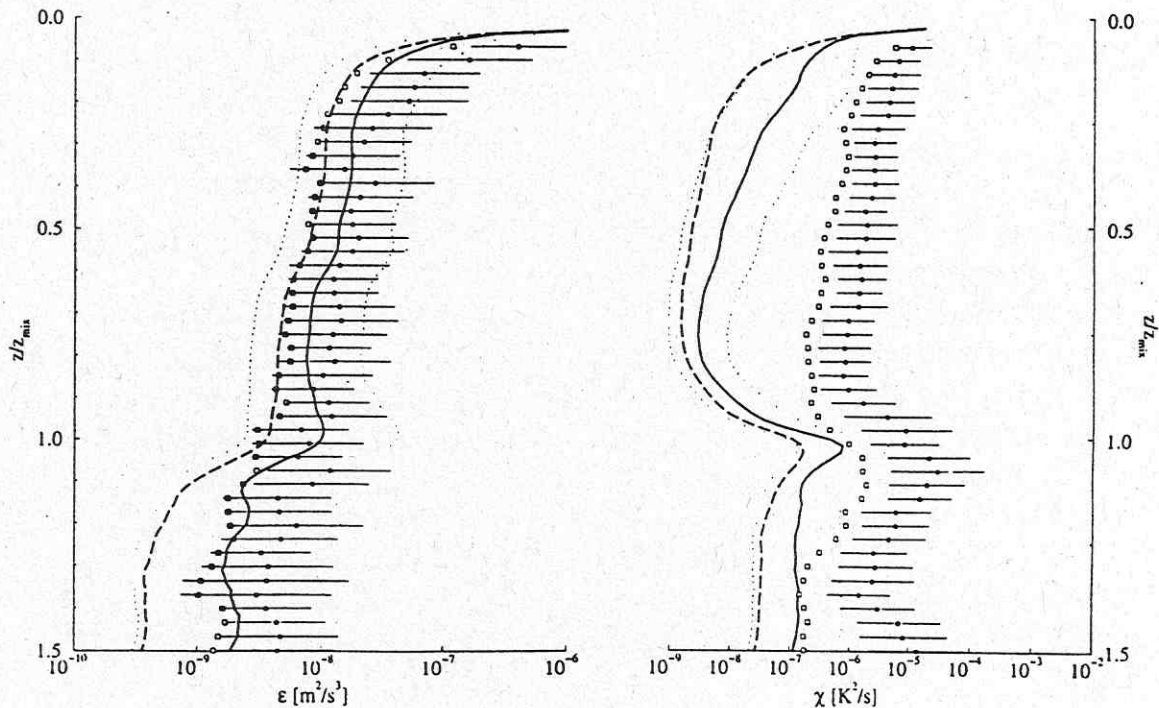In contrast the results from LES are three dimensional and derive from time-averaged

Figure 1. vertical profiles of ε and χ. notation for Observation/LES: Dots/ thick line indicate arithmetic mean, with symmetric errorbars/ thin dashed lines as 1σ confidence interval. Open squares/ thick dashed line show geometric mean. Z_{mix} is about 7±1 m during the investigated period of time.

constant forcing. Therefore profiles for ε and χ, horizontally averaged and vertically normalized to the mixed layer depth, develop with time approaching steady state. Hence, only the last profile is utilized for the comparison.

4. RESULTS

Averaged in the sense mentioned above, results for ε and χ are presented in figure 1. Obviously, ε is being reproduced very well by our LES. Only close to the boundaries minor deviations occur, which may derive according to two problems. On the one hand, the assumption of stationary isotropic turbulence closer to the boundaries and at higher turbulence levels is critical for a wave number domain extending towards high k. Therefor the method for evaluating ε and χ tends to become less appropriate. On the other hand, the vertical resolution of the model remains equidistant, while ε increases exponentially towards the surface.

As shown in figure 1, χ is underestimated by the model. Within the mixed layer χ from observations are about two order of magnitudes larger than corresponding values from LES.

Looking at the temperature profiles besides the microstructure we find fine scale fluctuations, which come along with locally extremely high temperature gradients. Figure 2 presents three observed successive temperature profiles, typical for the investigated period of time. The first profile displays rather pure microstructure, while within the following 20 minutes the temperature profile is being disturbed and a significant fine structure builds up. According to the local guts of high temperature gradients the χ increases by approximately three orders of magnitude.

In this example the temperature situation has
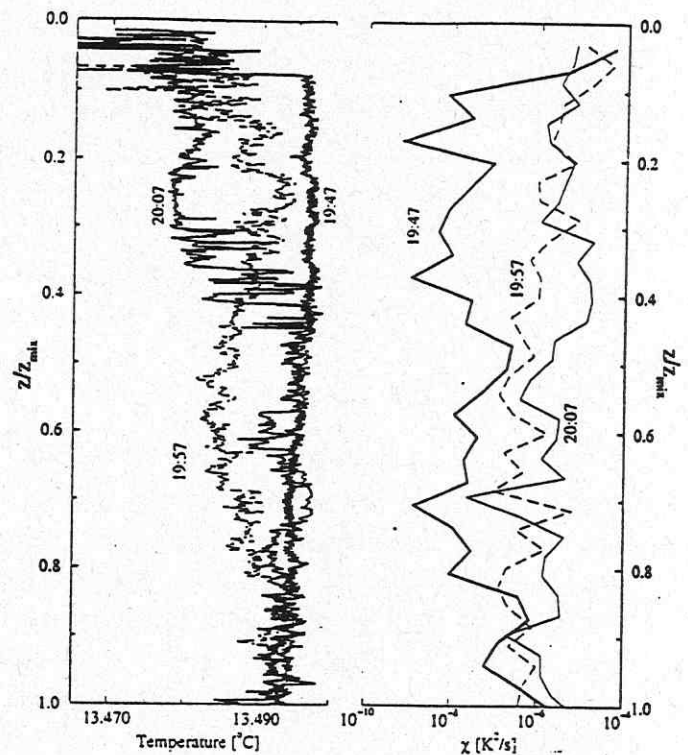
Figure 2. Left: Temperature microstructure profiles for different times as indicated. Right: Corresponding fit estimations for χ. Z_{mix} is about 8 meter

changed in a way that neither a realistic heat flux nor the vertical velocity scale derived from the surface buoyancy flux could explain the fast cooling. Therefor the disturbances cannot be the result of vertical convection but are entrained laterally. Here a lens of colder water seems to have intruded into the observed domain at around $z/z_0 = 0.6$. The finestructures disappear within the following 10 profiles, leaving only the micro scale fluctuation behind.

The chosen example is representative for the investigated period of time. Obviously the regime significantly features lateral advection. Since our LES cannot handle these effects as well as our measurement do not reveal side boundary conditions, we expect the model to represent microstructure only. Therefor our LES is underestimating χ if the investigated regime is dominated by lateral advection as in this case.

5. REFERENCES

Gloor M., Kocsis O., Omlin M., Schurter M., Wüest A.: *Temperaturmikrostrukturen. Eine Methode zur Bestimmung der Mischungs-intensität in geschichteten Gewässern*; Gas, Wasser, Abwasser, 12/95, 1995.

Kocsis O., Prandke H., Stips A., Simon A., Wüest A.: *Comparison of dissipation of turbulent kinetic energy determined by shear and temperature microstructure*; J. Marine Systems, submitted, 1998.

Schemm C. E., Lipps F.B.: *Some results from a simplified three-dimensional numerical model of atmospheric turbulence*; J. Atmosph. Sci., 33, 1021-1041, 1976.

Schmidt H., Schumann U.: *Coherent structure of the convective boundary layer derived from large-eddy simulations*; J. Fluid Mech., 200, 511-562, 1989.

TURBULENT FLUXES PARAMETERIZATION
IN THE UPPER BLACK SEA LAYER

Vladimir M. Kushnir

Marine Hydrophysical Institute HAS Ukraine.

2Kapitansaya st. 335000 Sevastopol. Ukraine

ABSTRACT

Experimental data of the vertical profiles of currents and hydrological parameters in the Northwest Black Sea (R/V " Jakov Gakkel" expedition, August 1992) were used for definition of average meanings and statistical characteristics of the vertical diffusion coefficient Kz in conditions of the strong density stratification in the upper layer of the Sea. The mode of the vertical diffusion in such layers is close to molecular according to received estimations and the average Kz meanings exceeds the molecular thermal diffusivity coefficient to 20% approximately. Basic vertical transport ($Kz = 0.1...1$ cm^2/s) is carried out by the local turbulente "flares" which probability is equal about to 2...5 %. These local turbulent "flares" are formed to many accidental reasons: the shifts of current speed in internal waves and eddy-wave structures "billows" type, etc.

Probability's distribution W(F) of the vertical flows F of various passive substantions with a vertical gradient G are calculated on the basis of definition of the statistical characteristics of the vertical diffusive coefficient and the following ratio for an average flow $<F> = 0.77 \nu G$ (ν - kinematic viscosity) is received in particular for the Black Sea layer of the density jump.

Key words: Turbulent diffusion, density stratification

INTRODUCTION

Steady density stratification is formed in natural basins in summer period owing to intensive heating and wind hashing of the top layer. High gradient layers (vertical density gradients reach to $10^{-4}...10^{-5}$ g/cm^4) place in the depth of 15-25 m in the Black Sea and considerably hinder the exchange between surface and near bottom waters. This renders the strong influence on the vertical transport of the nutrients and oxygen, as well as on dynamics (change of concentration) various impurity and pollution. In this connection, determination of the main parameter of the vertical turbulent exchange and vertical fluxes - vertical diffusion coefficient Kz - has the large significance at mentioned conditions and in many cases is necessary for decision of many problems of applied biology, diffusion of pollution and dynamics of the basin ecosystem as a whole.

Mentioned factors are typical for many marine and lake conditions and so the problem of the turbulent exchange in stratified on density water medium was intensivily studied for the last 50...60 years.

Significant vertical density gradient rises the costs of energy for overcoming of the Archimed's forces and so the turbulence exists as the located areas with stochastic space-temporary structure. Vertical diffusion carring happens mainly at the expense of the stochastic "flares" of the local turbulence (Ozmidov,1997). These "flares" arise owing to many reasons: shifts of currents speed in internal waves or eddy formations "billows" type, local deformations of the density gradients and other ones. Regime of sporadic turbulent "flares", probably, is the main form of the vertical exchange through the high gradient layers and so the valuation of statistical Kz characteristics and vertical diffusive fluxes of the nutrient and oxygen are especially important.

Present work is devoted to analysis of this problem on the basis of the data of the measurements of the currents and density profiles in the Black Sea by summer heating (Fig.1) at formation of the strong vertical gradients of density (expedition R/V Yakov Gakkel, August,1992).

The data of the similar measurements in the Loch Ness (Thorpe,1977) and in the Lake Kinneret (submitted by Prof. B.Steinman) were also used
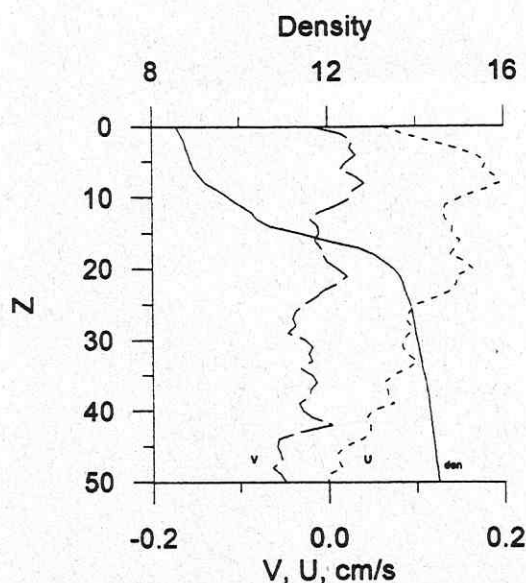
Fig.1. Characteric profiles of density (den) and current speed vector's meridian (V) and parallel (U) components in the upper Black Sea

ANALYSIS OF THE EXPERIMENTAL DATA

The main idea of the present work consists in similarity of the physical processes of formation of the density structures and vertical current shifts in the top layers of water column by summer heating. It means the similarity of these characteristics in following normalized dimensionless form: depth $z_* = z/z_m$, where z_m - the depth of the density gradient maximum (Brunt-Vaisala frequency is equal to Nm); Brunt-Vaisala frequency $N_* = N/Nm$; Richardson numbers Ri significance. Logarithms of these values are used owing to large range of their changes.

Analysis of the dimensionless dependences $logN_* = f(z_*)$ and $logRi = f(z_*)$ for the Black Sea, the Loch Ness and the Lake Kinneret conditions has shown the opportunity of approximation of average significances $<logN_*>$ and $<logRi>$ by regressions $a_0 + a_1 z_* + a_2 z_*^2 + a_3 z_*^3$ type and that these regressions have the identical character and are close among themselves. This confirms the similarity of physical processes of formation of the top layer in natural basins by summer heating (Fig.2 and Fig.3)

Experimental dependences $logRi = f(2logN)$ received on the data of the measurements in the Black Sea and the Loch Ness admit the approximation by linear regression $logRi = c_0 + 2c_1 logN_*$ form and thus have relatively close parameters:for the Black Sea $c_0 = 4.2663$, $c_1 = 1.0394$; for the Loch Ness $c_0 = 4.8258$, $c_1 = 1.1217$. Correlation coefficients between $logRi$ and $2logN_*$ for the Black Sea and the Loch Ness are equal to 0.75 and 0.74 correspondently.High correlation between Richardson numbers and vertical density gradients is stipulated by increasing of energy concentration of internal waves and eddy structures "billows" type in the layers with the maximal vertical density gradients (Thorpe, 1977; Duchno & Kushnir,1990).
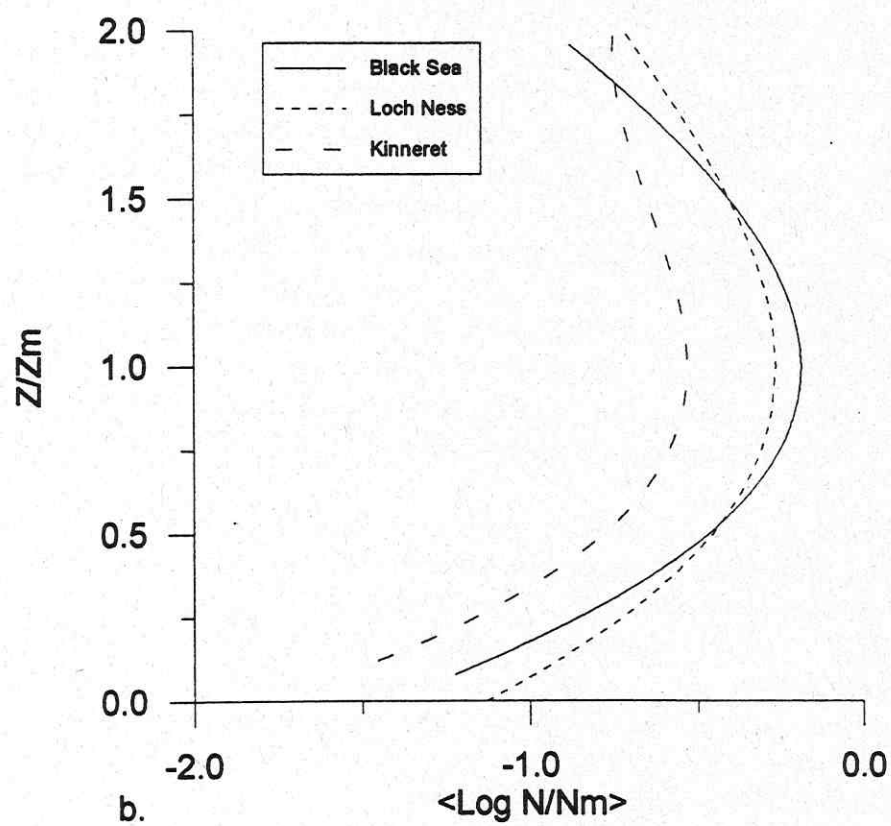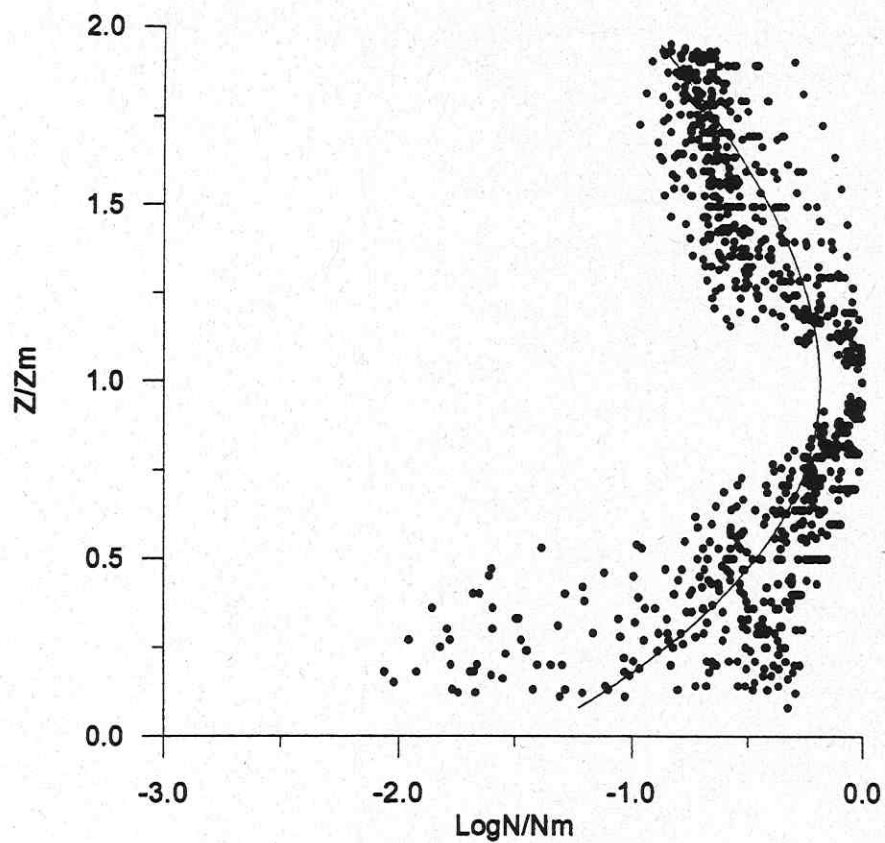
Fig.2.Experimental dependence $\log(N_*) = f(z_*)$ and regression line for the upper Black Sea (a); regression lines $<\log(N_*)> = f(z_*)$ for the Black Sea, Loch Ness and Lake Kinneret.
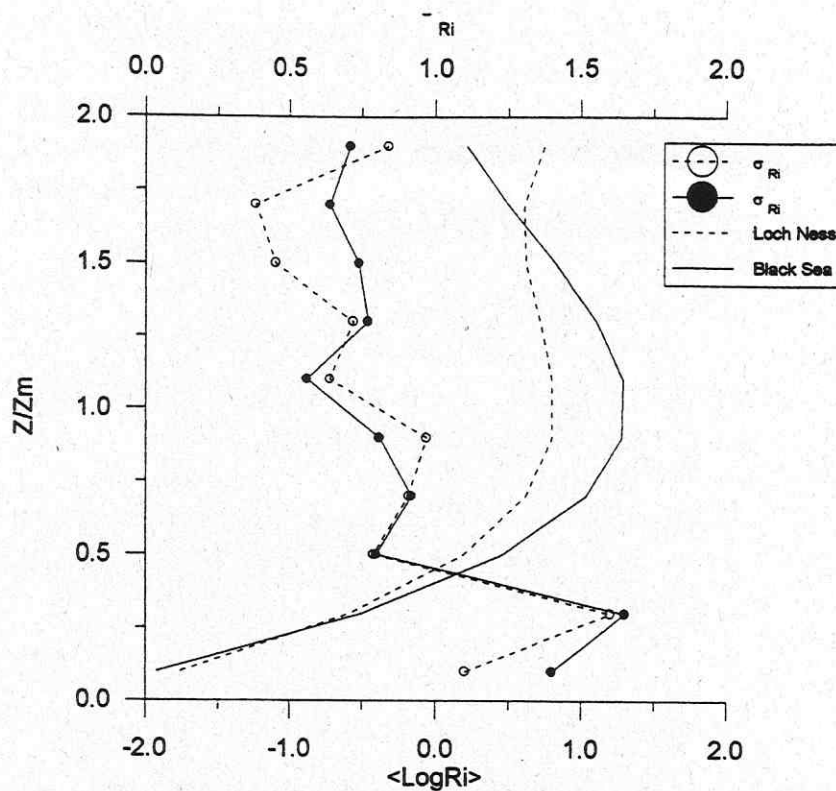
Fig.3.Regression lines $\langle Ri \rangle = f(z_*)$ and standart log Ri deviations $\sigma = f(z_*)$ for the Black Sea and Loch Ness.

RESULTS AND DISCUSSION

Semi-empirical Ozmidov's model (1965) is used for calculation of the vertical diffusion coefficient Kz:

$$Kz = C_1 \varepsilon^{1/3} Lo^{4/3}, \tag{1}$$

where $C_1 = 0.1$- the constant, $\varepsilon = 7.5\nu E^2$ - the rate at which energy is dissipated per unit volume, ν - kinematic viscosity, $E^2 = (\partial u/\partial z)^2 + (\partial v/\partial z)^2$ - square of module of the vertical shift of horizontal current speed, $Lo = \varepsilon^{1/2} N^{-3/2}$ - Ozmidov's scale.

Ratio (1) is transformed easily to the following form:

$$Kz = 0.75\nu Ri^{-1}. \tag{2}$$

Vertical turbulent diffusion can be developed at condition $Lo > L_K = \nu^{3/4} \varepsilon^{-1/4}$ - Kolmogorov's scale. Maximal (critical) significance of the Richardson number Ri_{kr} at which vertical turbulent diffusion can exist is equal to 7.5 and appropriate to significance $Kz/\nu = 0.1$ that is about equal to the molecular thermal diffusivity coefficient k_T.

Average significance of the vertical diffusion coefficient $\langle Kz \rangle$ with account of the mentioned regression $\langle \log Ri \rangle = a_o + a_1 z_* + a_2 z_*^2 + a_3 z_*^3 = Rz$ is equal:

$$\langle Kz \rangle = 0.75\nu 10^{-Rz}. \tag{3}$$

Rz is equal to -2.54 in the top layer of the Black Sea and $\langle Kz \rangle = 3.65 cm^2/s$; at $z_* = 0.5$, $\langle Kz \rangle = 0.044 cm^2/s$ (3ν); $z_* = 1$ in layer of density jump and $\langle Kz \rangle = 0.0016 cm^2/s$ $(1.2 k_T)$; $\langle Kz \rangle = 0.0025 cm^2/s$ $(2k_T)$ at $z_* = 1.5$. Just so, the average significances of the vertical diffusion coefficient

are close to the sizes of the molecular thermal diffusivity in the high gradient layers which are formed in the Black Sea by intensive summer heating.

Statistical valuations of the vertical diffusion coefficient and parameters connected with the vertical fluxes are especially important in this connection.

Thorpe (1977) has shown that probability distribution of the logRi values are close to the normal (Gauss) in the Loch Ness. Calculations of the asymmetry and excess coefficients for the logRi and logn significances for the Black Sea conditions have shown, that their sizes are relatively small and correspondent to the Kolmogorov's criterion for normal probability distribution. So, the ratio (2) is recorded in following kind:

$$Kz = 0.75 \ v10^{-x}, \quad W(x) = (2\pi\sigma^2)^{-0.5} \exp[-(0.5(x - x_o)^2/\sigma^2)],$$

$$logRi = x, \quad <logRi> = x_o, \quad <(x - x_o)^2> = D(x) = \sigma^2. \tag{4}$$

Probability distribution of the $Kz/v = Y$ values is calculated on the base of the common rule of nonlinear transformations of stochastic sizes and has the following form:

$$W(Y) = 0.173(\sigma Y)^{-1} \exp[-0.5\sigma^{-2}(-0.124 - x_o - logY)]. \tag{5}$$

Analysis of the probability distributions $W(Y) = f(Y)$ for various normalized depths has shown, that they are characterized by significant positive asymmetry, which is displayed in relatively slow reduction $W(Y)$ at Y increasing (Fig.4).
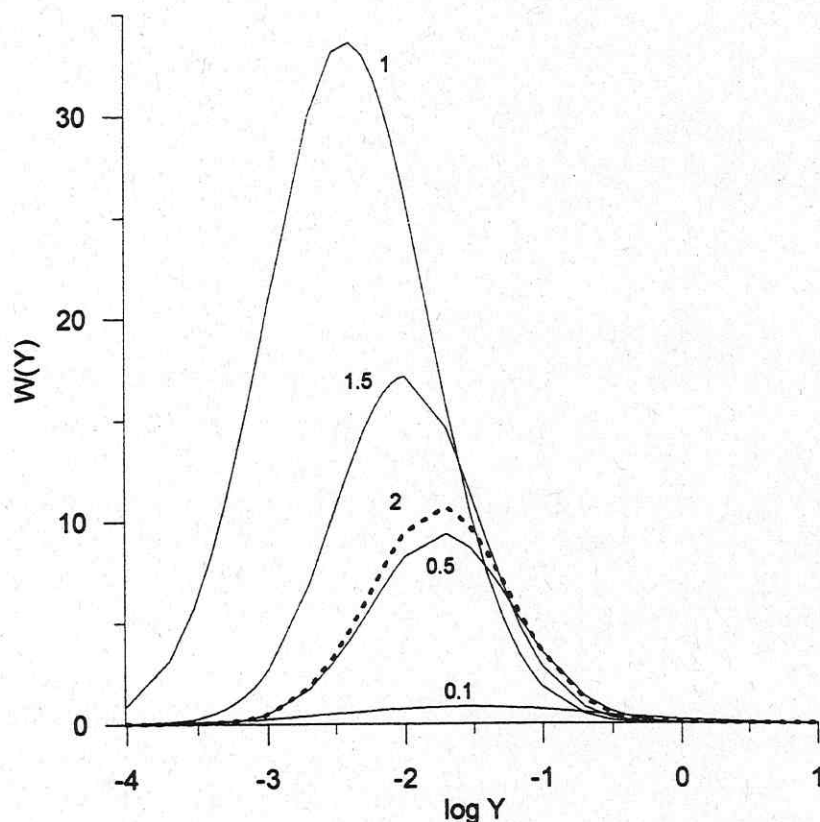
Fig.4.Probability distribution $W(Y) = f(logY)$ at various significances z_*.

$W(Y)$ dependenses are possible to use for definition of the probability of the local turbulent "flares" which are appropriated to certain vertical diffusin coefficient. Probability of these "flares", appropriated to range $Kz= 5...50cm^2/s$ is equal to 27% for near surface layer ($z_* = 0$, $<Kz> = 3.65$ cm^2/s); at $z_* = 0.1$ ($<Kz> = 0.66 \ cm^2/s$, $N = 0.0056 \ rad/s$, $T = 2\pi/N = 18.6 \ min$); probability of "flares", appropriate to range $Kz = 1...5cm^2/s$, is equal to 20%. Probabilities of formation of the

local turbulent "flares" for high gradient layers are equal to 2.86% ($z_* = 1$, density jump), 5.1% ($z_* = 1.5$), 2% ($z_* = 2$) for Kz range 0.1...1cm^2/s (such significances are usually used in hydrodinamical models).

Thus, the high gradient density layers are difficultly obstacle for receipt of oxygen from atmosphere on the depth more than 15-25 m and nutrients from deep-water layers to the top euphotic layer of the Sea. Considerable reduction of the oxygen concentration and accumulation of the nutrients in layers located deeper than density jump should be the chemical and biological consequences of such regimes. Present hydrochemical data confirm to such picture.

Phytoplankton meal is executed in the top layer above the density jump, basically, at the expense of regeneration of organic substance. The main source of reception of new production in this layer is expansion of the nutrients through the high gradient density layers in the euphotic zone, and the main mechanism of the such expansion is the mentioned local turbulent "flares". The probability distribution of vertical fluxes W(F) and their average significance <F> are calculated on the next ratio:

$$W(F) = (vG)^{-1}W(F/vG), \quad <F> = vG<Y>, \qquad (6)$$ where G - vertical gradient of considered biogenic element.

<F> value is equal to 0.77vG in considered case of the density jump in the Black Sea .

CONCLUSIONS

1.Analysis of the vertical diffusion characteristics in the upper Black Sea by summer heating has shown that the effective vertical carrying (Kz = 0.1 - 1cm^2/s) in the high gradient layers is executed mainly by stochastic local turbulent "flares", probability of which is equal to 2...5%. The main diffusion processes background in the stratified Black Sea layer is the slowly proceeding, languid processes of vertical exchange, speed of which slightly exceeds to the speed of the molecular vertical diffusion.The exception is the thin near surface layer, where the average Kz significances are equal to 0.6...3.65cm^2/s, and probability of the local turbulent "flares" is equal to 20...27% for large Kz significances in the range of 5...50 cm^2/s.

2.High correlation between logRi and logN$_*$ significances also with the similarity of the logRi = f(z_*), logN$_*$ = f(z_*) characteristics permits to use for statistical parameterization of vertical turbulent fluxes the density profiles, measurements of which are considerably easier than synchronous measurements of currents and density profiles and archives of which are already present for many natural basins.

REFERENCES

Duchno L.A.,Kushnir V.M. 1990. The top ocean layer in condition of warm inflow and layered current structure: laboratory and natural experiments. Izv. Acad. Sci. of the USSR. Physics of Atmosphere and Ocean. Vol. 26. No. 4. P. 421-429. (in Russian).

Ozmidov R.V. 1965. Turbulent exchange in steadily stratified Ocean. Izv. Acad. Sci. of the USSR. Physics of Atmasphere and Ocean. Vol.1. No.8. P.853-859. (in Russian).

Ozmidov R.V. 1997. Vertical exchange through the layers with large vertical density gradients in Ocean. Oceanology. Vol. 34. No. 4. P. 492 - 496. (in Russian).

Thorpe S.A. 1977. Turbulence and mixing in a Scotish Loch. Phil. Transaction of Royal Soc. of London. Vol.286. No. 1334. P.125-181.

Direct heat flux estimates in the oceanic boundary layer – results from measurements with a horizontal profiler

Fabian Wolk
Joint Research Centre, Ispra

Rolf G. Lueck
Centre for Earth and Ocean Research, University of Victoria, BC

Introduction

Fluxes of mass, heat, and momentum are important factors of ocean circulation. In the past, these fluxes have been estimated indirectly from measurements of the dissipation of temperature variance, χ (*Osborn and Cox*, 1972) or the dissipation of turbulent kinetic energy, ϵ (*Osborn*, 1980). The "direct" measurement of the vertical fluxes of scalars by correlation methods is a well developed technique in the atmospheric boundary layer (*Kaimal* et al., 1972), but in the oceanic boundary layer, these measurements are challenging because rigid platforms are seldom available. In recent years, promising attempts have been made to directly determine the oceanic turbulent heat flux from simultaneous measurements of the vertical velocity fluctuations and the temperature fluctuations, w' and T', respectively (*Moum*, 1990; *Yamazaki and Osborn*, 1993; *Fleury and Lueck*, 1994).

Here, we present data from direct heat flux measurements collected with our horizontal profiler, TOMI[1]. With this contribution to the yet limited set of direct observations of vertical oceanic fluxes, we are beginning to discern common characteristics. When normalized by the Ozmidov scale, the co-spectra between w' and T' exhibit a universal character.

Observational Background

We tow TOMI at night in the oceanic mixed layer between 15 m and 25 m depth. During the eight hour tow, wind speeds are between 8 ms^{-1} and 12 ms^{-1}, and the oceanic boundary layer is loosing heat to the atmosphere at a rate of approximately 100 Wm^{-2}. The data are collected during Phase II of the Marine Boundary Layer Experiment, in

---

[1]Towed Ocean Microstructure Instrument

April/May 1995 in Monterey Bay, California. w' is measured with a conventional airfoil probe (shear probe), and T' is measured with a fast thermistor.

Instrumentation and Data Processing

The outputs of the shear probe and thermistor are filtered at 0.03 Hz with a zero phase shift high-pass filter. This operation eliminates a small pyroelectric effect of the shear probe, which is evident in regions of large horizontal temperature gradients (e.g. temperature fronts). Thus, the smallest wavenumber resolved is 0.02 cpm (50 m wavelength). The shear probe yields vertical velocity shear, $\partial w/\partial x$, from which the vertical velocity is reconstructed by applying an anti-derivative (low-pass) filter. This velocity signal is still contaminated by the motions of the vehicle and spurious irrotational velocity signals induced by surface waves. These erroneous velocity signals are extracted by applying a special motion compensation algorithm to the measured velocity signal (*Wolk*, 1997). This yields the fluctuating vertical velocity w'.

Time series of the instantaneous heat flux are obtained by directly multiplying the quantities w' and T'. Average heat fluxes are computed by integrating the co-spectrum, between w' and T' over the wavenumber range to be resolved, here between 0.02 cpm and 45 cpm. One flux spectrum is computed for a 1600-second record of w' and T'. The spectrum for one record is obtained by block-averaging the spectral estimates of thirty-seven half overlapping data sections of length 64 seconds.
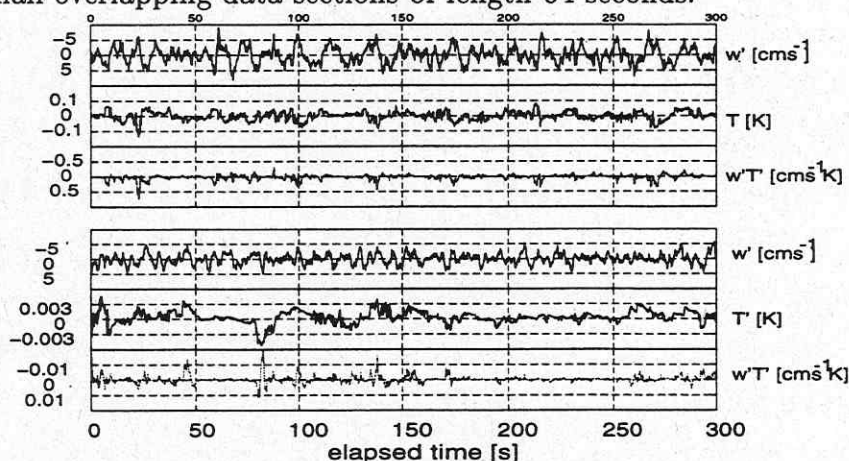
Figure 1. Time series of w' T' for a stably stratified region (upper panels) and a convective region (lower panels).

Results

Figure 1 shows time series of w', T', and instantaneous $w'T'$ taken from a stably stratified region in the boundary layer (upper panels) and from a convective region (lower panels). In the coordinate system chosen here, z is positive downwards, so that negative value of $w'T'$ represents either downward transport of cold water or upward transport of warm water.

In the $w'T'$ time series from the stable region, there are numerous examples of upward heat transports (negative spikes), but the average heat flux is downward. This is indicative of wind driven boundary layer, in which turbulent overturns act in such a way as to reduce the background temperature stratification. For the convective region, the situation is reversed: most spikes are negative, indicating cold water is transported downward, which represents an upward, non-local heat transport. The negative spikes are caused by plumes of cold water sinking from the sea surface. The variance of the vertical velocity in the stable section is approximately two times larger than in the convective section. The temperature variance in the stable region is about 500 times larger than in the convective region. For the segments shown, the repective avarage heat fluxes are $+950\text{Wm}^{-2}$ (stratified) and -14Wm^{-2} (convective).

Figure 2 shows the ensemble averaged co-spectrum from stratified regions. The co-spectrum represents the average of approximately 4.5 hours of data and it is shown as a solid, heavy line (hereafter referred to as WL). Also shown for comparison, are the flux spectra calculated by Yamazaki and Osborn (1993, solid thin line, hereafter YO) and Fleury and Lueck (1994, dotted line, hereafter FL). The spectra are plotted in variance preserving form, so that the area underneath the curve equals the total variance. To facilitate the comparison, the magnitudes of the spectra are non-dimensionalized by $g\alpha/\epsilon$, where g is the constant of gravity, α is the thermal expansion coefficient, and ϵ is the dissipation rate of turbulent kinetic energy. The wavenumber axis is scaled by the Ozmidov wavenumber $k_o = L_o^{-1} = (2\pi)^{-1}(N^3/\epsilon)^{1/2}$ (in cpm), where L_o is the Ozmidov wavelength and N is the buoyancy frequency. The co-spectra of YO and WL, which are fully resolved, both have their maxima at $k_o/2$. In both studies, the maximum heat flux occurs on scales of twice the Ozmidov length, even though the data originate from different regimes: the WL data is sampled in an active mixed layer, while the YO data is sampled at the bottom of the thermocline. The FL spectrum is not fully resolved but exhibits a similar slope at $k_o = 1$ and thus lends support to the common characteristic.

Conclusions

By employing a motion compensation algorithm, we are able to extract the environmental velocity fluctuations w' from velocity shear data sampled with our horizontal profiler. Correlation of w' with the fluctuating temperature T' yields a direct, instantaneous estimate of the vertical heat flux. The average flux spectrum from a stratified region oceanic boundary layer exhibits a peak at $0.5k_o$. Comparison with previous studies suggests a universal character of the heat flux spectrum in stratified environments.
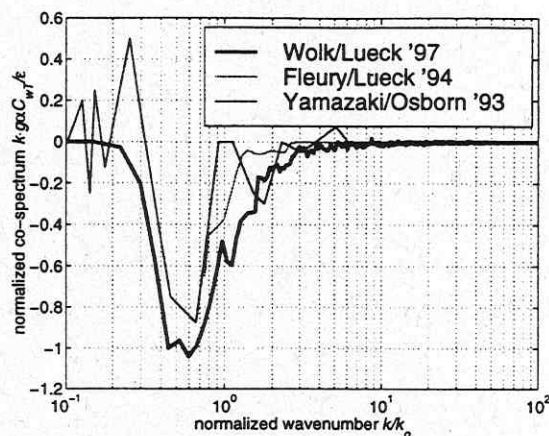
Figure 2. Ensemble averaged co-spectra (solid heavy line) from a stratified section. Show as a comparison are the co-spectra obtained by Yamazaki and Osborn (1993) (thin line) and Fleury and Lueck (1994) (dotted line).

References

Fleury, M., and R. G. Lueck, Direct heat flux estimates using a towed vehicle, *Journal of Physical Oceanography, 24*, 801–818, 1994.

Kaimal, J. C., J. C. Wyngaard, Y. Izumi, and O. R. Coté, Spectral characteristics of surface-layer turbulence, *Quarterly Journal of the Royal Meteorological Society, 98*, 563–589, 1972.

Moum, J. N., The quest for k_ρ – preliminary results from direct measurements of turbulent fluxes in the ocean, *Journal of Physical Oceanography, 20*, 1980–1984, 1990.

Osborn, T. R., Estimates of the local rate of vertical diffusion from dissipation measurements, *Journal of Physical Oceanography, 10*, 83–89, 1980.

Osborn, T. R., and C. S. Cox, Oceanic fine structure, *Geophysical Fluid Dynamics, 3*, 321–345, 1972.

Wolk, F., Near surface heat flux measurements with a towed vehicle, M.Sc. Thesis, Univeristy of Victoria, Dec., 1997.

Yamazaki, H., and T. Osborn, Direct estimation of heat flux in a seasonal thermocline, *Journal of Physical Oceanography, 23*, 503–516, 1993.

Near-Bottom Turbulence in the South Basin of Lake Baikal

Tom Ravens, Michael Schurter, and Alfred Wüest

Swiss Federal Institute of Environmental Science and Technology
(EAWAG) and Swiss Federal Institute of Technology (ETH)
CH-8600 Dübendorf, Switzerland

Abstract

Daily near-bottom velocity bursts collected in the south basin of Lake Baikal (Russia) between December 1995 and December 1997 were studied. The inertial range of the velocity spectra was analyzed and dissipation of turbulent kinetic energy estimated. Dissipation estimates in conjunction with velocity were used to estimate a bottom drag coefficient ($C_{1m} = 2.3 \times 10^{-3}$). Both linear and non-linear models of the kinetic energy budget were developed to interpret and explain the data. Time constants for the under-ice decay of kinetic energy and dissipation were 40 days and 28 days, respectively.

1   Bottom current dynamics

Near-bottom water velocity was measured for about two years (Dec. 1995-Dec. 1997) from a mooring in the south basin of Lake Baikal in a water depth of 1390 m. The velocity meter was a 2-D acoustic velocity meter (SACM3, EG&G Marine Instruments, Burlington, MA). Velocity was measured at either 105 m (for the first and fourth deployment) or 4 m above bottom (for the second and third, Fig. 1). Velocity fluctuations were much stronger immediately above the bottom presumably a result of turbulence generated in the bottom boundary layer. Larger scale (though less energetic) structures were visible 105 m above bottom. The velocity data indicated significant damping during the periods when the south basin was ice-covered (Fig., 1a and 1b – the thick horizontal bars indicating periods of ice cover). The time constant of the decay of kinetic energy under ice was about 38 days (Table 1). By the end of the period of ice cover, the measured velocity fell to near zero (< 1 mm s^{-1}) confirming our laboratory calibration. The velocity data following ice break-up indicated a relatively slow recovery of velocity in spring 1996 compared to that observed in spring 1997. The faster recovery observed in 1997 may have been a result of the stronger wind energy input seen that year (Fig. 1a). In the 2 months following ice breakup, the flux of wind energy (10 m above water) was 0.087 and 0.141 W m^{-2} in 1996 and 1997, respectively. Assuming a typical water velocity of 3 cm s^{-1}, a 1000-m water depth, and a 0.1% efficiency of energy transfer from wind to water, the time scales for recovery of water kinetic energy, are 66 and 41 days in 1996 and 1997, respectively. Velocity spectra (Fig. 2a) from energetic periods indicated a significant peak at 1.7 d^{-1}. The fact that this frequency corresponds to the Coriolis frequency (= $2\,\Omega \sin\theta = 9.9$ rad d^{-1} = 1.6 d^{-1}) in conjunction with the fact that the peak is missing during calm, low velocity periods (Fig., 2b), indicate that the Coriolis force is responsible for this effect. Large scale eddies, with length and time scales of 5 km and 5 days, respectively, were also evident in the velocity data.

2   Dissipation estimation from the velocity spectra.

a) **Method:** Within the inertial subrange (between the energy containing range and the dissipative range), the velocity power spectra (E(k)) shows a $k^{-5/3}$ dependence and is related to the rate of dissipation (ε) by the expression:

$$E(k) = \alpha \varepsilon^{2/3} k^{-5/3}$$

where k is the radial wave number (radians m^{-1}) and α is the three-dimensional Kolmogorov constant ($\alpha = 1.56$ (Wyngaard and Cote, 1971). Typically, one-dimensional turbulence only is measured. Assuming isotopic turbulence, the velocity spectra are written:

$$\phi_{11} = \alpha_1 \varepsilon^{2/3} k_1^{-5/3}$$
$$\phi_{22} = \phi_{33} = \alpha_2 \varepsilon^{2/3} k_1^{-5/3}$$

where ϕ_{11} is the spectra of the longitudinal velocity, ϕ_{22} and ϕ_{33} are the spectra of the horizontal and vertical transverse velocities, respectively, $\alpha_1 = 18/55\alpha$, $\alpha_2 = 4/3\alpha_1$, and k_1 is the one-dimensional radial wave number. Initially, velocity spectra were calculated in the frequency domain. Then, the Taylor's frozen turbulence assumption was invoked to convert the spectra to the radial wave number domain. The distance above the lake bottom of the velocity sensor (h_{meas}) established the minimum wave number ($2\pi/h_{meas}$) at which isotopic turbulence could be expected and the above relations would be valid. Following Terry *et al.* (1996), $\phi_{22} k^{5/3}$ was calculated producing a "flat spectrum" from which dissipation mean and standard deviation could be readily calculated.   Only dissipation estimates greater than the standard deviation were used.

The dissipation estimates ranged from 10^{-12} W/kg to 10^{-8} W/kg (Fig 1d). They were greatest in the second and third deployments where the velocity sensor was only 4 m above bottom. Under ice cover, dissipation estimates showed a marked decrease with a 28-day time constant (τ_{Diss}= 26 and 30 days in the 1996 and 1997 ice coverage periods, respectively). Given that dissipation (Diss) goes as the cube of velocity and kinetic energy (KE) as velocity squared, $\tau_{KE} = 1.5$ τ_{Diss}, and the corresponding kinetic energy time scales are 39 and 45 days for the 1996 and 1997 ice coverage periods, respectively. These results are in very good agreement with those of section 1, and we can conclude that the time scale for energy decay is $\tau_{KE} = 40 \pm 3$ d.

In the second and third deployments, when the velocity meter was 4 m above bottom, the dissipation estimates were found to be linearly related to the cube of the velocity magnitude (U^3) (Fig. 3). This suggests the velocity meter was in the logarithmic layer where the dissipation can be written: $\varepsilon(z) =$ (τ_o/ρ) ($\partial U/\partial z$) = $u_*^3/\kappa z$ = $C_{4m}^{1.5} U_{4m}^3$ /κz = $C_{1m}^{1.5} U_{1m}^3/\kappa z$ where τ_o is the bottom shear stress, u_* is the friction velocity, κ (= 0.41) is the von Karman constant, C_{4m} and C_{1m} are the 4-m and 1-m drag coefficients, and U_{4m} and U_{1m} are the velocity magnitudes at 4-m and 1-m above bottom (Imboden and Wüest, 1995). Linear regression of the data in Figure 3 lead to C_{4m} estimates of 1.5 and 1.8 x 10^{-3} for the second and third deployments, respectively.   Using the law of the wall relationship, $C_{1m} = C_{4m}(\ln^2(4/z_o))/(\ln^2(1/z_o))$, C_{1m} estimates of 2.0 and 2.7 x 10^{-3} were made for the second and third deployments, respectively. The bottom roughness parameter, z_o, was assumed equal to 0.1 mm, approximately equal to $0.1\nu/u_*$ (the roughness

parameter associated with smooth turbulent flow). Order of magnitude variation in z_o lead to only a 10% variation in the C_{1m} estimate.

3   Kinetic Energy

The measured near-bottom kinetic energy (throughout the four deployments) was compared with a linear (quasi-steady) model which assumed a balance between wind energy input ($E_{in} = f_{eff} P_{10}$) and decay of water kinetic energy (E/τ), where f_{eff} is the fraction of wind energy at 10 m ($P_{10} = \tau_{wind} U_{wind}$) which enters the water and τ is the energy loss time constant. The model was optimised when f_{eff} was 1.05 10^{-3} and $\tau = 50$ days (dashed line in Fig. 1c). In addition, a non-linear model, which (more realistically) assumed a kinetic energy loss that went as $E^{3/2}$ ($\approx U^3$) was considered (i.e., $f_{eff} \tau_{wind} U_{wind} = C E^{1.5}$) where C is a constant. This model was optimised with $f_{eff} = 0.0014$ and $C = 9 \times 10^{-6}$. From the constant C, a time constant of 53 d was obtained ($\tau = C^{-1} E_{ave}^{-0.5}$ where E_{ave} is the average kinetic energy = 5.9×10^{-4} $m^2 s^{-2}$). The mean square error of the models was 5.3×10^{-4} $m^2 s^{-2}$ and 5.5×10^{-4} $m^2 s^{-2}$ for the linear and non-linear models, respectively. Considering the whole data set, the time constant for decay of kinetic energy was a little greater than that observed under the ice. This may be because the ice provides an additional surface with which to dissipate energy.

4.   Conclusions

- The kinetic energy balance was reasonably well represented by a linear model which assumed that 0.1% of the wind energy (at 10m) was transported into the water and assumed a time constant of 50 days.

- The kinetic energy balance (as well as accompanying microstructure measurements, see below) indicate that bottom boundary layer dissipation accounts for about of the deep water (below 250 m) dissipation in Baikal

- The decay time constants of kinetic energy and dissipation under ice in the south basin are 40 d and 28 d, respectively.

- Dissipation estimates ranged from 10^{-12} to 10^{-8} W kg^{-1}.

- The one meter drag coefficient (C_{1m}) was 2.3 10^{-3}.

- At times of relatively high velocity (under open water conditions), most of the variance in velocity was at the inertial frequency.

NOTE: The above work is a part of the paper: Small-scale turbulence and diapycnal mixing in the stratified deep water of Lake Baikal by O. Kocsis, T. Ravens, A. Wüest, and N. Granin (in review)

Table 1: Summary of the TKE Balance during 1996 and 1997.

Period From-to	Length (d)	Ice/open Water	Height h above bottom (m)	Bottom current $\langle u_h\rangle$ (cms⁻¹)³	Dissipation $\langle\varepsilon_{LOW}\rangle$[1] 10⁻¹⁰ Wkg⁻¹	$\langle\varepsilon_{ID}\rangle$[2] 10⁻¹⁰ Wkg⁻¹	P_{bot}[3] μWm⁻²	Decay time τ_{KE}[4] (d)	$1.5\cdot\tau_{Diss}$[4] (d)	Wind W_{10}^3 (m³s⁻³)
8.12.95-17.1.96	(38)	Open	105	102	.077	.92 ± 0.3	102	-	-	185
18.1.96-3.5.96	(106)	Ice	105	51	.038	.28 ± 0.1	51	38	39	106
30.6.96-16.1.97	(200)	Open	4	55	24.1	30.1 ± 5	122	-	-	117
17.1.97-27.4.97	(100)	Ice	4	25	11.0	14.4 ± 2.7	55	39	45	182
28.4.97-9.7.97	(72)	Open	4	23	10.1	13.5 ± 5	51	-	-	106
12.7.97-26.11.97	(138)	Open	105	77	.058	1.2 ± 0.4	77			86
Mean	(206)	Ice	4/105	53			53	39±2		144
Values:	(448)	open	4/105	95			95			111

(1) ε_{LOW} is determined from $\langle u_h\rangle$ by using $\varepsilon_{LOW} = u*^3/(\kappa h)$, where $\kappa=0.41$ is the von Karman constant, $u* = C_h^{1/2} u_h$, and h=height above lake bottom; $C_{1m} = 2.3\ 10^{-3}$, C_h is calculated according to $C_h = C_{1m}\ ln^2(1m/z_0)/ln^2(h/z_0)$ with $z_0 = 0.1$ mm.

(2) ε_{ID} is determined from the current fluctuations u_h at height h above bottom by using the inertial dissipation method.

(3) P_{bot} is determined by using $P_{bot} = \rho C_{100}\langle u_{100}^3\rangle$; C_{100} and u_{100} corrected assuming Law of the Wall (LOW).

(4) τ_{KE} determined from the decay of kinetic energy $(\langle u_h^2\rangle/2)$ under ice; τ_{Diss} determined the decay of near-bottom dissipation under ice.
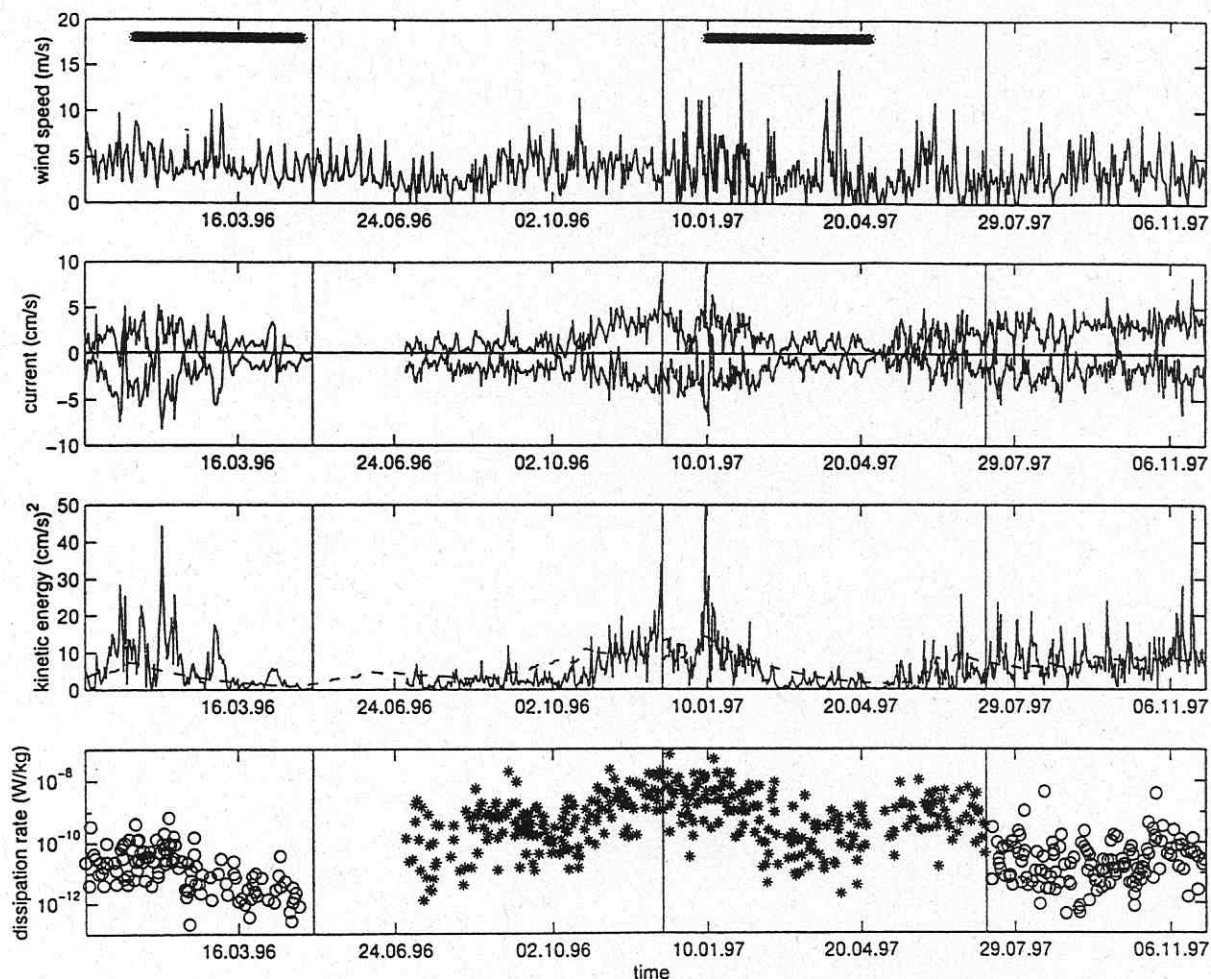
Figure 1:

(a) Upper panel: Wind speed throughout the time of the four velocity meter deployments: 8 Dec. 95 to 3 May 96, 28 Jun 96 to 11 Dec. 96, 12 Dec. 96 to 8 July 97, and 9 July 97 to 26 Nov. 97. The two thick horizontal lines indicate the time of ice cover. The light vertical lines demarcate the various deployment periods.

(b) Second panel: The north (lower line) and the east component (upper line) of velocity during the four deployments. The position of the velocity meter was 105 meters above bottom in the first and fourth deployment and 4 meters above bottom in the second and third.

(c) Third panel: Measured kinetic energy during the four deployments (solid line). The dotted line indicates the linear model calculation.

(d) Bottom panel: Dissipation rate during the deployments based on analysis of the inertial subrange of the velocity spectra.

(a)

(b)
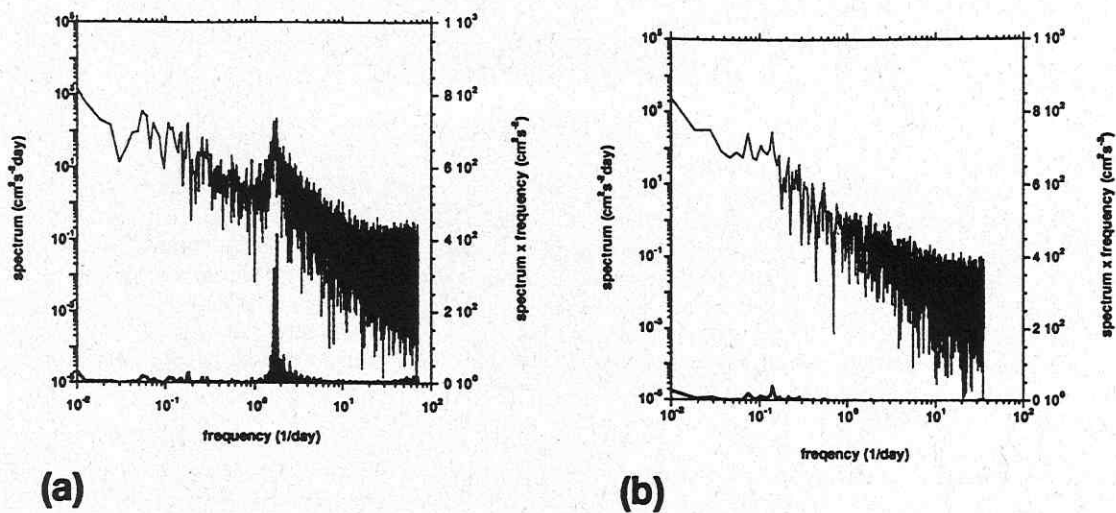
Figure 2: Velocity spectrum (light, upper line) and the variance-preserving spectrum x frequency (heavy, lower line) during (a) an open water period (June 30 - December 11, 1996) and (b) under ice (January 17 - April 27, 1997). Under open water conditions, where the currents are higher, a spectral peak at 1.6 days^{-1} is visible. The peak is not visible during ice-covered calm periods.
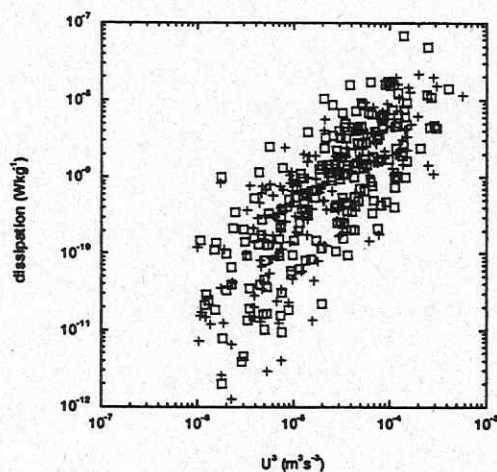
Figure 3: Dissipation versus the cube of velocity (U^3) during the second (+) and third ( ) deployments. A near-linear relationship is evident suggesting that these velocity measurements at 4-m were in the bottom boundary layer.

Application of Turbulence Models to Lakes—

The Role of Internal Seiches

G.-H. Goudsmit[1], H. Burchard[2], P. Reichert[1], and A. Wüest[1]

[1]Department of Environmental Physics, Swiss Federal Institute of Environmental Science and Technology (EAWAG) and Swiss Federal Institute of Technology (ETH), Dübendorf.
[2]Joint Research Centre, Space Application Institute, Ispra, Italy

1. Introduction

During the past decades, various turbulence closure models such as bulk models (e.g., Kraus and Turner, 1967) and one- or two equation differential models (such as k-l and k-ε) for the simulation of the dynamics of natural basins have been developed and applied. Most of these models are focused on an accurate prediction of the mixed layer depth. In stratified lakes, major difficulties arise below the thermocline for 1-D versions of such models, because TKE breaks usually down and diffusivities fell to molecular values; in contradiction with experimental observations.

This contradiction has been explained by the fact that part of the kinetic energy introduced at the water surface by wind is transferred to internal seiches and becomes therefore indirectly available for turbulent mixing. A common solution is the introduction of a minimum threshold value for TKE, an approach, which does not allow for any variations of TKE within and below the thermocline.

The present approach was motivated by experimental observations (temperature microstructure and dye tracer experiments) in Lake Alpnach where was shown that (1) hypolimnetic dissipation rates increased according to wind excitation and decayed with a typical time constant of approx. 3 days (Gloor et al., 1998) and (2) that vertical mixing in the hypolimnion is predominantly determined by mixing near the bottom boundary (Wüest et al., 1996).

Therefore our lake model comprises not only a k-ε turbulence closure scheme but also an additional simple seiche excitation and damping model. This seiche model with wind forcing and bottom friction as energy source and sink, respectively, is added to compute the diffusivity below the thermocline of the basin. In a first application, the temperature stratification and turbulent diffusivity in Lake Alpnach and Lake Baldegg were modelled. Results show that the lake model is appropriate for the simulations of deep, stratified basins.

2. Modelling Approach

The host model is adapted from the buoyancy-extended k-ε model (Rodi, 1984) to describe the vertical density structure and mixing. As this has been already described in detail elsewhere (Burchard and Baumert, 1995), we confine ourselves to a brief description of the framework.

The one-dimensional model equations are based on the assumption that horizontal gradients are negligible, which is usually the case for small or mid-size basins. In the one-dimensional vertical model (z-axis pointing upwards) the basic set of equations for temperature T, mean horizontal velocity components with respect to x and y, u and v, turbulent kinetic energy per unit mass (TKE) k, and the dissipation rate of TKE ε, are:

$$\frac{\partial T}{\partial t} = \frac{1}{\rho_0 c_p} \frac{\partial F_{sol}}{\partial z} + \frac{1}{A} \frac{\partial}{\partial z}\left(A\left(v_t' + v'\right)\frac{\partial T}{\partial z}\right) \tag{1}$$

$$\frac{\partial u}{\partial t} = \frac{1}{A} \frac{\partial}{\partial z}\left(A\left(v_t + v\right)\frac{\partial u}{\partial z}\right) - fv \qquad \frac{\partial v}{\partial t} = \frac{1}{A} \frac{\partial}{\partial z}\left(A\left(v_t + v\right)\frac{\partial v}{\partial z}\right) + fu \tag{2}$$

$$\frac{\partial k}{\partial t} = \frac{1}{A} \frac{\partial}{\partial z}\left(A v_k \frac{\partial k}{\partial z}\right) + P + \phi_S P_{Seiche} + B - \varepsilon \tag{3}$$

$$\frac{\partial \varepsilon}{\partial t} = \frac{1}{A} \frac{\partial}{\partial z}\left(A v_\varepsilon \frac{\partial \varepsilon}{\partial z}\right) + \frac{\varepsilon}{k}\left(c_{\varepsilon 1}\left(P + \phi_S P_{Seiche}\right) + c_{\varepsilon 3} B - c_{\varepsilon 2} \varepsilon\right) \tag{4}$$

where A represents the surface area of the lake at the depth z, F_{sol} the short-wave solar irradiation. $\phi_S P_{Seiche}$ [W kg^{-1}] is the production of TKE due to internal seiching (see below). All other definitions, boundary conditions, and discretization are equal those in (Burchard and Baumert, 1995), except the boundary condition for temperature, where measured surface temperatures were prescribed.

The balance of total energy E_{Seiche} per surface area [J m^{-2}] of an internal seiche can be described as:

$$\frac{dE}{dt} = PW - \int_{z=bottom}^{z=surf} \phi_S P_{Seiche} \tag{5}$$

where PW and $\phi_S P_{Seiche}$ [W m^{-2}] are the source and sink of seiche energy by wind excitation and bottom friction, respectively. Wind excitation is parameterized as

$$PW = \alpha \rho_{air} c_{10} \left(\left| u_{10}^3 \right| + \left| v_{10}^3 \right| \right) \tag{6}$$

where ρ_{air} is the density of air, u_{10} and v_{10} the wind speed measured at a height of 10 m above the water surface, and c_{10} the drag coefficient (0.001 - 0.0025, depending on wind speed; Amorocho and de Vries, 1980). The model parameter α measures the portion of total wind energy, which is consumed for the production of internal seiches and depends mainly on the magnitude of the mixed layer H_E of the water column. Assuming that the loss of seiche energy is entirely balanced by dissipation, α can be approximated by the average ratio of dissipation ε to wind energy flux at the surface. For the ocean ($u_{10} \approx 8$ m s^{-1}, ε integrated over the stratified part of the water column $\approx \int_{0m}^{100m} \approx 0.5$ mW m^{-2} (Gregg and Sanford (1988)), $H_E \approx 100$ m) this ratio is approximately 0.001. For lakes, where the thickness of the mixed layer is much less ($H_E \approx 5$ m), α is approximately 0.01 (A. Wüest, personal communication, based on Wüest et al. (1996)). Thus, acceptable values for α should lie within this interval.

The bottom friction term $\phi_s P_{Seiche}$ (flux of energy from the boundaries) was parameterized similar to Gloor et al. (1998):

$$\int_{z_{bottom}}^{z_{surf}} \phi_S P_{Seiche} = \gamma E^{3/2} \tag{7}$$

where γ is a damping factor, which depends on the friction coefficient and the basin geometry (mainly the mean depth of the hypolimnion). Assuming a logarithmic velocity profile above the lake bottom, the loss of seiche energy is approximately:

$$\frac{\partial E}{\partial t} \approx \rho_0 C_D \left| U_{SB} \right|^3 \tag{8}$$

where C_D is the bottom friction coefficient. The constant U_{SB} can be estimated by taking the total kinetic energy of the seiche into account. Assuming that the temporal mean over a seiche period of potential energy equals the temporal mean of the kinetic energy, E is given by:

$$E = 2E_{kin} \approx \frac{2}{A} \int_{z_{bottom}}^{z_{surf}} A \frac{1}{2} U_S^2 \cdot \rho \, dz \approx \rho_0 h \cdot U_{SB}^2 \tag{9}$$

where h is the mean depth of the lake (i.e. total volume divided by lake surface), U_S the temporal mean of the absolute horizontal velocity, and U_{SB} the horizontal velocity at the basin bottom. Thus γ is given by:

$$\gamma = C_D \rho_0^{-1/2} h^{-3/2} \tag{10}$$

In order to verify this parameterization, the decay time τ_{Seiche} for internal seiche energy (which can be easily deduced from Eq. 5 and 7)

$$\tau_{Seiche} = \frac{2 \left(\sqrt{e} - 1 \right)}{\gamma \sqrt{E_{Seiche}(t=0)}} \tag{11}$$

was compared with the value obtained from Lake Alpnach ($\tau_{Seiche} \approx 3$ days (Gloor et al., 1998). The mean depth h was known from lake volume (0.10 km^3) and lake surface (4.76 km^2)). Simulations of Lake Alpnach (see below) yielded $E_{seiche} \approx 20$ J m^{-2}. Assuming a bottom friction coefficient $c_D = 0.002$ (Elliot, 1984), τ_{Seiche} was estimated to be 4 days, in reasonable agreement with observations. The distribution function of seiche energy ϕ_s was derived from theoretical considerations and from measurements in Lake Alpnach. As bottom friction is the main factor for seiche damping (Gloor et al., 1998, Goudsmit et al., 1997), ϕ_s should be proportional to the bottom surface area per volume at depth z. This is equal to a constant flux of TKE from the bottom boundary layer into the water column. However, theoretical considerations and measurements have shown that the system mixing efficiency γ_{mix}, i.e. the amount of kinetic energy used for buoyancy production, strongly varies with stability N^2. Figure 1 sows the variation of γ_{mix} and N^2 with depth in Lake Alpnach. From this point of view, ϕ_s was parameterized to be also a function of N^2:

$$\phi_S = c \frac{1}{A} \frac{dA}{dz} N^{2q} \tag{12}$$

where c is a normalization coefficient, i.e. $\int \phi_s \, dz = 1$, and q [-] a model parameter. The differing dynamics of mixed layers over a sloping bottom boundary as compared to the flat bottom near the deepest site of the lake may be the reason for the increase of the system efficiency with decreasing depth and increasing stability. Mixing over a flat bottom at the deepest site of the lake where a quasi-stationary layer persists is inefficient. In contrast periodical generation of well-mixed layers and their subsequent intrusion into the lake interior offers the possibility of mixing repeatedly restratification which is more efficient.

3. Application of the Model

As a first test, the model was applied for Lake Alpnach during the period of approximately three weeks in summer (June 18 – July 9, 1995). The lake water temperature was measured quasi-continuously by two moored thermistor chains (Aanderaa, Bergen, Norway). Additionally, meteorological quantities such as wind speed, air temperature, and solar radiation were measured by a weather station (Aanderaa, Bergen, Norway), installed at the airport near the lake.

In Figure 3 (lower panel), a contour plot of the measured temperatures shows the pronounced oscillations in the hypolimnion of the internal seiches in Lake Alpnach. As shown in Figure 3, the simulated temperatures are very close to the observed values. As the oscillations of the internal seiches are not included explicitly into our model, the simulated results lack this effect. However, on larger time scales, deviations are relatively small.

In order to compare vertical transport in the hypolimnion, turbulent diffusivities v_t computed using the budget-gradient method (Powell and Jassby, 1974). As shown in Figure 2, the temporal average values of simulated v_t (line) is in reasonable agreement with the observations (dots).

In a second application, the thermal stratification and mixing processes is the upper layers of Lake Baldegg was modelled. Lake Baldegg is a eutrophic lake on the Swiss Plateau, approximately elliptical, and has a maximum depth of 65 m. Due to intense eutrophication problems, the lake has been artificially oxygenated during summer and airated during winter since 1982. Like in Lake Alpnach water temperature was measured quasi-continuously by a moored thermistor chain at a sampling rate of 0.1 min^{-1} from 1 to 16 m depth for a nearly two-year period. Additionally, two meteorological stations were installed near the lake shore. Below 16 m, mixing and stratification is strongly influenced by artificial aeration and oxygenation, which was not accounted for in the model. As shown in Figure 4, the model results are in good agreement with the measurements. Some slight deviations occur in the thermocline, which may be already influenced by the aeration.

| Figure 1: Stability (N^2) and system mixing efficiency γ_{mix} in Lake Alpnach during June 18 – July 9, 1995. | Figure 2: Comparison of diapycnal diffusivities using heat-budget method (dots) with average model results (line). |

Time after 1.1.1995 [days]
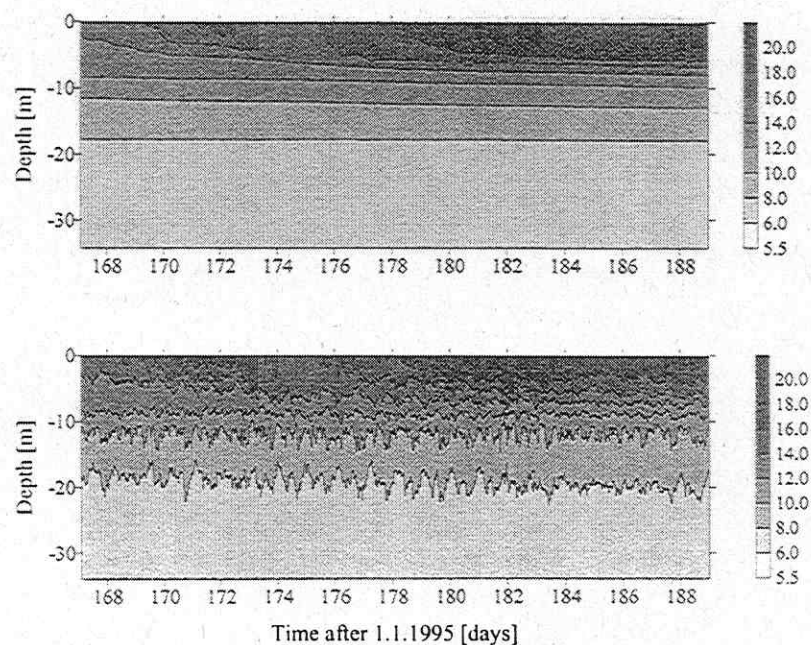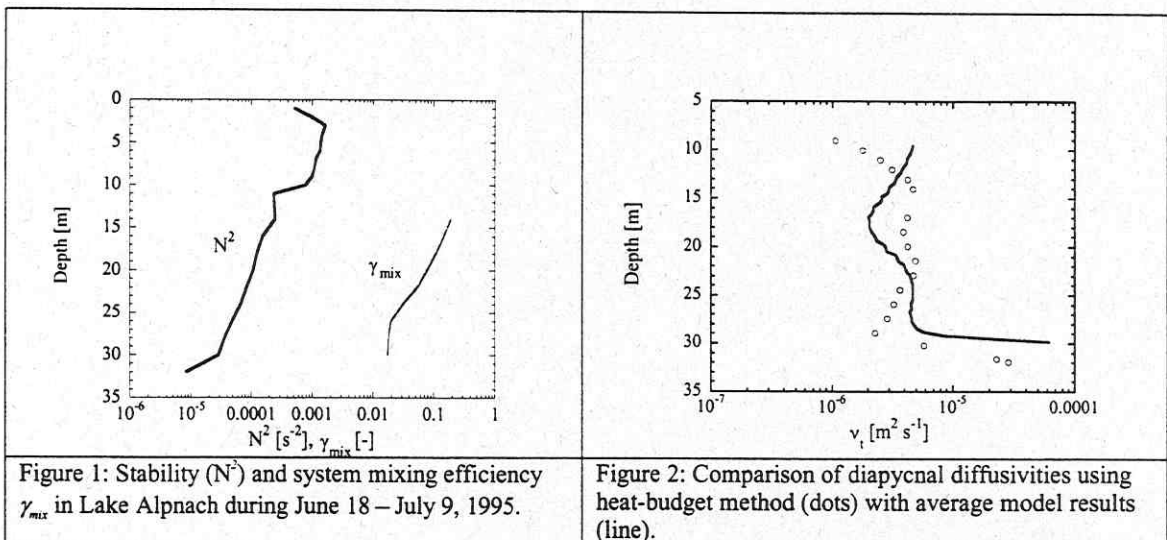
Figure 3: Simulated (upper) and measured (lower) temperature distribution in Lake Alpnach from June 18 – July 9, 1995.
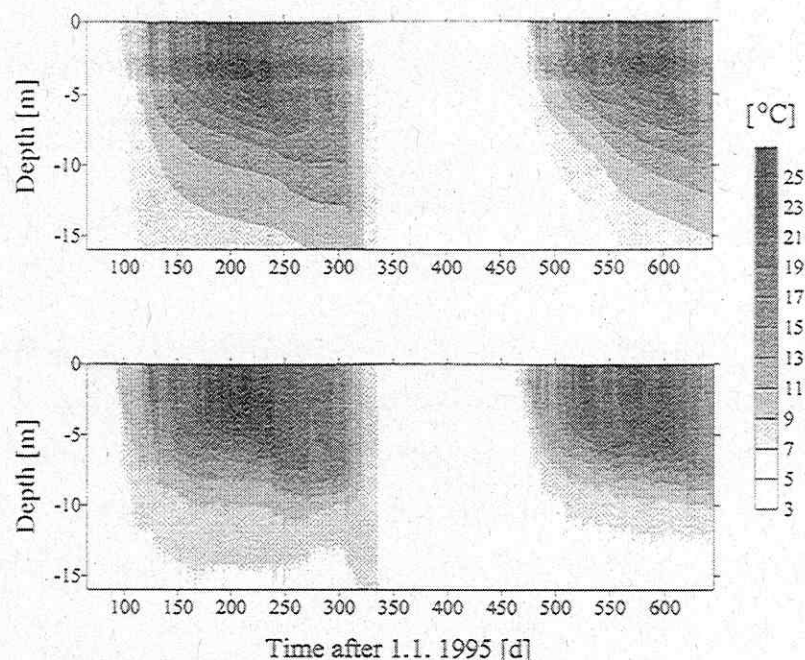
Figure 4: Simulated (upper) and measured (lower) temperature distribution in Lake Baldegg from March 1995 - October 1996.

References

Amorocho, J., and J.J. de Vries, A new evaluation of the wind stress coefficient over water surface, *J. Geophys. Res.*, *85*, 433-442, 1980.

Burchard, H., and H. Baumert, On the performance of a mixed-layer model based on the k-e turbulence model, *J. Geophys. Res.*, *100* (C5), 8523-8540, 1995.

Elliot, A.J., Measurements of the turbulence in an abyssal boundary layer, *J. Phys. Oceanogr.*, *14*, 1779-1786, 1984.

Gloor, M., A. Wüest, and D.M. Imboden, Dynamics of mixed bottom boundary layers in a stratified, natural water basin, *J. Geophys. Res.*, *submitted*, 1998.

Goudsmit, G.-H., F. Peeters, E. Gloor, and A. Wüest, Boundary versus internal mixing in stratified natural waters, *J. Geophys. Res.*, *102* (C13), 27903-27914, 1997.

Gregg, M.C., and T.B. Sanford, The dependence of turbulent dissipation on stratification in a diffusively stable thermocline, *J. Geophys. Res.*, *93* (C10), 12381-12392, 1988.

Kraus, E.B., and J.S. Turner, A one-dimensional model of the seasonal thermocline, *Tellus*, *19* (1), 98-105, 1967.

Powell, T., and A. Jassby, The estimation of vertical eddy diffusivities below the thermocline in lakes, *Water Resour. Res.*, *10* (2), 191-198, 1974.

Rodi, W., *Turbulence models and their application in hydrodynamics - a state of the art review*, Karlsruhe, 1984.

Wüest, A., D.C. Van Senden, J. Imberger, G. Piepke, and M. Gloor, Comparison of diapycnal diffusivities measured by tracer and microstructure techniques, *Dyn. Atmos. Oceans*, *24*, 27-39, 1996.

Numerical Studies of Lake Baikal Hydrodynamics

E.A.Tsvetova

Institute of Computational Mathematics and Mathematical Geophysics ,
Siberian Division of Russian Academy of Sciences, 630090,Novosibirsk

The construction of the numerical models of Lake Baikal hydrodynamics is fulfilled in the frames of a concept which consideres interactions in the system "lake - atmosphere of the region" for ecology and climate (Penenko, Tsvetova, 1998). Due to the concept interactions in a wide range are taken into account. In the atmospheric part a hemispheric model and a mezo-regional model are developed. The former is used as a background for the latter. The lake part includes some models of various complexity. A set of numerical models is used to investigate the main features of lake hydrodynamics. It includes 2D and 3D models for the whole lake and local zones. The most developed of them is a 3D multilevel, primitive equation, free surface, hydrostatic numerical model which is applied to the simulation of overall lake circulation. A scenario approach is involved to take into account climatic atmospheric data as an external forcing.

The atmospheric and lake parts are oriented to investigate problems of pollution. That is why the hydrodynamical models are supplemented by models of transport and dispersion of pollutants. In the atmospheric part the processes of chemical transformation are also taken into accountl (Penenko, Tsvetova et al.,1997). Previously the atmospheric and lake parts have been developing separately. And now a combined model is in progress.

From the mathematical point of view, the realization of all the models is based on the same principles: variational formulation , splitting technique, domain decomposition. The variational formulation gives an integral identity that cooperates the systems of equations with boundary and initial conditions. It is the base for all further constructions. Following some rules, we can derive numerical approximations of given properties and quality from it. The splitting technique is a well-known and widespread powerfull mean to solve complex problems. It allows to reduce an initial problem to the series of less complicated problems.

The present report is primarily concentrated on some results concerning the lake part of the system.

Non-hydrostatic model

The non-hydrostatic numerical model is specially developed for better understanding of deep lake physics. The focus is on convective processes and natural phenomena like thermal bar. This phenomenon occurs twice a year in the lakes of the temperate latitudes due to the anomalous behavior of fresh water density. It manifests itself as a dynamical front of temperature and density that separates the nearshore waters from the open lake. These two water masses posess different properties, especially in stability conditions. In the vicinity of the front the convergence and sinking of water may be observed. In deep lakes the thermal bar has some specific features because a decrease in the temperature of maximum density with increasing pressure or depth has essential influence on all processes in such lakes.

The statement of the problem is done under the assumption that all three components of vector velocity are included but the gradients of the state functions in y-direction are omitted. This assumption seems to be acceptable taking into account the fact that measurements display that the main changes are in the direction perpendicular to the front, and moreover, that characteristics in the parallel direction are sufficiently uniform. The system of equations has the form

$$\frac{du}{dt} - lv - kw = -\frac{1}{\rho}\frac{\partial p'}{\partial x} + \frac{\partial}{\partial z}v\frac{\partial v}{\partial z} + \frac{\partial}{\partial x}A\frac{\partial v}{\partial x},$$

$$\frac{dv}{dt} + lu = \frac{\partial}{\partial z}v\frac{\partial v}{\partial z} + \frac{\partial}{\partial x}A\frac{\partial v}{\partial x},$$

$$\frac{dw}{dt} + ku = -\frac{1}{\rho}\frac{\partial p'}{\partial z} + \frac{\partial}{\partial z}v\frac{\partial w}{\partial z} + \frac{\partial}{\partial x}A\frac{\partial w}{\partial x},$$

$$\frac{d\rho}{dt} + \frac{\partial\rho u}{\partial x} + \frac{\partial\rho w}{\partial z} = 0,$$

$$\frac{dT}{dt} - \gamma\frac{dp}{dt} = \frac{\partial}{\partial z}v_T\frac{\partial T}{\partial z} + \frac{\partial}{\partial x}\mu\frac{\partial T}{\partial x},$$

$$\rho = \rho(p, T, s_0).$$

The boundary and initial conditions are:

at z = 0: $\qquad p = p_a, \qquad w = -\frac{1}{g\rho}\frac{\partial p'}{\partial t},$

$$v\frac{\partial u}{\partial z} = -\frac{\tau_x}{\rho}, \qquad v\frac{\partial v}{\partial z} = -\frac{\tau_y}{\rho}, \qquad v_T\frac{\partial T}{\partial z} = -\frac{Q}{\rho c_p},$$

at z = H(x): $\qquad u = v = w = 0, \frac{\partial T}{\partial N} = 0,$

at the lateral boundaries: $u = v = w = 0, \dfrac{\partial T}{\partial N} = 0,$

at $t = 0$: $\qquad u = v = w = 0, \dfrac{\partial T}{\partial N} = 0.$

Here most of notations are common, except for a few ones: p' is the pressure deviations from hydrostatic values when system are at the given T_0 and s_0,

l and k are the components of the Coriolis force, γ is the adiabatic lapse rate, $\dfrac{\partial}{\partial N}$ is

the co-normal derivative, $\dfrac{\partial}{\partial N} = \mu \cos(n, x) \dfrac{\partial}{\partial x} + \nu_T \cos(n, z) \dfrac{\partial}{\partial z}$, n is the outer

normal vector to the boundary.

With the help of the described model a series of numerical experiments has been done for the simulation of thermal bar in conditions like those in Lake Baikal (Tsvetova 1995,1997,1998). The results show that the model reproduces the main features of the phenomenon. Due to the heat flux through the surface the front forms which gradually moves from the shore to the center of the domain. An intensive downwelling is in the convergence zone while upwellings occur near the far boundaries of convective cells.

Combined use of models and data of measurements

There are some ways to describe the natural processes. One is to collect and analyze the data of measurement. A second one is to design a mathematical model and make numerical experiments. It seems, a remarkable progress can be reached if we move along a third way: to combine data of measurement and modeling.

In our concept of lake-region system two possible procedures of the combined use of data and models are considered and realized. They are based on the methods of inverse modeling .The procedures are started with the construction of a quality functional which consists, at least, of two terms that define a measure of deviations of the computed values from the measured ones and the model errors. Then a minimum of the functional with respect to input parameters and the state functions is found out. In general case this optimization procedure can be realized by means of gradient-type methods using the sensitivity functions of quality functionals with respect to the variations of input data. For the calculation of the sensitivity functions the adjoint problems, that correspond to the choosen functionals, have to be solved. The adjoint problems and sensitivity functions give a possibility to realize direct links between the

variations of quality functionals and the variations of the parameters to be found. This technique is comparatively simple but it needs huge power of computers.

The second algorithm, that we propose, can be used as a mean for fast data assimilation. Unlike the first one, the local optimization of the quality functionals is done with respect to the current phase trajectory of the system. As for realization this procedure in combination with the splitting techniques is the most effective remedy at the present time.

Using this approach the philosophy of model verification, validation, calibration etc. should be changed. As a model and data take part in the process of solution simultaniously the errors of the model show the quality of the latter. From the other hand, the optimization procedure gives a minimum of the quality functional. And if this minimum has been reached but the residual of the model are greater than an admissible value, it is nesessary to revise the model. The optimization procedure allows to find the key parameters of the model which are responsible for the description of the process under investigation.

References

Penenko V.V., Tsvetova E.A. 1998. The Structure of a Model Set for the Investigation of Ineractions in the System "Lake Baikal - Atmosphere of the Region". Atmospheric and Ocean Optics, v.11, N 6

Penenko V.V., Tsvetova E.A. et al. 1997. Numerical Modeling of Chemical Kinetics and Transport of Pollutants in the Atmosphere of Industrial Regions. Chemistry for Sustainable Development, V.5, N5, pp. 505-510.

Tsvetova E.A. 1995. Convective Currents Associated with Thermal Bar in Lake Baikal. Proc. AMCA-95, NCC Publisher, pp.386-393.

Tsvetova E.A. 1997. Numerical Model of the Thermal Bar in Lake Baikal. Meteor. and Hydrol. N 9, pp.58-68.

Tsvetova E.A.1998. Enfluence of Coriolis Force on the Thermal Bar in a Deep Lake. J.Appl.Mech and Theor.Phys. V.39, N4, pp. 127-134.

Comparing two topography-following primitive equation models for lake circulation

L. Umlauf   Y. Wang   K. Hutter

Institut für Mechanik
TU Darmstadt
D-64289 Darmstadt

July 3, 1998

1   Introduction

A precise three-dimensional prediction of water quality is always based on a reliable turbulence closure and requires stability of the hydrodynamical model over a large range of horizontal and, in particular, vertical turbulent diffusivities. The most severe time step limitation arises from the vertical CFL criterion and may be overcome by the formulation of (semi-)implicit temporal integration procedures. However, there are still other effects discussed in this paper that are related to the small length scales of a lake that make it a difficult task to economically integrate the shallow water equations in a lake over several months.

In this paper we shall compare two such models and test their applicability to the calculation of the wind forced response of a lake or a reservoir. Both are based on SPEM by HAIDVOGEL ET AL. [4] and HEDSTROM [5] but have been slightly modified to suit the special conditions envisaged by us.

Model A is a semi-implicit generalized σ-coordinate model and employes a vertical finite difference technique (see SONG AND HAIDVOGEL [6]). It has been modified by GUETING [3], and a k-ϵ-closure has been added. However, here the specialities of turbulence closure will not be discussed.

Model B is the original semi-spectral σ-coordinate model (SPEM) that uses a vertical Chebyshev polynomial expansion. It has been modified by WANG AND HUTTER [7] to allow for a semi-implicit (vertical) time stepping of either Crank-Nicholson or backward Euler type. In the horizontal direction both models employ an identical centered FD discretization on a staggered Arakawa grid in connection with a conformal mapping of the irregular shoreline to a rectangle to achieve higher smoothness of the horizontal boundary conditions.

2   Model Formulation

Common numerical techniques for the solution of the shallow water equations employ a Cartesian coordinate system where the vertical grid size can be easily arranged to allow higher resolution in regions of strong gradients in the surface layer of a lake (epilimnion) and near the thermocline (metalimnion). However, in this approach the bottom topography has to be approximated by a series of steps which may lead to difficulty in applying the flux boundary conditions and also induces instability.

Since varying topography and sediment exchange processes play a crucial role in lake modelling we use a model with generalized vertical σ-coordinates ("s-coordinates") that follow the bathymetry and greatly simplify the computation and formulation of the flux boundary conditions. Through the s-coordinates a stretching factor H_θ and extra terms are introduced to the shallow water equations.

To sidestep the approximation of an irregular lateral lake boundary by a horizontally Cartesian grid and to avoid the interpolation of lateral boundary conditions to the numerical boundary both models

make use of a horizontal conformal mapping. The resulting curvilinear boundary-following coordinate system is able to provide a spatially variable horizontal grid resolution. We used a software-package developed by WILKIN AND HEDSTROM [8] for the generation of the two-dimensional orthogonal grid. For lakes that have a suitably smooth boundary this package provides the metric coeffcents m and n of the conformal mapping from an irregular lake shoreline to a rectangle.

Stability of the numerical models is strongly related to the diffusive terms, representing the divergence of the turbulent fluxes. The diffusive turbulent fluxes $\mathcal{F}_\varphi^i$ for heat and momentum have been formulated by gradient laws. They can be written in s-coordinates for a dummy variable φ (either u, v or T) as follows:

$$
\begin{aligned}
\mathcal{F}_\varphi^\xi &= D_H^{(\varphi)} m \left(\frac{\partial \varphi}{\partial \xi} - H_\theta \frac{\partial z}{\partial \xi} \frac{\partial \varphi}{\partial s} \right), \\
\mathcal{F}_\varphi^\eta &= D_H^{(\varphi)} n \left(\frac{\partial \varphi}{\partial \eta} - H_\theta \frac{\partial z}{\partial \eta} \frac{\partial \varphi}{\partial s} \right), \\
\mathcal{F}_\varphi^s &= -m \frac{\partial z}{\partial \xi} \mathcal{F}_\varphi^\xi - n \frac{\partial z}{\partial \eta} \mathcal{F}_\varphi^\eta + D_V^{(\varphi)} \frac{1}{H_\theta} \frac{\partial \varphi}{\partial s},
\end{aligned}
\tag{1}
$$

where D_H and D_V are the horizontal and vertical turbulent diffusivities, respectively, and ξ and η the (mapped) horizontal coordinates. In contrast to Cartesian models (see, e.g., CASULLI AND CATTANI [1]) in σ-type models always extra flux correction terms appear (in this case the second terms in the brackets of $(1)_1$ and $(1)_2$ and the first two terms in $(1)_3$). Without these extra terms and without coordinate transformation ($n = m = H_\theta = 1$) the traditional form of the fluxes in Cartesian coordinates may be discovered.

The vertical (s-) derivative of the third term in $(1)_3$ is the only one that is treated by an implicit time-stepping scheme in our models as to remove the most severe time step limitation. An implicit scheme on the vertical divergence of the additional flux correction terms could be performed only at extremely high costs since they involve mixed horizontal and vertical derivatives.

It is clear that in all σ-type models these terms, to which in this case only an explicit scheme is applied, will be an extra soure of numerical instability. We found that the maximum stable timestep in our model runs was reduced by a factor of three to five by the flux correction terms. However, in topographical coordinates the boundary conditions can be formulated in a smoother way compared to step-like Cartesian models. Therefore both models require only very little numerical smoothing and all types waves may be recognized without beeing damped immediately (see below).

Note that the linear system arrising from the implicit procedure leads to a tridiagonal, easily solvable matrix in model A (FD), but to a fully occupied matrix in model B (SP).

3 Accuracy, Stability and Performance

The convergence of each model and the difference between model A and B have been analyzed in terms of a rms-error. Since the horizontal discretizations in both cases are identical we introduced a local volume-weighted rms-error for each vertical column of N datapoints. Further, a global measure of error was introduced by defining a global rms-error as the area-weighted average over all L × M horizontal grid points.

We compared the convergence of both models by means of the global rms-error of the velocity fields. The values at the collocation points of model B have been interpolated to the collocation points of model A by Chebyshev polynomials, if necessary. We found that for a sufficiently high vertical resolution the local rms-error between both models could be made less than 1% at all points. This indicates that both models reliably solve the shallow water equations.

Fig. 1 (left) showes the convergence of both models with decreasing vertical grid spacing. According to the theory of spectral methods (see, e.g., GOTTLIEB AND ORSZAG [2]) model B exhibits an extremely fast convergence, whereas model A (with vertical centered finite differences) shows an approximately quadratic convergence.
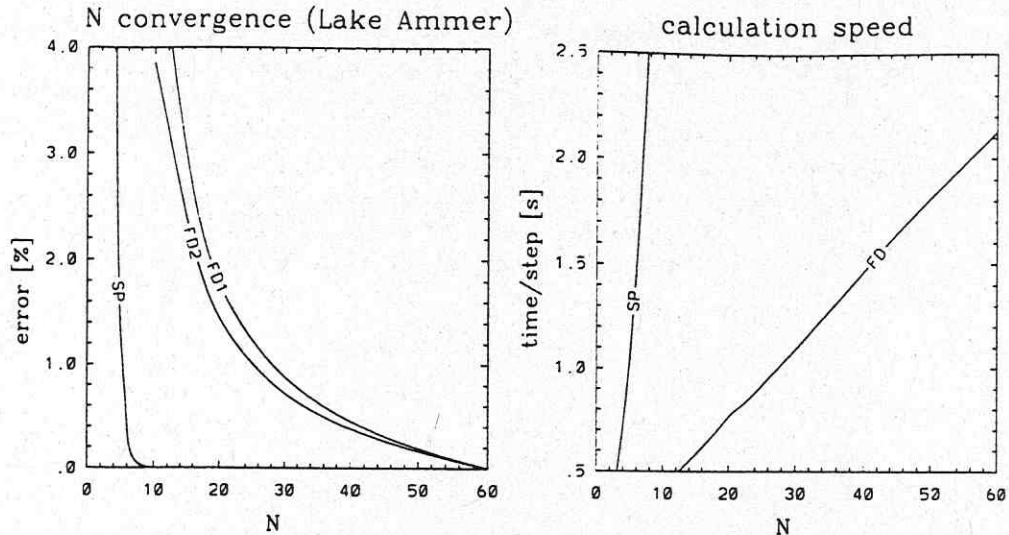
Figure 1: *Global rms-error of the velocity field with increasing number of vertical grid points N in Lake Ammer (left) for Model A (FD1: σ-coordinates; FD2: generalized σ-coordinates) and model B (SP). For the reference run (error ≡ 0%): N = 60 (FD), N = 20 (SP) and Δt=10s). The right panel shows the time required for one time step on a pentium computer.*

The right panel of Fig. 1, however, reveals a great disadvantage of the spectral model: As mentioned above, for each implicit time step, in general, a fully occupied matrix must be inverted leading to an integration time that grows quadratic with increasing grid resolution N, whereas in the FD-model only a tridiagonal matrix has to be inverted. For a moderate global error of 1% (N=6 SP, N=30 FD) the integration CPU-time for one time step was 1.1s for the FD-model and 1.5s for the spectral model. The actual calculation time for a particular simulation, however, depends on both the intergration time for one time step and the maximum time step size. With a maximum stable time step for Lake Ammer of 90s for model A (FD) and 190s for model B (SP) the actual calculation time for the spectral model is smaller by a factor of ≈ 1.5. We want to point out that this is only a rhough estimate that depends on a number of factors like smallest gridsize, error requirements, machine architecture and solver.

It may seem from the above that the spectral model B is slightly superior in view of stability and accuracy. However, we found that the Chebyshev polynomials show high sensitivity to large gradients in the thermocline leading to negative diffusivities in the k-ε-model and thus violating the entropy inequality (see GUETING [3]). This seems to be a crucial disadvantage of the spectral model from a practical point of view.

4 Results

Concluding we very briefly discuss the response of Lake Ammer to a Heavyside wind force from South with a typical Summer temperature stratification. We used sinusoidal diffusivities in the epilimnion and small constant diffusivities in the meta- and hypolimnion.

Fig. 2 (left) shows the longshore velocity at the mid points of the western shore as a function of time. From the graph one of the two main types of waves may be identified: The "seiching" with the first baroclinic mode of a period of $T_k \approx 25h$ is caused by a superposition of two Kelvin-type waves circulating counterclockwise around the basin.

Evidence of the second, Poincaré-type waves, can be found in the whole basin. The right panel of Fig. 2 shows an oscillation in the transverse component of the velocity with a period $T_p \approx 3.75h$ in the middle of the lake that may be interpreted as a standing Poincaré-type wave. This oscillation can be found at almost all points of the basin. After three days the hypolimnetic oscillation has almost come to an end and the thermocline must have tilted sufficiently to set up a hydrostatic pressure gradient,
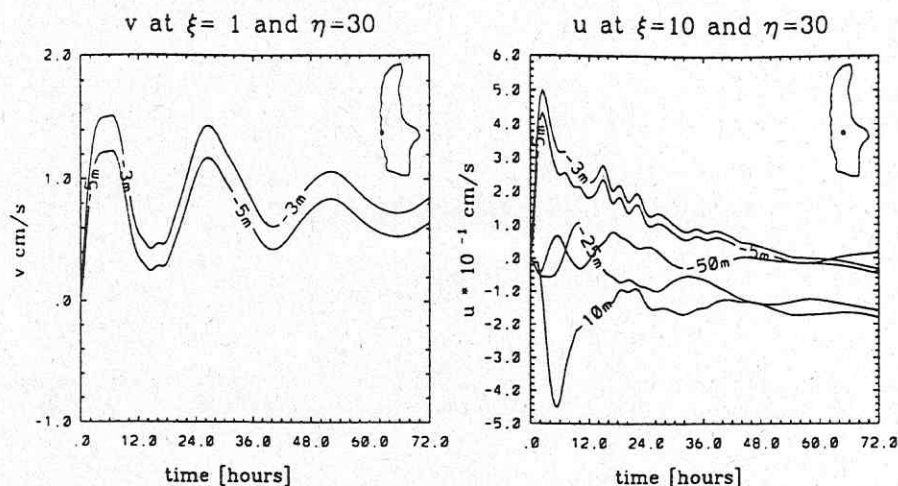
Figure 2: *The longshore component of the velocity (top) at the western and eastern shore at the depth levels of 3m and 5m. The bottom panels show the velocity in the middle of the lake at the depth levels of 3m, 5m, 10m, 25m and 50m. Position labels are shown in the upper right corner of the plots.*
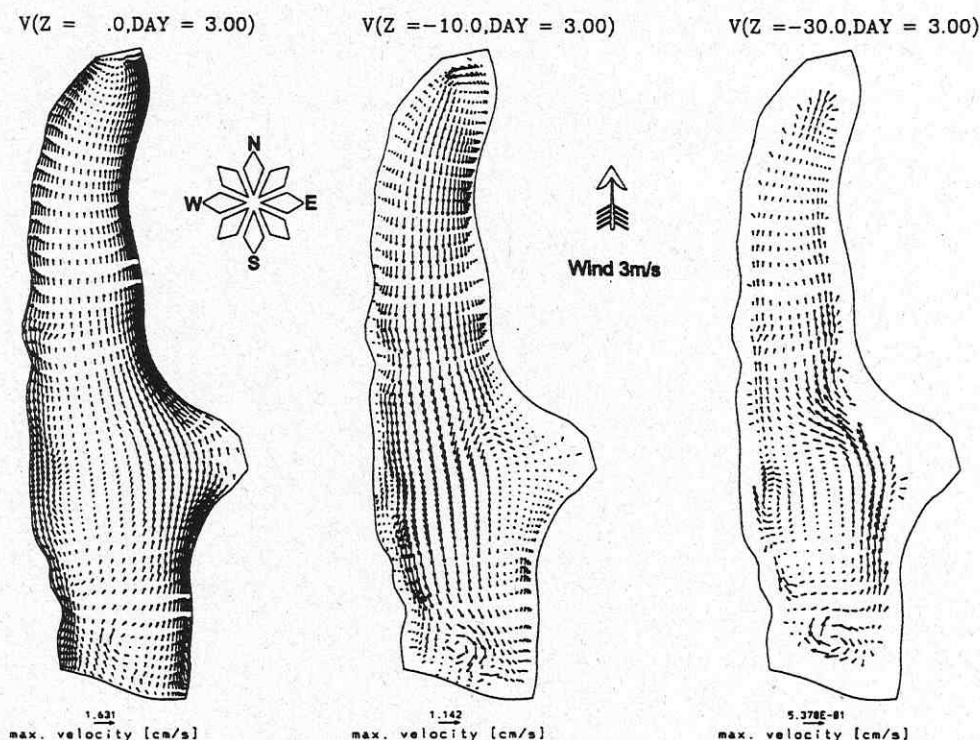
Figure 3: *Currents after three days of baroclinic simulation in L. Ammer at depth levels of 0m, 10m and 30m (form left to right)*

which just balances the surface stress. At this stage of motion the hypolimnion does not counter the surface flow any longer by a motion in the reverse direction. Thus the motion changes from a whole basin circulation to two closed vertical gyres, one each in the hypolimnion and the epilimnion, and the counter flow occurs in the metalimnion as displayed in Fig. 3.

References

[1] V. Casulli and E. Cattani. Stability, accuracy and efficiency of a semi-implicit method for three-dimensional shallow water flow. *Computers Math. Applic.*, 27(4):99–112, 1994.

[2] D. Gottlieb and S. A. Orszag. *Numerical analysis of spectral methods: Theory and applications.* Society for Industrial and Applied Mathematics, 1977.

[3] P. Güting. *Dreidimensionale Berechnung windgetriebener Strömungen mit einem k-ε Modell in idealisierten Becken und im Bodensee.* PhD thesis, University of Technology at Darmstadt, FB6, 1998.

[4] D. Haidvogel, J. Wilkin, and R. Young. A semi-spectral primitive equation ocean circulation model using vertical sigma and orthogonal curvilinear horizontal coordinates. *J. Comp. Phys.*, 94:151–184, 1991.

[5] K. S. Hedstrom. User's manual for a semi-spectral primitive equation regional ocean-circulation model. Technical Report SR-1, Institute for Naval Oceanography, July 1990.

[6] Y. Song and D. Haidvogel. A semi-implicit ocean circulation model using a generalized topography-following coordintate system. *J. Comp. Phys.*, 115:228–244, 1994.

[7] Y. Wang and K. Hutter. A semi-implicit semispectral primitive equation model for lake circulation and its stability performance. *J. Comp. Phys.*, 139:209–241, 1998.

[8] J. Wilkin and K. Hedstrom. *User's manual for an orthogonal curvilinear grid-generation package.* Institute for naval Oeanography, 1991.

Density measurements in mining lakes

M. Schimmele

UFZ Centre for Environmental Research, Brückstr. 3a, D-39114 Magdeburg

Introduction

Post mining pit lakes vary in their contents of dissolved substances (Schultze & Geller 1996, Schimmele 1995a). Especially the strongly acidified lakes (pH < 3) show high concentrations of sulphate and iron (Friese et al. 1998). The chemical composition influences the measurement of some properties, e.g. electrical conductivity (Schimmele 1998), in these waters. Furthermore it affects directly the density structure and the light climate and therefore the stratification, the biological development, and the formation of oxic/anoxic layers (Schimmele 1995b). This paper deals with the influence of dissolved substances on density in mining lakes. Particles and especially the internal production of particles are not considered.

Methods

Water samples were taken at various depths and at various seasons and transported to the laboratory cool and dark. Samples, where reaction with air could change conductivity or density, respectively, were treated under Argon – atmosphere. For density measurements 7 ml of the samples were injected in an temperature - controlled u-tube-oscillator (Anton Paar, Graz, Austria) by a syringe. Oscillation frequencies were determined at least 5 times and averaged. Due to outgassing at higher temperatures and particles in the samples, which disturb the measurement, relative uncertainties were usually about $2 \cdot 10^{-5}$ - $5 \cdot 10^{-5}$ (instead of $2 \cdot 10^{-6}$ for clear water) with higher values at higher temperatures. The uncertainties of el. conductivity $\kappa 25$ stem mainly from the temperature correction and are about 1% or less (see Schimmele 1998). The contribution of gases to density in air saturated samples is in the order of $3 \cdot 10^{-6}$ (Millero & Emmet 1976). Therefore in this case the major effect of outgassing of surface samples is the disturbance of the measurement itself. Chemical analysis are described in Herzsprung et al. (1998) and Friese et al. (1998).

Results and discussion

Figure 1 shows the relation between el. conductivity $\kappa 25$ and density at 5°C together with calculations from temperature and el. conductivity after Bührer & Ambühl (1975) for fresh water and Fofonoff & Millard (1983) for seawater. It can be seen that these relations do not hold for mining lakes. In most cases, measured densities are higher than calculated.
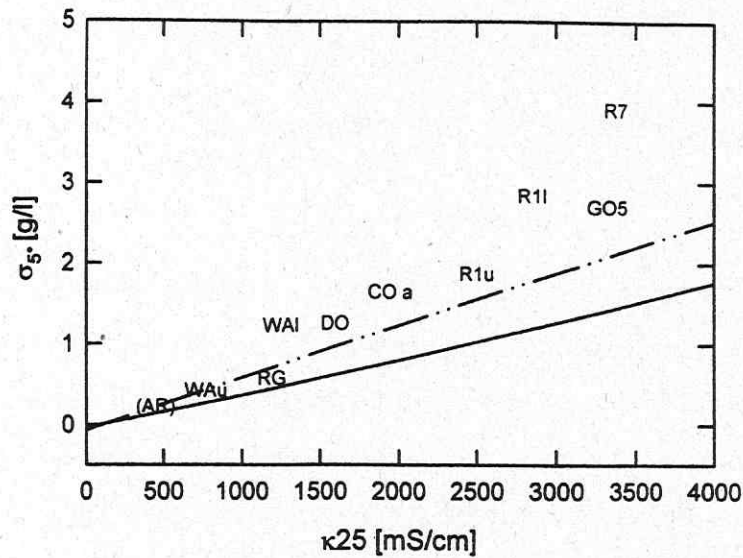
Fig 1: Relation between el. conductivity κ25 and density at 5°C (σ_T = density – 1000 kg·m^{-3}) for samples from various lakes: COa = Cospuden, DO = Döbern, GO5 = Niemegk, R1l = ML111 monimolimnion, R1u = ML111 surface, R7 = ML107, RG = ML117, Wal = Waldsee monimolimnion, Wau = Waldsee surface, (AR) = Arendsee (natural, not a mining lake) and relation according to Bührer & Ambühl (1975; solid line) and Fofonoff & Millard (1983; dash - dotted line). (from Schimmele & Herzsprung 1999)

This may have two reasons. Firstly el. conductivity is not a good estimator for dissolved substances because there is a relative high amount of neutral substances and/or chemical composition changes due to internal processes (see Schimmele & Herzsprung 1999).

Even using the Chen & Millero (1986) formula with input – salinities equal to the sum of measured concentrations of the main constituents yields densities lower than measured (see figure 2; please note, that most of the shown salinities are beyond the upper limit of validity of the Chen & Millero formula of S=0.6).

A look on partial molal volumes helps to estimate the influence of the composition of dissolved substances to density.

The partial molal volume is the change of volume V upon the addition of one mole of electrolyte i to a large reservoir at constant temperature T, pressure p, and moles of the other

components n_j: $\overline{V}_i^0 = \left(\dfrac{\partial V}{\partial n_j} \right)_{T,p,n_{j \neq i}}$. In table 1, conventional partial molal volumes $\overline{V}_{conv}^0$

at infinite dilution at 25°C (Millero 1972) are listed, where $\overline{V}_i^0 = \overline{V}_{conv}^0 + z\overline{V}_{H^+}^0$ for cations and

$\overline{V}_i^0 = \overline{V}_{conv}^0 - z\overline{V}_{H^+}^0$ for anions. The estimates for the absolute partial volume of the proton

$\overline{V}_{H^+}^0$ are varying from -0.9 cm^{3}mol^{-1} to -7.6 cm^{3}mol^{-1} (Millero 1972). Zana & Yeager (1966, 1967, cited by Millero 1972) determined it experimentally to –5.4 ± 2 cm^{3}mol^{-1} at 25°C.
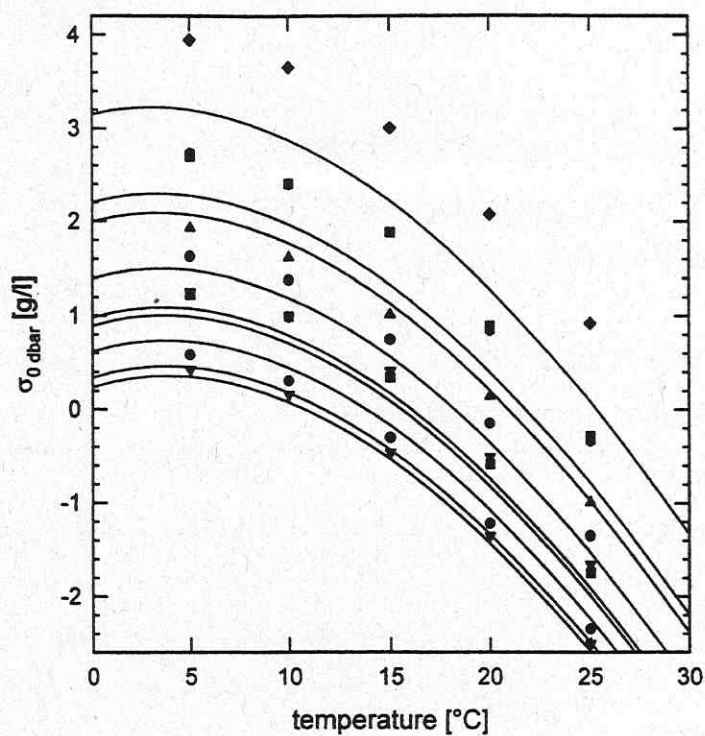
Fig. 2: Measured densities (σ= density – 1000 kg·m^{-3}) for samples from different mining lakes with corresponding calculated densities after Chen & Millero (1972).

Table 1: Conventional partial molal volumes $\overline{V}^0_{conv}$ at infinite dilution at 25°C (Millero 1972)

Ion	$\overline{V}^0_{conv}$ [cm^{3}mol^{-1}]	Ion	$\overline{V}^0_{conv}$ [cm^{3}mol^{-1}]
H$^+$	0	HCO$_3^-$	23.4
Na$^+$	-1.21	Cl$^-$	17.83
K$^+$	9.02	CO$_3^{2-}$	-4.3
Mg^{2+}	-21.17	SO$_4^{2-}$	13.98
Ca^{2+}	-17.85		
Fe^{2+}	-24.7		
Al^{3+}	-42.2		
Fe^{3+}	-43.7		

For diluted solutions additivity is valid and the relative change in density then is given by

$$\frac{\Delta\rho}{\rho} = -\sum_j \overline{V}_i^0 m_j + \frac{1}{\rho}\sum_j m_j M_j \quad,\text{ where } m_j = \frac{n_j}{V} \text{ is the molarity and } M_j \text{ the molar weight. The}$$

first term represents the change of volume and the second represents the increase of density due to the additional mass.

The relative changes in density were calculated for different "typical" mixtures with the values from table 1 and are listed in table 2.

Table 2: Density differences about addition of 1g salt / 1kg water (1 $^0/_{00}$) for different mixtures (under assumption of infinite dilution)

	Ion	Relation	$\frac{\Delta\rho}{\rho} * 10^3$
"seawater"	Na^+	1	0.72
	Cl^-	1	
"lake"	Ca^{2+}	1	0.82
	HCO_3^-	2	
"mining lake"	SO_4^{2-}	13	1.05
	Ca^{2+}	10	
	Fe^{3+}	2	

It can be seen that for the same salinity and different compositions the density change varies widely. The density difference in the above example lies in the same order of magnitude as epi / hypolimnion differences in spring and autumn stratifications of temperate lakes. Furthermore, the molal volumes of the various substances have different temperature dependencies. In figure 3, density measurements from a sample from highly acidic mining lake ML107 (pH ~ 2.3) are drawn at 5 temperatures. In this figure the temperature dependence of pure water (with an additional offset of 4 g/l) and the outcome of the Chen & Millero (1986) formula with a salinity of S=5.0 are added. It can be seen that the true temperature dependence of that specific sample lies in between the both estimates. Especially in acidic mining lakes, the chemistry is mostly dominated by three species: Ca^{2+}, SO_4^{2-} and Fe^{3+}. Therefore it may be possible to construct equations of state, which hold for groups of mining lakes with only few adjustments.

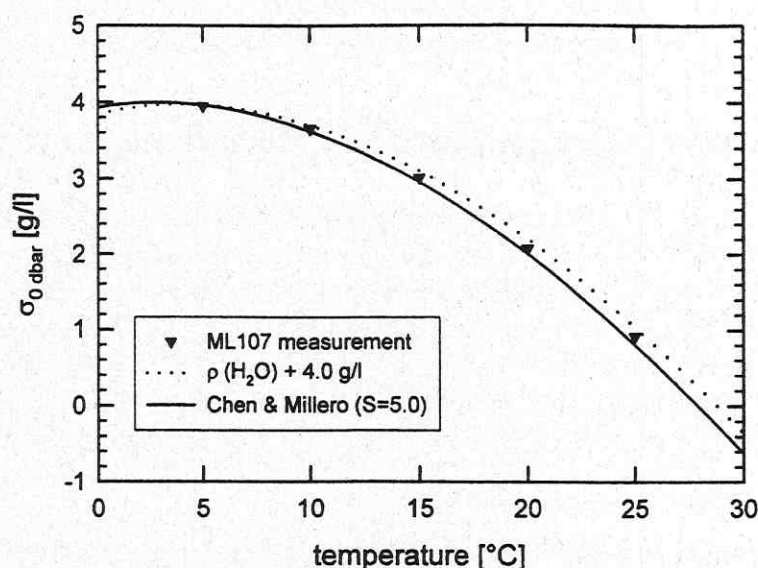*Fig. 3:* Measured densities (σ= density – 1000 kg·m^{-3}) for a sample from lake ML107 at various temperatures compared to Chen & Millero (1986) formula with salinity of S=5.0 and pure water with an offset of 4.0 g/l .

References

BÜHRER, H. & AMBÜHL, H., 1975: Die Einleitung von gereinigtem Abwasser in Seen. Schweiz. Z. Hydrol. 37(2): 347-369.

CHEN ,C.T. & MILLERO, F., 1986: Precise thermodynamic properties for natural waters covering only the limnological range. Limnol. Oceanogr. 31(3): 657-662

FOFONOFF, N. P. & MILLARD JR., R.C., 1983: Algorithms for computation of fundamental properties of seawater. UNESCO technical papers in marine science 44, 53pp.

FRIESE, K., HUPFER, M., SCHULTZE, M., 1998: Chemical Characteristics of Water and Sediment. In Acid Mining Lakes of the Lusatian Lignite District. In: Geller, W., Klapper, H., Salomons, W. (Eds.) Acidic mining lakes. Springer Verlag, Berlin, 1998.

HERZSPRUNG, P., FRIESE, K., PACKROFF, G., SCHIMMELE, M., WENDT-POTTHOFF, K., WINKLER, M., 1998: Vertical and Annual Distribution of Ferric and Ferrous Iron in Acidic Mining Lakes. Acta Hydrochim. Hydrobiol. 26 (1998) 5.

MILLERO, F.J., & EMMET, R.T., 1976: The effect of dissolved air and natural isotopic distributions on the density of water. J. mar. Res. 34: 15-24.

MILLERO, 1972: The Partial Molal Volumes of Electrolytes in Aqueous Solutions. In: Horne, R.A. (ed.): Water and Aqueous Solutions, pp 519-564. Wiley, New York.

SCHULTZE, M. & GELLER, W., 1996: The Acid lakes of Lignite Mining District of the former German Democratic Republic. In: R. Reuther (ed.): Geochemical Approaches to Environmental Engineering of Metals. Springer Verlag 1996.

SCHIMMELE, M., 1995a: Zur Schichtungsproblematik in Braunkohlerestseen. DGL Erweiterte Zusammenfassungen der Jahrestagung 1994 in Hamburg: 749-753, Deutsche Gesellschaft für Limnologie, Krefeld, 1995.

SCHIMMELE, M., 1995b: Beeinflussung des Schichtungsaufbaus eines Abgrabungssees durch Wind, Lufttemperatur und Strahlung. In: Geller, W., Packroff, G. (Hrsg.): Abgrabungsseen - Risiken und Chancen. Limnologie aktuell Vol. 7 , S. 91-98. Gustav Fischer Verlag.

SCHIMMELE, M., 1998: Die Messung der elektrischen Leitfähigkeit in Bergbaurestseen. Erweiterte Zusammenfassungen DGL Jahrestagung, Frankfurt a.M., 22. - 26. September 1997: 769-773. Deutsche Gesellschaft für Limnologie, Krefeld 1998.

SCHIMMELE, M. & HERZSPRUNG, P., 1999: Limnology of sulfur acidic lignite mining lakes. I. Physical properties: Influence of dissolved substances on el. conductivity and the density structure. Verh. Int. Verein Limnol. (submitted)

ZANA, R. & Yeager, E. (a) 1966: J. Phys. Chem. 70, 954; (b) 1967a: J. Phys. Chem. 71,521; (c) 1967b: J. Phys. Chem. 71, 4241.

Thermodynamic properties of sea-water and sea-ice

Rainer Feistel

Institut für Ostseeforschung, Warnemünde

Thermodynamic properties of sea-water like density or heat capacity can be expressed mathematically as functions of three independent variables. In practical oceanography these variables are pressure p, temperature t, and salinity S, which can be measured in-situ by e.g. common underwater probes („CTD"). Intense physico-chemical investigations, mainly in the 70s, led to an internationally accepted standard on seawater properties, documented in the *International Oceanographic Tables Vol.4* (IOT-4, Unesco,1987, 1991). This document describes the shape of basically three different quantities – density, heat capacity, and sound speed of sea-water – in the range of oceanographic interest (-2 to 40°C, 0 to 100 MPa, 0 to 4%) to a high degree of accuracy (4 g/m³ in density, 0.6 m/s in sound speed, 0.5 J/kgK in specific heat).

A closer view onto these so-called Unesco-formulas reveals a number of weaknesses. The three different functions are not fully consistent with each other, as thermodynamic cross-relations show. They are incomplete in the sense that they do not suffice to compute thermochemical properties like entropy, enthalpy, chemical potential, dilution heat, or freezing points. They are not very reliable to compute maximum density points of seawater (deviations up to some 0.1 K), and they deviate systematically about 0.5 m/s from best known sound speed measurements.

To improve the basis for studies of energetic and irreversible processes in the water the Unesco formulas have been unified using additionally available data, like dilution heats, melting points, temperatures of maximum density, del-Grosso-74 sound speeds etc. As a result the thermodynamic potential function G(S,t,p) - Specific Free Enthalpy or Gibbs Potential – was expressed as a polynomial in pressure and temperature and as an 'almost-polynomial" in the square root of salinity. The latter structure is predicted by theory: in the case of very low salinity dilute electrolytes obey the so-called Debye-Hückel limiting laws. Altogether, 87 double precision coefficients needed to be determined, including four of them specified by an arbitrary choice of reference states.

Many oceanic processes can be assumed to be adiabatic, i.e. they are running without exchange of heat with their environment. For their description, entropy σ is the most suitable independent variable, substituting temperature as thermal property. Due to thermodynamic rules, enthalpy H(S,σ,p) is then required as mathematical potential function. Based on an explicit formulation of H the computation of quantities like adiabatic compressibility, lapse rate, sound speed, potential temperature and potential density becomes essentially simplified. Energy conservation in ocean currents is expressed in terms of enthalpy as well (Bernoulli function).

The knowledge of ice properties is much less complete and precise than that of water. History-dependent crystal structures and aging processes make accurate measurements of ice properties more difficult. There are only few recent studies; most results have been obtained in the first half of the century. A number of ice properties has been selected from a review of Yen et al.(1981, 1991) and assembled to form a Gibbs potential G(t,p) of ice, valid in the vicinity of the freezing point (up to about –10°C and 10 MPa), a polynomial with 9 derived coefficients.

Sea-ice is a mixture of solid water and liquid sea-water, called brine, in phase equilibrium. Instead of a sharp freezing point it has a phase transition range, instead of diverging heat capacity and compressibility at the first order phase transition point it exhibits exceptional large values. Below about -8.2°C the brine becomes saturated and precipitation sets in. For sea-water properties are known only up to 4% salinity of brine, sea-ice can be described here only above –3°C. Due to the equilibrium condition (equal chemical potentials of water in ice and brine) the Gibbs potential function G(s,t,p) turns out to be a merely linear function in sea-ice salinity s.

In regions effectively separated from the global oceans, like the Baltic, the Red or the Bering Sea, or in fully enclosed basins like Lake Qarun, Egypt, the chemical composition of sea salt may become modified by e.g. evaporation or river discharge processes. Because of the unknown conductivity of these mixtures, salinity determination by usual conductivity measurements becomes uncertain, and so do all quantities derived from the triple (S,t,p). Typically, these deviations cause density errors of some 10 g/m³. Most thermodynamic properties are entirely unknown for sea salt mixtures different from standard composition. However, for a number of mechanical (PVT) properties the so-called Absolute-Salinity Rule proved to be a good approximation tool. Additional directly measured quantities like sound speed or refractive index, which could help to overcome such difficulties, have not yet been made sufficiently reliable by now.

Literature:

Yen, Y.C., 1981: Review of thermal properties of snow, ice and sea ice. USA Cold Regions Research and Engineering Laboratory, CRREL Report 81-10, Hanover, New Hampshire

Unesco, 1987: International oceanographic tables, Vol.4. Unesco technical papers in marine science 40, Unesco

Unesco, 1991: Processing of oceanographic station data. Unesco

Yen, Y.C., Cheng, K.C., Fukusako, S., 1991: Review of intrinsic thermophysical properties of snow, ice, sea ice, and frost. In: J.P. Zarling and S.L. Faussett (Eds), Proceedings 3rd International Symposium on Cold Regions Heat Transfer, Fairbanks, Alaska, 187-218

Feistel, R., 1993: Equilibrium thermodynamics of seawater revisited. Progress in Oceanography, 31, 101-179

Feistel, R., Hagen, E.1995: On the Gibbs thermodynamic potential of seawater. Progress in Oceanography 36, 249-327

Feistel, R. 1998: On the Physical Chemistry of Seawater with Deviating Ion Composition. Zeitschrift für Physikalische Chemie 204, 27-44

Feistel, R., Hagen, E., 1998: A Gibbs Thermodynamic Potential of Sea Ice. Cold Regions Science and Technology (in press)

Thermophysical properties of lake sediments, water-sediments heat interaction and thermal cycling in moderate lake

Sergei V.Ryanzhin

Limnology Institute, The Russian Academy of Sciences, Sevastyanova 9, St.Petersburg, 196199 RF, Phone 7 812 2948020, 298 7327, Fax 7 812 E-mail: ryanzhin@lake.spb.su

General approach. Temporal variations of heat flux $F(t,H)$ at lake water-sediments boundary considerably contributes a heat storage E_w and an annual heat budget b_w of moderate shallow lakes and lake sites. However, the problems of the heat interaction remain poorly studied so far. Variations of heat storage of water-sediments system can be described in a frame of 1-D Fourier problem as

$$\frac{\partial}{\partial t} E_w(t) = F(t,0) - F(t,H), \text{ lake water at } 0 \leq z \leq H, \tag{1}$$

$$\frac{\partial}{\partial t} E_b(t) = F(t,H) - F(D), \text{ sediments at } H \leq z \leq D, \tag{2}$$

where z is downward directed axis with $z=0$ at lake surface; E_b is a heat storage in sediments; H is a lake depth; $D=(2k_b/\omega)^{1/2}$ is wavelength of temperature harmonic with ω-frequency in sediments characterised by thermal diffusivity k_b and volumetric heat capacity $c_b\rho_b$; $F(D)=-c_b\rho_b k_b G$ is steady-state geothermal flux with geothermal gradient G at $z=D$. Kinematic form of a heat flux F^* is related with buoyancy flux as $B=\alpha g F^*$.

Effects of geothermal flux. To evaluate geothermal effects on lake heat budget and to calculate global average estimates 202 and 446 probing of G and $F(D)$ obtained from 78 European, American, Asian and African lakes have been compiled and processed in [12]. The review of recent relevant measurements has been given in [13]. It was shown that G varies from $0.009 K \cdot m^{-1}$ in L.Nyasa (Malawi), to $0.28 K \cdot m^{-1}$ in L.Windermeer, England, giving the global avg $0.9(\pm 0.05) K \cdot m^{-1}$. In turn, $F(D)$ ranges from $-6.28 \cdot 10^{-3} W \cdot m^{-2}$ in L.Malawi, to $-3.12 \cdot 10^{-1} W \cdot m^{-2}$ in L.Baikal, yielding the global avg $-7.45(\pm 4.31) \cdot 10^{-2} W \cdot m^{-2}$ that is close to the global avg terrestrial value. It should be stressed, that only absorbed radiation term and $F(D)$ always tend to a lake heating in a year cycle. Thus, in spite of its small value, the contribution of $F(D)$ into lake heating increases with a decrease of absorbed insolation. Particularly, $F(D)$ considerably contributes to a heat budget of, e.g. cold amictic (perennially ice-covered) lakes [12, 13].

Seasonal cycling at air-water and water-sediments boundaries. Expressions (1) and (2) are used to calculate annual variations of heat flux at air-water and water-sediments boundaries, heat storage and budget of water and sediments through time sequences of vertical temperature profiles obtained in a lake and sediments. Similar data have been received for freezing dimictic

L.Mendota, Stewart's Dark L., L.Tub, Wisconsin [1, 6-8], L.Beloye, Russia [11], Tver and Karelian lakes [5], L.Velen, Sweden [15], L.Kubenskoye, Lacha and Vozhe, NW Russia [4], etc.

The unique 20-year long term water temperature profile measurements at the deepest site (10m) of dimictic freezing Lake Punnus-Jarvi, 60.6°N, 29.7°E, Karelia, NW Russia, accompanied by 13-year vertical sediments temperature profile measurements (3m-layer of sediments) have been carried out [13, 14]. It was shown, that seasonal thermal variations in water-sediments system satisfactorily described both by expressions (1) and (2) and by solutions of 1-D Fourier problem. Particularly, seasonal variations of heat storage in lake water are shifted by 1/8 (1.5 month) and 1/4 (3 month) period with respect to those of surface temperature and surface heat flux. Similar shifts are clearly seen for seasonal variations of heat storage in sediments and rhose of temperature and heat flux at water-

Fig.1. Seasonal temperature course and thermal cycling at air-water and water-sediments boundaries of moderate dimictic lake. Derived from 13-year long-term temperature data on Karelian Lake Punnus-Jarvi (ozero Krasnoye), lake maximum depth 10m, modified from (Ryanzhin, 1997)
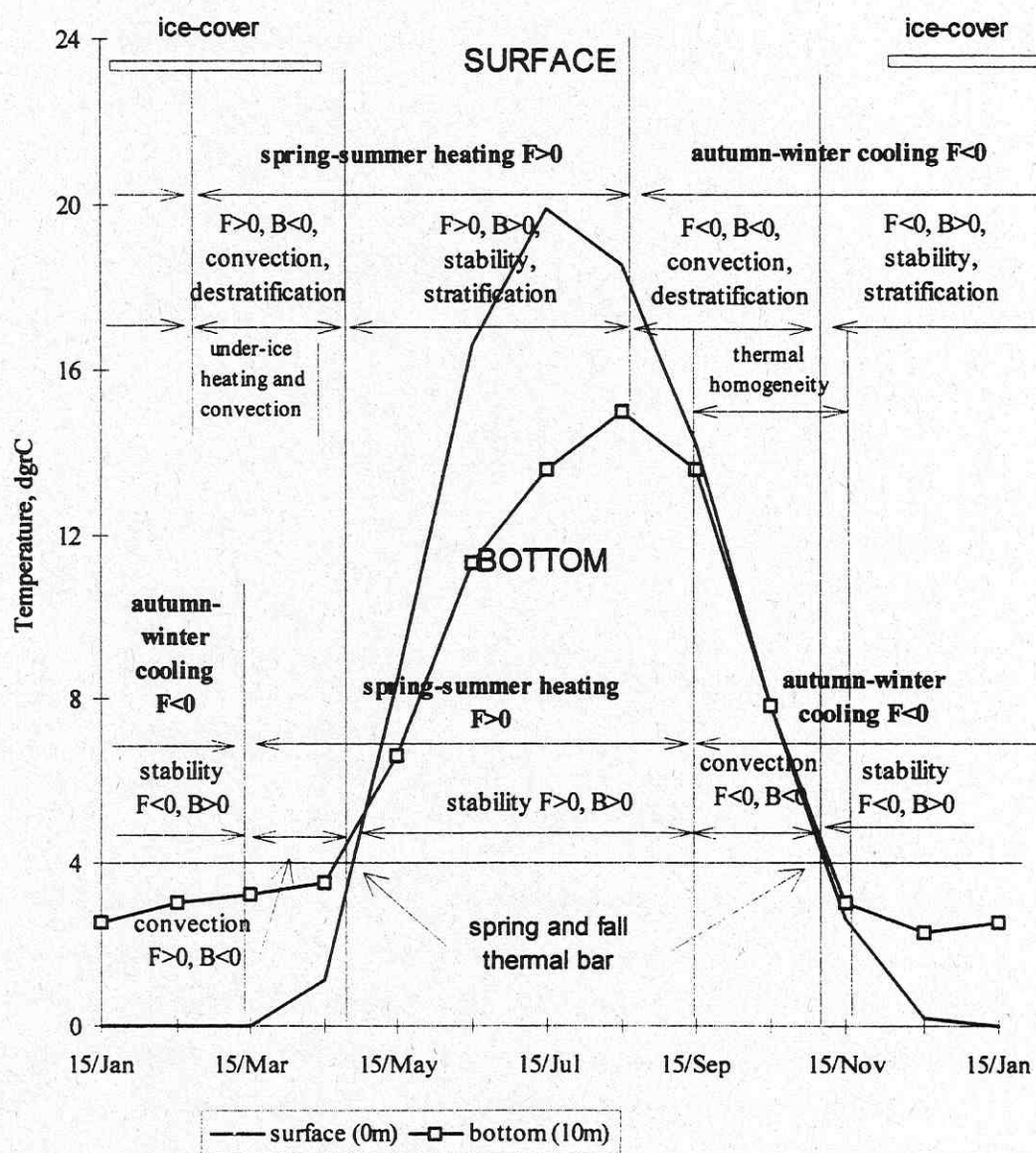
-sediments boundary. Thus, the following seasonal cycling at air-water and water-sediments boundaries both consisting of time interval of the *spring--summer heating* (SSH) at $F > 0$ and *autumn-winter cooling* (AWC) at $F < 0$, as well as induced thermal regimes of con-vection and stratification could be concluded from the analysis of the above data [13] (Fig. 1).

SSH and AWC each consists of two intervals characterised with negative and positive buoyancy flux, $B = agF < 0, > 0$, denoted here as − and + (e.g. SSH−, SSH+). At water-air boundary SSH− (spring heating, $F > 0$, $B < 0$) characterised by convection begins at minimal Ew and is completed at 4°C (spring thermal bar). Usually SSH− starts already in ice-covered lake due to the under-ice penetration of insolation. Then SSH+ (summer heating, $F > 0$, $B > 0$)

Fig. 2. Lake sediments to water heat budget ratio for seasonal variations depending on Fourier heat number Fo. The curve corresponds to the expression (5). Field data are taken or recalculated from the cited publication.

Fo=k/wH^2 -Fuorier number
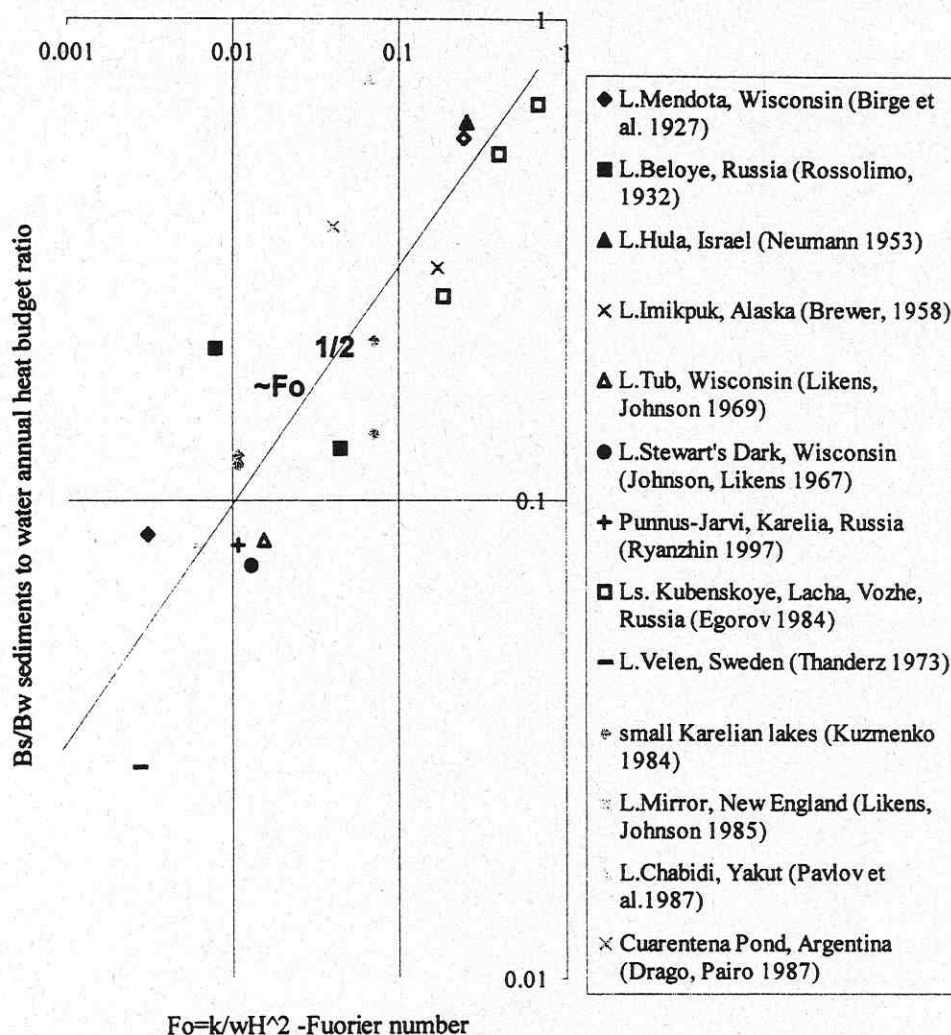
characterised by stratification takes place and finishes at maximum E_w when AWC− (autumn cooling, $F < 0$, $B < 0$) begins. The latter characterised by convection is completed at 4°C (fall thermal bar). Next, AWC+ (winter cooling, $F < 0$, $B > 0$) characterised by stratification develops till the reaching of the minimum E_w. Although, the above sequences of events are well known, notice that in contrast to annual variations of F, value of B reveals semi-annual variability. It should be stressed, that the similar behaviour is revealed at lake water-sediments boundary

$F>0$, $B<0$) and SSH+ (summer heating, $F>0$, $B>0$). In turn, AWC consists of AWC- (autumn cooling, $F<0$, $B<0$) and AWC+ (winter cooling, $F<0$, $B>0$). However, the intervals SSH-, and AWC- both at negative buoyancy flux at sediments boundary $B<0$, should be of especial interest. Negative buoyancy induces gravity convection from sediments towards lake water that seems releases nutrient, contaminants, etc. Long-term data on Punnus-Jarvi for SSH-, and AWC- give 1 month (April-May), $F(H)\sim3.1\text{W}\cdot\text{m}^2$, $B(H)\sim-2\cdot10^{-3}\text{cm}^2\cdot\text{sec}^{-3}$, and 1.5-2 month (September-November), $F(H)\sim -8.6\text{W}\cdot\text{m}^2$, $B(H)\sim-0.11\text{cm}^2\cdot\text{sec}^{-3}$, respectively. Similar intervals have been found and calculated in [13] from the field data obtained from L.Mendota [1], and L.Velen [15].

Heat budget of lake water and sediments. Heat budget of lake water and sediments and their ratio can be derived from the simplest temperature -wave solutions of 1-D-heat conductivity equation under certain assumptions and simplifications. Assume $A(0)$, $A(H))$ to be amplitude of temperature harmonic with frequency ω at air-water and water sediments boundary. Then, kinematic heat budget of water and sediments can be estimated as

$$b_w^* = 2A(0)\cdot H, \ b_b^* = 2A(H)\cdot(k_b/\omega)^{1/2}. \tag{3}$$

Then a combination of budgets (3) yields for sediments to water heat budget ratio

$$\frac{b_b}{b_w} = C_1 \frac{A(H)}{A(0)} Fo^{1/2}, \tag{4}$$

where $C_1 = c_b\rho_b/c_w\rho_w$; $c_w\rho_w$ is volumetric heat capacity of freshwater; $Fo = k_b/H^2\omega$ is analogy of Fourier heat number for sediments. Since under the natural conditions $c_b\rho_b$ ranges from ~0.50 cal/$^\circ$C cm^3=2.09 MJ/K m^3 (for hard rock bottom, e.g. granite) to $c_w\rho_w$=1.00cal/$^\circ$C cm^3=4.18 MJ/K m^3 (very soft and wet sediments, e.g., organic silt), the dimensionless coefficient in (4) can be taken as C_1=0.5-1.0. Besides, $A(H)$ can vary from $A(0)$ (high mixing lake) to 0 (meromictic lake). Therefore, (4) is reduced for the estimate from above (at C_1=1, $A(H)/A(0)$=1) to

$$\frac{b_b}{b_w} = Fo^{1/2}. \tag{5}$$

Fig. 2, where expression (5) is compared with the field data for annual heat budget ratio, shows that (5) is adequate. Thus, (4) and (5) state that a contribution of heat storage of lake sediments into the heat storage of lake water increases with a decrease of lake depth and an increase of thermal diffusivity of sediments. Since, thermal diffusivity k_b increases from some minimum of $\sim1.2\cdot10^{-3}$ cm$^2\cdot$sec^{-1} (e.g., organic silt) to some maximum of ~8-$9\cdot10^{-3}$ cm$^2\cdot$sec^{-1} (granite), b_b/b_w can ~2.6 times differ in lakes with a similar depth, but different sediments.

smoothed. On the other hand according to (5), under similar values the ratio b_b/b_w should be higher for long-term and lower for diurnal temperature variations as compared with seasonal variability.

References

1. Birge E.A., Juday C., March H.W. 1927. The temperature of the bottom deposits of Lake Mendota, *Trans. Wiscon. Acad. Sci.*, 23: 187-231
2. Brewer M.C. 1958. The thermal regime of an Arctic lake, *Trans. Amer. Geophys. Union*, 39(2): 278-284
3. Drago E.C., Paira A.R. 1987. Temperature and heat budget in a floodplain pond of the middle Parana River (Argentina), Revista De La Asociacion De Ciencias Naturales Del Litoral (RCNLDW), 18(2): 193-201
4. Egorov A.N. 1984. The role of lake bottom sediments in heat exchange processes, In: Geogr. Hydrol. Methods Inland Waters Study, Nauka Publ., Leningrad, 87-94
5. Forsh L.F. 1968. Thermal regime and thermal storage of lake bottom sediments, In: N.I.Semenovich (ed.), Lakes of Various Landscapes of the north-western USSR, Nauka Publ., Leningrad, 166-209 (in Russian)
6. Johnson N.M. Likens G.E. 1967. Steady-state thermal gradient in the sediments of a meromictic lake, *JGR*, 72(12): 3049-3052
7. Likens J.E., Eaton J.S., and Johnson N.M. 1985. Physical and chemical environment, In: (ed.) G.E.Likens, Ecosystem Approach to Aquatic Ecology: Mirror Lake and Its Environment, Springer, New York, 89-108
8. Likens J.E. Johnson N.M. 1969. Measurements and analysis of the annual heat budget for the sediments in two Wisconsin Lakes, *Limnol. Oceanogr.*, 14(1): 115-135
9. Neumann J. 1953. Energy balance and evaporation from sweetwater lakes of the Jordan Rift, *Bull. Res. Council Israel*, 2: 337-357
10. Pavlov A.V., Skryabin P.N., Skachkov Yu.B., and Varlamov S.P. 1987. Annual course of thermal regime of a shallow lake in Central Yakut, *Geogr. Nat. Res. (USSR)*, 1: 91-97
11. Rossolimo L. 1932. Die thermik der bodenablagerungen des Beloje-sees zu Kossino, Arbeiten der Limnologischen station zu Kossino, 15: 44-66
12. Ryanzhin S.V. 1992. The global statistical estimates for terrestrial heat flow in freshwater lake bottom sediments, *Dokl. (Trans.) Acad. Nauk (Russia)*, 324(3): 562-566 (in Russian; transl. into English by Scripta Technica, USA)
13. Ryanzhin S.V. 1997. Thermophysical Properties of Lake Sediments and Water-Sediments Heat Interaction, Report N 3214, Dept.Water Res. Engin. Lund University, Lund, Sweden, 95p.
14. Ryanzhin S.V. L.G.Kuzmenko. 1993. Long-term and seasonal variability of hydro-meteorological processes in shallow lakes of the middle latitudes, In: (ed.) K.Kreiman, Heat and Matter Transfer Processes in Shallow Water Bodies, Nauka Publ., St.Petersburg, 5-21 (in Russian; with Summary and Contents in English)
15. Thanderz L. 1973. Studies of heat budgets, In: M.Falkenmark (ed.), Dynamic Studies in Lake Velen. Int. Hydrolog. Decade, Sweden Rept.31: 67-78

Year to year differences in the temperature regime below the ice-cover in Lake Erken during the last ten years

Gesa A. Weyhenmeyer and Donald C. Pierson, Erken Laboratory, Institute of Limnology, Uppsala University, Norr Malma 4200, 761 73 Norrtälje, Sweden
email: Gesa.Weyhenmeyer@natgeog.uu.se; Don.Pierson@limno.uu.se

Introduction

Like many other lakes at northern latitudes, Lake Erken in central Sweden is frequently ice-covered for about three to four months each year. Even though ice-cover dynamics are known to influence lake oxygenation (Stewart, 1976; Livingstone, 1993), fish winterkills (Greenbank, 1945; Barcia and Mathias, 1979) and phytoplankton production, species composition and abundance (Rodhe, 1955; Maeda and Ichimura, 1973; Pettersson, 1985; Smol, 1988) relatively few limnological studies during periods of ice-cover have been undertaken. In this paper, temperature regimes below the ice-cover in Lake Erken are determined by continuous temperature measurements at the 1 m and 14 m water depths between 1988 to 1998. These data together with measurements of global radiation, snow depth and nutrient concentrations in the lake water are used to examine variations in the occurrence of the spring phytoplankton bloom. The overall intention of this paper is to provide a clear description of ice-cover dynamics and to examine the ecological consequences of variable ice cover dynamics on phytoplankton blooms.

Methods

Lake Erken is a dimictic mesotrophic lake in central Sweden, about 50 km E of Uppsala and 60 km NNE of Stockholm (59° 25'N 18° 15'E). The lake has a surface area of 24 km^2, a mean water depth of 9 m and a maximum water depth of 21 m. Frequent measurements of water chemistry show yearly mean total phosphorus concentrations of 24 µg L^{-1}, yearly mean chlorophyll *a* concentrations of 3.7 µg L^{-1}, and yearly mean total nitrogen concentrations of 620 µg L^{-1}. The yearly mean Secchi depth is 4.5 m.

In 1988, an automatic meteorological station was installed on a small island 500 m from the southern shore. From the meteorological station average hourly measurements of air temperature, vapor pressure, global radiation, photosynthetically active radiation (PAR), wind speed, wind direction, rainfall and water temperatures at 1 m and at 14 m are collected. Snow data are available from a meteorological station 10 km south of Lake Erken.

Water samples were collected, either monthly, biweekly or weekly, with an intergrating tube-sampler from a station situated 700 m offshore above the deepest part of the lake. When the lake was unstratified a volume-proportional mixture of water from 0 m to 10 m was taken. When the lake was stratified the volume-proportional mixture was from 0 m to the depth of the thermocline. The molybdate reactive phosphorus, nitrate and chlorophyll *a* concentrations of the water samples were immediately determined in the laboratory.

Results and discussion

The onset of ice-cover could be identified in the water temperature record by the development of temperature differences between the 1 m and 14 m water depths, and the end of ice-cover corresponds to the end of temperature differences between these depths (Fig. 1). The duration of ice-cover is dependent on wind and air temperatures, and is, therefore, quite variable from year to year. During the last ten years the duration of ice-cover ranged from 25 days in winter 1992/93 to 139 days in winter 1995/96.
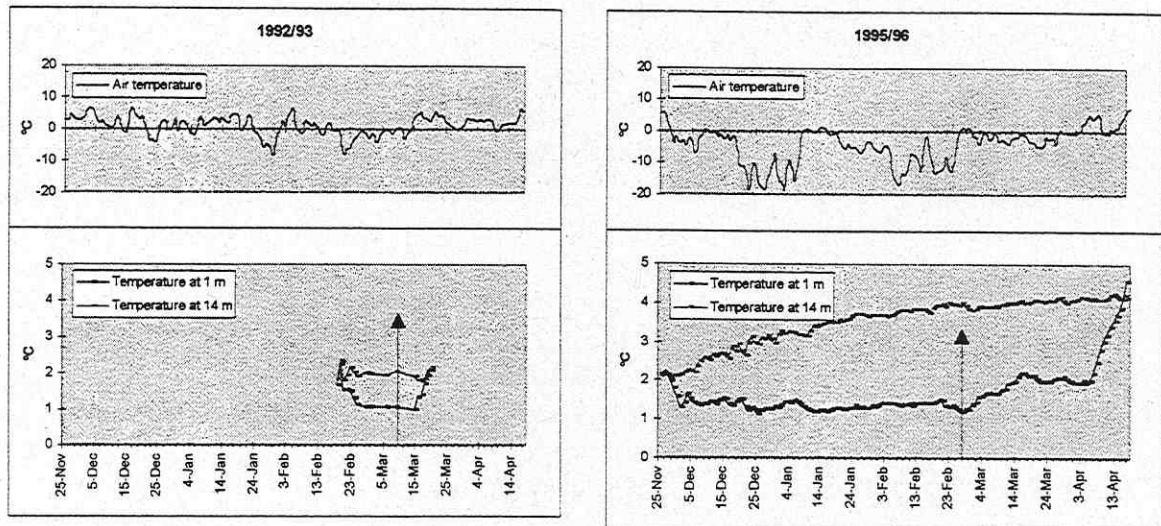
Fig. 1. Daily mean air temperatures and daily mean water temperatures at the 1 m and 14 m depths in Lake Erken during the extremely warm winter 1992/93 and the extremely cold winter 1995/96. The arrow shows the time of the maximum temperature difference between 1 m and 14 m water depth and divides the ice-cover period into a pre-rising and rising period, based on temperatures measured at the 1 m depth.

Not only the duration of ice-cover, but also the temperature regimes below the ice-cover are variable from year to year. Since 1988, the isothermal lake temperature at the beginning of ice-cover varied from 0.18 to 2.15 °C, and the difference between this temperature and that just following ice loss varied from 0.03 to 2.39 °C. During the period of ice-cover, the maximum temperature differences between the 1 m and 14 m water depths ranged from 0.93 to 2.77 °C (Table 1). This maximum temperature difference appeared approximately at the time when the temperature at 1 m began to rise. The magnitude and duration of this temperature rise varied significantly from year to year.

Despite the variability in the temperature regime, temperatures at 1 m and 14 m below the ice-cover follow a certain pattern, which can be represented as a triangle. One side (A) represents increasing temperatures at 14 m during the total duration of ice-cover, one side (B) represents a decreasing or constant temperature at 1 m during a pre-rising period and one side (C) represents the rising temperature at 1 m prior to ice loss (Fig. 2).

Table 2. Duration of ice-cover temperature differences and the duration of the period, prior to ice loss, over which temperature rises at 1 m in Lake Erken from 1988 to 1998.

Year	Beginning of ice-cover	End of ice-cover	$D_{ice-cover}$ (days)	$T_{beg.}$ (°C)	$T_{diff.:beg.-end}$ (°C)	Max $T_{diff.:1-14m}$ (°C)	Beginning of $T_{rise\ at\ 1\ m}$	D_{Trise} (days)
88/89	1-Dec-88	9-Feb-89	70	0.43	1.18	1.92	2-Jan-89	38
89/90	7-Dec-89	6-Feb-90	61	0.51	2.14	m. d.	m. d.	m. d.
90/91	11-Jan-91	21-Mar-91	69	0.47	2.81	1.57	22-Feb-91	27
91/92	25-Jan-92	12-Mar-92	47	0.83	1.43	0.93	23-Feb-92	18
92/93	21-Feb-93	18-Mar-93	25	1.81	0.03	0.98	9-Mar-93	9
93/94	12-Dec-93	12-Apr-94	121	1.00	2.39	m. d.	m. d.	m. d.
94/95	21-Dec-94	5-Apr-95	105	1.41	0.97	m. d.	m. d.	m. d.
95/96	28-Nov-95	15-Apr-96	139	2.15	1.98	2.77	27-Feb-96	48
96/97	19-Dec-96	13-Mar-97	84	0.32	2.72	1.97	22-Jan-97	48
97/98	1-Feb-98	4-Apr-98	62	0.18	1.83	m d	m. d.	m. d.

$D_{ice-cover}$: Duration of ice-cover
T_{beg}: Isothermal water temperature at the beginning of ice-cover
$T_{diff:beg.-end}$: Temperature differences between the isothermal temperatures at the beginning and end of the ice-cover period
Max $T_{diff.:1-14m}$: Maximum temperature differences between the 1 m and 14 m water depths
Beginning of $T_{rise\ at\ 1\ m}$: Time when the temperature begins to increase at 1 m began
D_{Trise}: Duration of the period over which the 1 m water temperature increased prior to ice loss
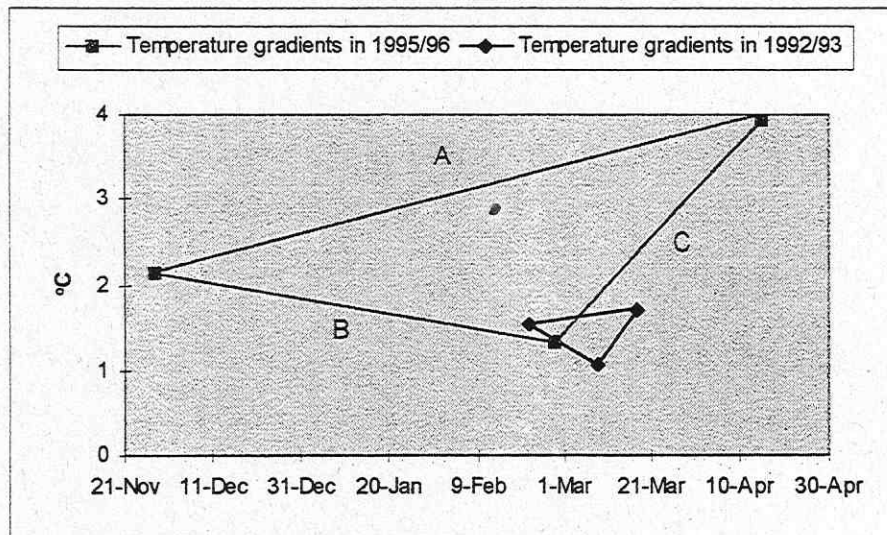m.d.: missing data

Fig. 2. The temperature gradient at 14 m water depth during the whole ice-cover period (A), the temperature gradient at 1 m water depth during the prerising period (B), and the temperature gradient at 1 m water depth during the rising period (C). The large triangle is for the coldest winter recorded (95-96) while the small triangle is for the warmest winter (92-93).

The triangles can be defined by the duration of ice-cover, the timing of the rising period at 1 m and the temperature gradients at the 1 m and 14 m depths. The duration of the ice-cover (length side A) was found to be inversely dependent on the mean air temperature calculated over the duration of ice-cover. The rate at which the temperature at 14 m increased (slope side A in°C/day), and thereby the sediment heat flux, was very similar from year to year, and found to be independent of the previous summer's lake temperatures, lake water temperatures at the beginning of ice-cover and the timing of the onset of ice-cover. More variable were the temperature gradients during the rising period at the 1 m water depth (slope side C in °C/day). These gradients were observed to be dependent on the solar radiation penetrating through the ice, which were in turn dependent on the characteristics of the ice and the depth of

the snow-cover on the ice. The beginning of the rising period equaled the time of the maximum temperature differences between 1 m and 14 m and was also dependent on solar radiation and snow cover. In general, the warmer the winter, the shorter the ice-cover period, the colder the temperature at 14 m, the smaller the maximum temperature difference between 1 m and 14 m and the more labile the stratification. This pattern is the opposite pattern of a warm summer where stratification becomes more stable.

Solar radiation penetrating through the ice was also observed to be the main factor influencing the occurrence of the spring phytoplankton bloom. In Lake Erken, a spring phytoplankton bloom always appeared at the beginning of April, whether the lake was still ice-covered or not, except during the winter 1995/96 when a deep snow-cover reduced sub-ice light intensity at the time normally associated with the spring bloom (Fig. 3). Nutrient limitation never seemed to be the reason for the absence of a spring phytoplankton bloom. However, during warm winters nutrient concentrations at the beginning of the spring phytoplankton bloom can clearly be reduced due to a continuous slow phytoplankton growth below the short lasting ice-cover (Fig. 3). More research is needed to determine how important ice-cover dynamics are in influencing the following summer stratification and summer phytoplankton blooms.
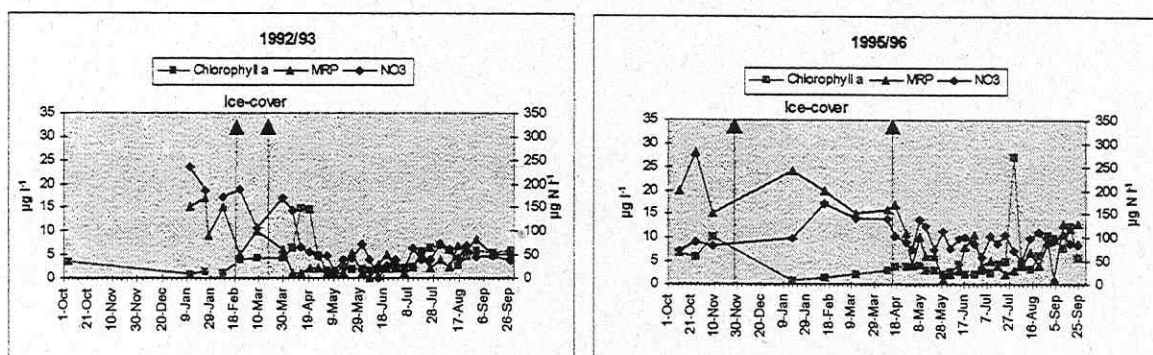

Fig 3. Chlorophyll a, molybdate reactive phosphorus (MRP) and nitrate (NO_3) concentrations in the upper water layer in Lake Erken during the extremely warm winter 1992/93 and the extremely cold winter 1995/96.

References

BARCIA, J., AND J. A. MATHIAS. 1979. Oxygen depletion and winterkill risk in small Prairie lakes under extended ice cover. J. Fish. Res. Board Can. **36**: 980-986.

GREENBANK, J. 1945. Limnological conditions in ice-covered lakes, especially related to winterkill of fish. Ecol. Monogr. **15**: 343-392.

LIVINGSTONE, D. M. 1993. Lake oxygenation: application of a one-box model with ice cover. Int. Revue Ges. Hydrobiol. **78**: 465-480.

MAEDA, O., AND S.-E. ICHIMURA. 1973. On the high density of a phytoplankton population found in a lake under ice. Int. Revue Ges. Hydrobiol. **58**: 673-685.

PETTERSSON, K. 1985. The availability of phosphorus and the species composition of the spring phytoplankton in Lake Erken. Int. Revue ges. Hydrobiol. **70**: 527-546.

RHODE, W. 1955. Can phytoplankton production proceed during winter darkness in subarctic lakes? Verh. Internat. Verein. Limnol. **12**: 117-122.

SMOL, J. P. 1988. Paleoclimate proxy data from freshwater arctic diatoms. Verh. Internat. Verein. Limnol. **23**: 837-844.

STEWART, K. M. 1976. Oxygen deficits, clarity and eutrophication in some Madison lakes. Int. Revue Ges. Hydrobiol. **61**: 563-579.

Energy considerations for the persistence of a monimolimnion – molecular diffusion

By Bertram Boehrer

UFZ - Gewässerforschung

Brückstraße 3a, D - 39114 Magdeburg, Germany

boehrer@monimo.gm.ufz.de

SCOPE

In an infinitly large water body with fresh water overlying salty water, the smoothing of an initially absolutely sharp salinity jump is considered (Fig. 1). No advective processes are present. Due to diffusion, salt is transfered vertically and the water column gains potential energy which can be evaluated analytically and numerically and a mathematical relation between potential energy gain and diffusion coefficient is achieved.
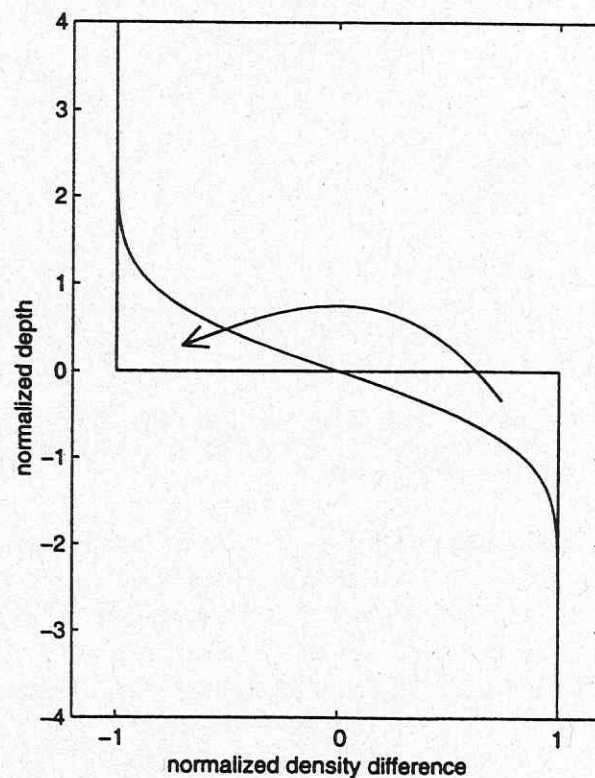

Figure 1: An initially sharp salinity gradient is smoothed by molecular diffusion. A salinity parcel gained potential energy by vertical transport

INTRODUCTION

Meromixis can establish, if the deep water body of a lake has sufficiently high density to resist the deep recirculation in the cold or windy season. Either this water of higher density has to be introduced from the outside by a salty inflow (like Fig. 2), or vica versa by a fresh inflow into a salt lake from surface ('exogenic', Wetzel 1983) or groundwater sources ('creogenic', Wetzel 1983). On the other hand, these denser waters can be produced internally by evaporation in a salt lake or by biological activity ('biogenic', Wetzel 1983), as the plants and animals contain a higher concentration of dissolved matter withing their shells. In addition, chemical transformation of solutes can cause a change in density, especially if supported by microbiological activity.
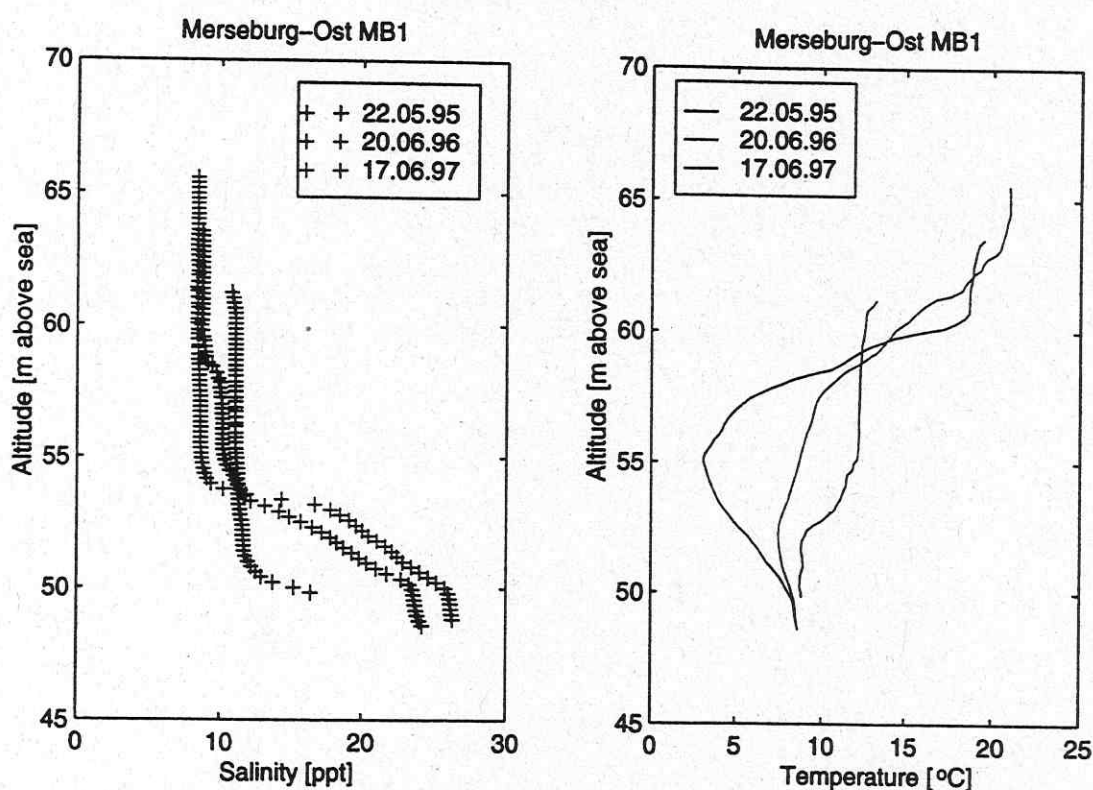
Figure 2: Salinity and temperature profiles in Merseburg-Ost Lake 1b at sampling point MB1 in the years 1995, 96, 97 while the waterlevel was recovering from its artificially low level by unforced groundwater inflows (also Boehrer and Zippel, 1997)

When a deep layer of dense water exists, a number of processes is involved in its dissolution into the overlying mixolimnion. As the stable stratification is at a lower potential energy than the perfectly mixed water column would be, energy has to be supplied from various sources to shift the lake towards a perfectly mixed water body.

Potential energy considerations allow a comparison of the importance of the various processes. In some meromictic lakes several of the contributions might be at a similar magnitude, while in others one factor might be dominant. Especially for artificial lakes, e.g. the mining lakes from opencast mines, predictions of the recirculation pattern would be desirable, even before the lakes exist in final form (e.g Boehrer et al. 1998).

The discussion of all contributions to meromixis, and all diluting processes would be

beyond the scope of this contribution. We concentrate on a model of an infinite water column, where a fresh water overlies salty water initially separated by a sharp interface. Temperature and advective processes are not considered. We evaluate the contribution of the diffusion to the potential energy of the water column, yielding a power per area.

DIFFUSION

Diffusion is the consequence of a stochastic movement of the individual particles of an observed substance. The process results in a down-gradient net transport. The salinity in the lower water body (corresponds to the monimolimnion of a meromictic lake) is higher than in the upper water body (corresponds to the mixolimnion of a lake). A net salt transport opposed to gravity is the result. Thus the potential energy of the stratification is increased.

We quantify this process, for an initially sharp density step. Fig. 1 shows, how the sharp density gradient has smoothed after a time span t. κ denotes the diffusion coefficient. For simplicity the vertical coordinate is chosen $z = 0$ in the density step, the density ρ is normalized by $M = 2(\rho - \bar{\rho})/\Delta\rho$, where $\bar{\rho}$ is the density of the fluid half across the density difference $\Delta\rho$. The problem is considered not to have any bounds. The diffusion obeys (e.g. Batchelor, 1967 pp 187):

$$\frac{\partial M}{\partial t} = \kappa \frac{\partial^2 M}{\partial z^2}, \qquad \text{with} \quad M(z, t = 0) = \pm 1 \quad \text{for} \quad z <> 0 \qquad (1)$$

The solution is known

$$M(z,t) = \frac{-1}{\sqrt{\pi \kappa t}} \int_0^z \exp(-\frac{z'^2}{4\kappa t}) dz' = -\text{erf}(\eta) \qquad (2)$$

including $\eta = z/\sqrt{4\kappa t}$. The question is now, how much potential energy was gained through the vertical transport of salinity of the lower shaded area to the upper shaded area. Because of symmetry, the energy for the tranport is double the potential energy gain due to the shaded area on one side of $z = 0$:

$$E_d = 2g \int_0^\infty z(\rho(z) - \bar{\rho} - \frac{1}{2}\Delta\rho) dz \qquad (3)$$

substitute ρ by M:

$$E_d = g\Delta\rho \int_0^\infty z(M(z,t) + 1) dz \qquad (4)$$

and $\eta = z/\sqrt{4\kappa t}$

$$E_d = 4g\kappa t \Delta\rho \int_0^\infty \eta(-\text{erf}(\eta) + 1) d\eta \qquad (5)$$

The evaluation of the integral yields 0.25, see appendix, and thus we can calculate the potential energy input by the molcular diffusion:

$$E_d = g \kappa \Delta\rho t \qquad (6)$$

CONCLUSIONS

A number of aspects of the result (eq. 6) disserve a closer look. Firstly a diffusing stable stratification is gaining potential energy. The amount of gained energy over time (power) is the derivative of eq. 6 after time

$$P_d = g\,\kappa\,\Delta\rho \tag{7}$$

and is constant with time. A density difference, as found in Merseburg-Ost Lake 1b, (Boehrer and Zippel, 1997) would indicate:

$$P_d = 9.81\mathrm{m/s^2} \cdot 1 \cdot 10^{-9}\mathrm{m^2/s} \cdot 15\,\mathrm{kg/m^3} \approx 1.5 \cdot 10^{-7}\mathrm{W/m^2} \tag{8}$$

Secondly the energy input over time (power) is linear in $\Delta\rho$. This means any shape of halocline can be approximated by a number of steplike salinity profiles. Therefore it can be concluded that the gain of potential energy over time depends only on the density difference between the waters at infinity, but not the shape of the gradient.

REFERENCES

BATCHELOR, G.K., 1983. *An introduction to fluid dynamics*, Cambridge University Press, Cambrigde, ISBN 0 521 04118x

BOEHRER, B., HEIDENREICH, H., SCHIMMELE, M. AND SCHULTZE, M., 1998. *Numerical prognosis for salinity profiles of future lakes in the opencast mine Merseburg-Ost*, Int. J. Salt Lake Research (in press)

BOEHRER, B. AND ZIPPEL, B., 1997. *Jahresbericht 1997 für den Tagebau Merseburg-Ost.* UFZ-Gewässerforschung, Brückstr. 3a, D-39114 Magdeburg.

BRONSTEIN, I.N. AND SEMENDJAJEW, K.A., 1981. *Taschenbuch der Mathematik*. 21st ed., Verlag Harry Deutsch, Thun und Frankfurt(Main), ISBN 3 87144-492-8.

WETZEL, R.G., 1983. *Limnology*, 2nd ed., Saunders College Publishing, ISBN 0-03-057913-9.

APPENDIX

With the help of Rainer Feistel (many thanks again!), the integral was evaluated analytically. We start from the eq. 4 including $M(z,t)$ from eq. 2.

$$E_d = g\Delta\rho \int_0^\infty z\left(\frac{-1}{\sqrt{\pi\kappa t}}\int_0^z \exp\left(-\frac{z'^2}{4\kappa t}\right)dz' + 1\right)dz' \tag{9}$$

Partial integration yields

$$E_d = g\Delta\rho\left[\frac{z^2}{2}\left(\frac{-1}{\sqrt{\pi\kappa t}}\int_0^z \exp\left(-\frac{z'^2}{4\kappa t}\right)dz' + 1\right)\right]_0^\infty + g\Delta\rho\int_0^\infty \frac{z^2}{2}\frac{1}{\sqrt{\pi\kappa t}}\exp\left(-\frac{z^2}{4\kappa t}\right)dz \tag{10}$$

From Bronstein (1981, p.66), the first term is zero, and the second term is:

$$E_d = g\Delta\rho\kappa t \tag{11}$$

Idealized calculation of the horizontal circulation in Lake Constance driven by deep density currents

Eckard Hollan
Institut für Seenforschung in Langenargen
at the Landesanstalt für Umweltschutz Baden-Württemberg, Germany

Extended abstract

During winter chilled water masses over the marginal region of the basin of Upper Lake Constance have been observed by CTD-measurements to drive deep density currents. This transport of surface waters may extend far into the deep regions of the lake and provides then partial exchange of the stagnant hypolimnetic layers as deep as the bottom layer depending on the deep stratification and the density of the penetrating water mass. Due to this driving agent there is the possibility of a weak horizontal circulation in the main lake water body overlying the density current, when the effect of deflection by the earth's rotation is taken into account. In order to provide first insight into this complementary motion a rough theoretical analysis is conducted in terms of a cylindrically symmetric basin with a typical radial bottom configuration and a forcing of the homogeneous water mass from below by the stress exerted from the density current. In a cartesian coordinate system with x eastward, y northward positive and z positive upward the transport in the homogeneous lake defined by vertical integration of the steady current from the top of the deep density current at $z = -H(x,y)$ to the surface at $z = \eta(x,y)$ is governed by the equations:

$$-fN = -gH\eta_x + A_h\Delta_h M + \frac{1}{\rho}(\tau_s - \tau_b)\cdot\mathbf{i},$$

$$fM = -gH\eta_y + A_h\Delta_h N + \frac{1}{\rho}(\tau_s - \tau_b)\cdot\mathbf{j}, \quad M_x + N_y = 0,$$

where Δ_h is the horizontal Laplace operator, A_h the horizontal eddy coefficient, g gravitational acceleration, f the Coriolis parameter, ρ density, τ_s and τ_b the stress at the surface and at the lower boundary, resp, and $\mathbf{i}, \mathbf{j}$ are unit vectors in x- and y-direction. The indices x,y denote derivation in the corresponding direction. When the components M, N of the transport vector are replaced by a stream function, ψ, according to: $M = -\Psi_y, N = \Psi_x$

and the frictional terms are approached by the linear relation: $A_h\Delta_h M = -R\,M$

with R a suitable friction coefficient, a partial differential equation of ψ of second order is obtained by elimination from the governing system of equations. The result reads in vector notation:

$$\Delta_h\Psi - \nabla\Psi\cdot\nabla(\ell nH) - \frac{f}{R}J(\Psi,\ell nH) = \frac{1}{\rho R}\mathbf{k}\cdot\left[\nabla\times(\tau_s - \tau_b) + \nabla(\ell nH)\times(\tau_b - \tau_s)\right]$$

where J is the Jacobian, $\quad J(\Psi,\ell nH) = \Psi_x\cdot(\ell nH)_y - (\ell nH)_x\cdot\Psi_y,$

and $\mathbf{k}$ is the unit vector in vertical direction.
By forming the divergence of the first two fundamental equations one obtains after some rearrangements a Poisson equation for the vertical deviation η of the surface from rest:

$$\Delta_h\eta = \frac{1}{gH}\left[RJ(\Psi,\ell nH) + f(\Delta_h\Psi - \nabla\Psi\cdot\nabla(\ell nH)) + \frac{1}{\rho}((\tau_b - \tau_s)\cdot\nabla(\ell nH) + \nabla\cdot(\tau_s - \tau_b))\right]$$

The boundary condition reads $\nabla\eta\cdot\mathbf{t} = 0$ at the lakeward rim of the shallow convection region with $\mathbf{t}$ the tangential unit vector there. The corresponding boundary condition for Ψ is $\Psi_e = 0$ and thus defines Ψ as the stream function of the longshore transport.

Confining to a cylindrical symmetric basin as represented in the diagram of Fig. 1 and introducing cylindrical coordinates as well as denoting by H*(r) and H(r) the configuration of the depth and the top of the density current, resp., letting $\tau_s = 0$, both the differential equations transform into the following representation:

$$\Psi_{rr} + \frac{1}{r}\Psi_r + \frac{1}{r^2}\Psi_{\phi\phi} - \Psi_r \cdot (\ell nH)_r + \frac{f}{rR}\Psi_\phi \cdot (\ell nH)_r = \frac{1}{\rho R}\left[\left((\ell nH)_r - \frac{1}{r}\right)\tau^\phi - \tau_r^\phi + \frac{1}{r}\tau_\phi^r\right],$$

$$\eta_{rr} + \frac{1}{r}\eta_r = \frac{1}{gH}\left[f\left(\Psi_{rr} + \frac{1}{r}\Psi_r - \Psi_r \cdot (\ell nH)_r\right) + \frac{1}{\rho}\left(\left((\ell nH)_r - \frac{1}{r}\right)\tau^r - \tau_r^r\right)\right],$$

where τ denotes the bottom stress with its components τ^r and τ^ϕ, resp. If rotational symmetry of Ψ is assumed, the third and fifth term of the left side and the third term on the right side of the equation for Ψ drop. This allows the term with the factor f on the right side of the equation for η to be replaced by terms consisting of τ^ϕ only and yields the equation:

$$\eta_{rr} + \frac{1}{r}\eta_r = \frac{1}{\rho gH}\left[\frac{f}{R}\left(\left((\ell nH)_r - \frac{1}{r}\right)\tau^\phi - \tau_r^\phi\right) + \left((\ell nH)_r - \frac{1}{r}\right)\tau_r - \tau_r^r\right].$$

The corresponding boundary conditions read $\Psi_e = 0$ and $\eta_{r,e} = const$ at the shoreward rim of the circulation and $\eta_{r,0} = 0$ at the centre of the basin. τ is defined at the top $z = -H(r)$ of the density current and has to be determined separately as forcing agent. This can be achieved by a local decomposition of the vertically integrated transports $\mathbf{M_c}$ and $\mathbf{M_b}$ of the compensating and density current, resp., according to an approach by Ekman (1905) gradient currents. The definition of quantities is shown in Fig. 2 for a three-dimensional Cartesian coordinate system x, y, z and the notations of the transport components read:

$$M_c = \int_{-H}^{0} u_c\,dz, \quad M_b = \int_{-H^*}^{-H} u_b\,dz, \quad N_c = \int_{-H}^{0} v_c\,dz, \quad N_b = \int_{-H^*}^{-H} v_b\,dz,$$

where $M_b = const$ is the constant rate of cold water surplus production by cooling over the shoreward shallow depth region in comparison to that over the deeper region of the basin. The decomposition into the vertical local current distribution has been explained during the talk on September 2, 1998, in terms of the simpler case for $f = 0$ in order to provide an easier understanding. In the following, the solution for $f \neq 0$ is given for the sake of consistency with the original problem.

The system of equations for the density current in terms of Ekman gradient currents is:

$$(1) -fv_b = g\rho' H_x^* - g\eta_x + A_v^* u_{b,zz}, \quad fu_b = A_v^* v_{b,zz}$$

with the boundary conditions: $u_b(-H^*) = v_b(-H^*) = 0$ and $u_{b,z}(-H) = v_{b,z}(-H) = 0$.

ρ' means the relative difference of density $(\rho_2 - \rho_1)/\rho_2$ as depicted in Fig. 2.

The system for the compensating current above reads:

$$(2) -fv_c = -g\eta_x + A_v u_{c,zz}, \quad fu_c = A_v v_{c,zz}$$

with its boundary conditions:

$$u_c(-H) = u_b(-H), \quad v_c(-H) = v_b(-H) \quad \text{and} \quad v_{c,z}(0) = u_{c,z}(0) = 0.$$

The quantities A_v^* and A_v denote constant different vertical eddy diffusivities of momentum in the layer of the density current and above, resp. It is possible to account for a logarithmic sublayer in the density current, where the friction at the bottom prevails. For this modification a final remark is added, when the treatment of the solutions is outlined as follows and provides formal evidence of the incorporation of this effect.
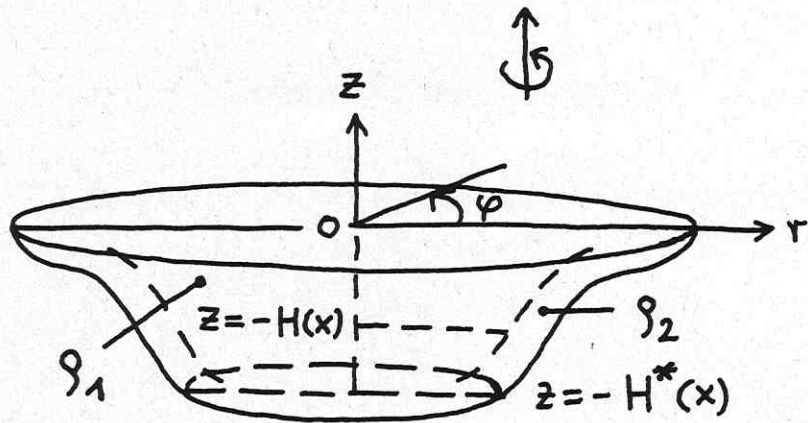
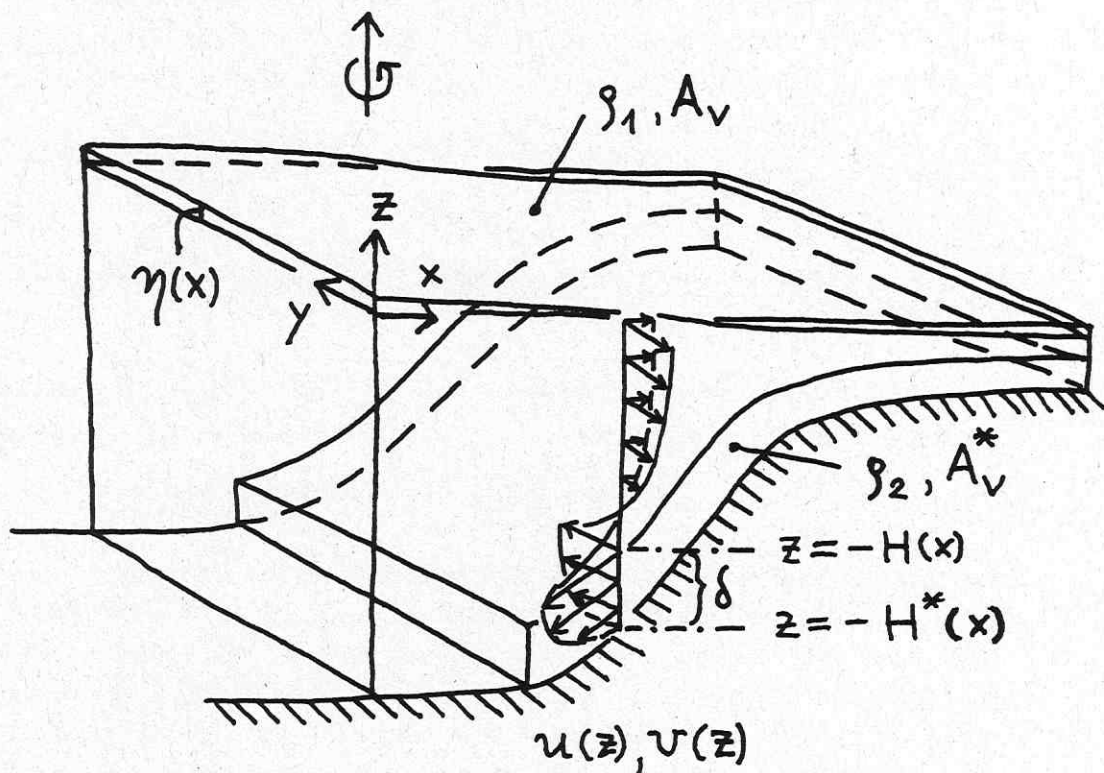Fig.1 Illustration of the cylindrically symmetric basin with deep density currents on its margin.

Fig.2 Schematic representation of convective density currents over the main margin of a large lake.

The solutions are obtained in complex notation as a concise formulation of the original theory by Ekman (1905) used by Krauss (1973) and read for the density current:

$$(3)\quad V_b = u_b + iv_b = \frac{i}{f}(F - g\eta_x)\left[\frac{\cosh\left((1+i)\gamma^*(z+H)\right)}{\cosh\left((1+i)\gamma^*(H^*-H)\right)} - 1\right]$$

with $\quad \gamma^{*2} = f/(2A_v^*), \quad F = g\rho' H_x^*$ and valid for $-H \geq z \geq -H^*$.

The solution for the compensating current is:

$$(4)\quad V_c = u_c + iv_c = \left[u_b(-H) + iv_b(-H)\right]\frac{\cosh\left((1+i)\gamma z\right)}{\cosh\left((1+i)\gamma H\right)} + i\frac{g\eta_x}{f}\left[1 - \frac{\cosh\left((1+i)\gamma z\right)}{\cosh\left((1+i)\gamma H\right)}\right]$$

with $\gamma^2 = f/(2A_v)$ and valid in the depth range $0 \geq z \geq -H$.

The corresponding vertically integrated transports in x-direction result in:

$$M_b = -\frac{1}{2\gamma^{*2}}\mathrm{Im}\left\{\frac{dV_b(-H^*)}{dz}\right\} = -\frac{1}{2\gamma^{*2}}\mathrm{Im}\left\{(i-1)\frac{\gamma^*}{f}(F - g\eta_x)\frac{\sinh\left((1+i)\gamma^*(H-H^*)\right)}{\cosh\left((1+i)\gamma^*(H^*-H)\right)}\right\},$$

$$M_c = -\frac{1}{2\gamma^2}\mathrm{Im}\left\{\frac{dV_c(-H)}{dz}\right\} = -\frac{1}{2\gamma^2}\mathrm{Im}\left\{(1+i)\gamma\left[u_b(-H) - i(v_b(-H) - \frac{g\eta_x}{f})\right]\cdot\frac{\sinh\left((1+i)\gamma H\right)}{\cosh\left((1+i)\gamma H\right)}\right\}$$

As to N_b and N_c corresponding expressions are obtained and not quoted here for sake of brevity. The derivation η_x is determined by the condition of mass continuity: $M_c+M_b+N_b = 0$. Evaluation by decomposition into real and imaginary parts yields the following relation for η_x:

$$(5)\quad g\eta_x = F - \frac{F}{\frac{2\gamma\widetilde{N}}{D_H}\left(\frac{L_\delta}{\gamma^*\widetilde{N}^*} - \delta\right) + \frac{S_H \cdot S_\delta}{D_H \cdot \widetilde{N}^*} + \frac{C_\delta}{\widetilde{N}^*}}$$

where δ is the constant thickness of the density current shown in Fig. 2. The remaining new expressions read:

$$\widetilde{N}^* = \cosh^2\gamma^*\delta\,\cos^2\gamma^*\delta + \sinh^2\gamma^*\delta\,\sin^2\gamma^*\delta, \quad \widetilde{N} = \cosh^2\gamma H\,\cos^2\gamma H + \sinh^2\gamma H\,\sin^2\gamma H,$$

$$S_H = \sinh\gamma H\,\cosh\gamma H + \sin\gamma H\,\cos\gamma H, \quad\quad D_H = \sinh\gamma H\,\cosh\gamma H - \sin\gamma H\,\cos\gamma H,$$

$$L_\delta = \sinh\gamma^*\delta\,\cosh\gamma^*\delta, \quad S_\delta = \sinh\gamma^*\delta\,\sin\gamma^*\delta, \quad C_\delta = \cosh\gamma^*\delta\,\cos\gamma^*\delta.$$

Some physical plausibility is evident, when formula (5) is evaluated for the limiting cases $H\rightarrow 0$ and $\delta\rightarrow 0$, which means that the water column consists of the heavy water or that the density current thickness is vanishing, resp. In the first case, from (5) results $g\eta_x = F$. Since there is no density difference any more, F is zero and thus $\eta_x = 0$. No density current is possible. In the second case, $g\eta_x = 0$ results directly, which is consistent with the vanishing thickness of the density current. From formula (5) either $g\eta_x$ or $F-g\eta_x$ can be replaced in the solutions (3) and (4) and the evaluation of the components of the compensating as well as the density current is straight forward, if a certain idealized configuration of $H(x)$ and $H^*(x)$ is introduced. It is to be expected, that the longshore circulation is weak. However, the compensating transport along the shore over the margin is not subjected to any boundary friction at the surface or at the top of the density current, instead, it is driven at the latter boundary. Thus its conditions of generation are favourable. On the basis of this local information on τ_b at $z = -H$ the original problem can be solved in terms of cylindrical functions for the radial dependency. The details

have still to be evaluated and will be given in a forthcoming paper on the interpretation of recent density current observations in Lake Constance.

Finally, a few hints on references are enclosed which concern the applied theory. A qualitative consideration is already given in Ekman's (1906) work in the section on currents caused by wind set up in enclosed seas. The mathematical approach had been used previously by the author in Serruya's et al. (1984) account on steady winter circulations compared between Lake Constance and Lake Kinneret, though convectively driven density currents were not included, as their pronounced contribution to the deep water renewal in Lake Constance was unknown at those times. The foregoing analysis does not consider the vertical component of motion, which is noteworthy in a slope-dominated problem. However, it is sufficient under usually not very steep marginal bottom configurations to treat the solution in horizontal projection. The vertical component is introduced via the additional continuity equation in the problems (1) and (2) with the meaning of a complementary quantity. Such a completed treatment is carried out, for instance, in Morozovsky's et al. (1998) investigation on a quasi-steady two-dimensional meteorological front. Also, the afore-mentioned notice on the frictional sublayer is incorporated in their theory which consists partially of the same method as used here. According to their formulation, the introduction as to the density currents would mean formally to fit the composed solution to an additional boundary condition at the top of the sublayer. This in turn would modify, for instance, relation (5), however, it would not alter essentially its physical sense. Detailed numerical calculations of convective circulations in lakes by Horsch and Stefan (1988) were confined to the slope in littoral regions and included the driving mechanism by cooling at the surface and the associated formation of thermals. In their second account (Stefan et al., 1989) a bulk formulation of the stronger cooling in less deep water columns is used for the estimation of the horizontal flow rates. Such an approach would suffice to specify roughly the driving transport of cooler water which enters the system at the upper edge of the main margin.

References

Ekman, V.W.(1905): On the influence of the earth's rotation on ocean-currents. Arkiv för matematik, astronomi och fysik, Vol.2, No.11, p. 1-52.

Ekman, V.W.(1906): Beiträge zur Theorie der Meeresströmungen. Annalen der Hydrographie und Maritimen Meteorologie, Vol.34, p. 423-430, 472-484, 527-540, 566-583.

Horsch, G.M. and H.G. Stefan (1988): Convective circulation in littoral water due to surface cooling. Limnol. Oceanogr. Vol.33, No.5, p. 1068-1083.

Krauss, W. (1973): Dynamics of the Homogeneous and Quasihomogeneous Ocean. Gebr. Bornträger, Berlin, 302 pp.

Morozovsky, E., G.I. Burde, L.N. Gutman and A. Zangvil (1998): A hydrodynamic model of a quasi-steady two-dimensional front. Tellus, Ser. A, Vol.50, No.4, p. 507-524.

Serruya, S., E. Hollan and B. Bitsch (1984): Steady winter circulations in Lakes Constance and Kinneret driven by wind and main tributaries. Arch. Hydrobiol./Suppl.70, p. 33-110.

Stefan, H.G., G.M. Horsch and J.W. Barko (1989): A model for the estimation of convective exchange in the littoral region of a shallow lake during cooling. Hydrobiologica 174, p. 225-234.

Winter cooling processes in Lake Geneva

I. Fer, S.A. Thorpe and U. Lemmin
LRH, EPFL, CH-1015 Lausanne, Switzerland

Over the past two winter seasons, CTD profiles have been repeatedly taken on transects from shore towards the deepest point (300m) of the lake. In all data, two processes of heat transport and winter cooling have been identified:

- the formation of cold water density currents on the lateral slope. A cold water bottom boundary layer of several meters thickness and at least 0.1K colder than the overlaying water column extends from the shore down to the seasonal thermocline (max. depth 200m). This boundary layer is a permanent feature of the winter cooling season, observed in all profiles when conditions favouring convection are prevalent at the surface. The lift-off at the depth of corresponding density and the subsequent penetration into the open waters as a horizontal plume are documented.

- the formation of sinking plumes in midwater. About 20 percent of the profiles where the total lake depth greater 40m consist of a sequence of statically unstable sections extending from the surface to the cold bottom boundary layer. These regions are typically several m thick and colder by more than 0.1K than the ambient. They are interpreted as an indication of vertical heat flux occurring in connection with plumes of cold water sinking from the surface to the bottom.

The two processes were further studied using a submarine equipped with a 1.5 m long vertical spar on which 12 high resolution thermistors were equally spaced. Running transects from shore into the open water at fixed depths, many plumes could be identified and a typical diameter of $O(10)$m was found. No significant difference in plume diameter can be seen between calm and windy days or between downwind runs and crosswind runs. The cold bottom boundary layer on the lateral slope was always evident. In addition, a general decrease in temperature from the center of the lake towards shore was observed in the whole water column above the thermocline.

The processes observed here are important in the context of deep water renewal and reoxygenation because they provide for water exchange on time scales much shorter than those of small scale turbulent diffusion.

Some Physical Features of Early-Spring Convection in Ice-Covered Lakes

Arkady Yu. Terzhevik[1,2,3] and *Joakim Malm*[1]

[1]Department of Water Resources Engineering, Lund University, Sweden
[2]Institute of Limnology, Russian Academy of Sciences, St. Petersburg, Russia
[3]Gefördert mit Forschungsmitteln des Kultusministeriums des Landes Sachsen-Anhalts
(Supported by research funds of the Ministry of Culture of the state Sachsen-Anhalt)

Within a field campaign programme in 1994-1995, measurements of temperature, conductivity, and currents were carried out in lakes Vendyurskoe, Rindozero, and Uros, located in the southern part of the Republic of Karelia, Russia (latitude 62°10' - 62°20'N; longitude 33°10' - 33°20'E) during the spring (April 1995). In the first two lakes, the penetrating solar radiation mainly heats the water close to the ice, until this layer becomes hydrostatically unstable and convection begins. The vertical thermal structure is then characterised by a thin boundary layer in the vicinity of the ice, where the temperature increases rapidly with depth, a convectively mixed layer with a depth constant temperature, and the "old" winter temperature structure in the lower part of the water column. Despite the fact that the temperature exceeds 277°K (temperature of maximum density) in the bottom layers, a higher salt content provides the hydrodynamic stability through that part of a water column.

In Lake Uros the vertical temperature development during the spring is different. When the temperature exceeds 277°K in the interior, hydrodynamic instability develops, since heavier and colder water lies above lighter and warmer water. As a result, a homogeneously mixed layer forms in the interior, which grows in thickness with time. There are presumably two main reasons for the absence of under-ice convection in Lake Uros, that are the higher vertical temperature gradient ($\sim$1°K$\cdot$m^{-1}) compared to the other two lakes (vertical temperature gradients are about 0.5°K$\cdot$m^{-1} in both lakes) before solar heating started, and different water characteristics in the three lakes, where Lake Uros has a comparatively smaller capacity for absorption of solar radiation per unit volume of water.

The temperature differences associated with the onset of convection in the investigated lakes are small (estimated to be less than 10^{-3}°K). The effects of penetrative convection were visualised by formation of a transition layer between the mixed layer and the stably stratified

and 0.2°K, respectively, after two days of convective mixing. Horizontal temperature differences of 0.2-0.3°K were observed during the period of convection, most likely caused by spatial differences in ice thickness and surface albedo.

References

1. Malm J., Terzhevik A., Bengtsson L., Boyarinov P., Glinsky A., Palshin N., Petrov M., 1997a, Temperature and salt content regimes in three shallow ice-covered lakes: 1. Temperature, salt content, and density structure. *Nordic Hydrology*, **2**, 99-128.

2. Malm J., Terzhevik A., Bengtsson L., Boyarinov P., Glinsky A., Palshin N., Petrov M., 1997b, Temperature and salt content regimes in three shallow ice-covered lakes: 2. Heat and mass fuxes. *Nordic Hydrol.*, **2**, 129-152.

Spring Convection in an Ice-Covered Lake: Observations, Scaling and a Simple Mixed-Layer Model

Dmitrii V. Mironov[1,2†] *and Arkady Yu. Terzhevik*[2,3‡]

[1]Alfred Wegener Institute for Polar and Marine Research, Bgm. Schmidt Str. 20, 27568 Bremerhaven, Germany
[2] Institute of Limnology, Russian Academy of Sciences, Sevastyanov str. 9, 196199 St. Petersburg, Russia
[3] Department of Water Resources Engineering, Lund University, P. O. Box 118, S-221 00 Lund, Sweden

1 Introduction

Recent observations in ice-covered lakes (Malm et al. 1997a, 1997b) indicate that in late spring a considerable part of the water column is well mixed and vertically homogeneous with respect to temperature. The homogenisation was shown to occur due to convection that originates from the vertically distributed heating by the solar radiation penetrating down through the ice. Convection in the oceanic upper layer (e.g. Price et al. 1986) and in fresh water lakes at temperature above the temperature of maximum density (e.g. Imberger 1985) is also affected by the vertically distributed solar heating. In that regime, however, convective motions are driven by surface cooling, whereas solar heating tends to stabilise the water column, arresting the mixed layer deepening. The regime of convection encountered in fresh water lakes at water temperature below that of maximum density is different in nature. In this regime, solar heating leads to de-stabilisation of the water column and thereby drives convective motions. We consider this regime of convection in some detail. Motivated by the observational evidence, we propose a mixed-layer scaling suitable for convection driven by vertically distributed heating. Based on this scaling, we develop a simple mixed-layer model and verify it against observational data.

Detailed observations of convection under the ice were taken in two lakes, Lake Vendyurskoe and Lake Rindozero, Russia, in spring 1995 (Malm et al. 1996, 1997a, 1997b; see also Bengtsson et al. 1995). During winter and early spring, a layer of snow overlying the ice prevents the solar radiation from penetrating downwards. The temperature changes in the water column occur due to molecular heat conduction and are very slow. When the snow cover vanishes, the solar radiation starts penetrating down through the ice. The radiation heating of the water column is vertically inhomogeneous – the upper layers gain more heat than the lower layers. Eventually, a part of the water column becomes hydrostatically unstable and overturns, leading to the formation of the convectively mixed layer. A sharp temperature increase over a thin layer at the bottom of the mixed layer suggests that convection is penetrative.

The temperature profiles representative of the period of penetrative convection (see Fig. 16 of Malm et al. 1997a) suggest that four layers can be distinguished. In a comparatively thin *surface layer* just beneath the ice, the temperature increases from the freezing point at the ice-water interface to the value characteristic of the bulk of the convectively mixed layer. Convective motions in the *mixed layer* effectively homogenise its properties in the vertical. The temperature in the bulk of this layer is nearly constant with depth. The *interfacial layer* at the bottom of the mixed layer is characterised by a sharp increase of temperature with depth. The kinetic energy of thermals is spent there for entraining the stably stratified fluid from below into the mixed layer. Therefore, the interfacial layer is also referred to as the *entrainment layer*. The stably stratified *quiescent layer* underlies the entrainment layer. The temperature changes in the quiescent layer occur due to the absorption of solar radiation and molecular heat conduction.

As the solar heating proceeds, the depth and the temperature of the mixed layer increase. Remarkably, the evolving temperature profile preserves its four-layer structure. This permits the use of a self-similar parametric representation of the temperature profile during penetrative convection.

[†]Phone: +49-471-4831501, fax: +49-471-4831797, email: dmironov@awi-bremerhaven.de
[‡]Phone: +7-812-2948050, fax: +7-812-2987327, email: Arkady.Terzhevik@tvrl.lth.se

2 The heat budget

We utilise the quadratic equation of state of the fresh water,

$$\rho = \rho_r \left[1 - \frac{1}{2} a_T \left(\theta - \theta_r \right)^2 \right], \tag{1}$$

where ρ is the density, θ is the temperature, $\rho_r \approx 10^3$ kg·m^{-3} is the maximum density of the fresh water at the temperature $\theta_r \approx 277$ K, and $a_T = 1.65 \cdot 10^{-5}$ K^{-2} is an empirical coefficient (Farmer and Carmack 1981).

Motivated by the empirical evidence discussed above, we adopt the following parameterisation of the temperature profile during penetrative convection:

$$\theta = \begin{cases} \theta_s & \text{at } 0 \leq z \leq \delta \\ \theta_m & \text{at } \delta \leq z < h \\ \theta_q & \text{at } h < z \leq D. \end{cases} \tag{2}$$

Here, z is depth; t is time; $\delta(t)$ is the depth of the surface layer beneath the ice; $\theta_s(t,z)$ is the temperature in the surface layer; $h(t)$ is the depth to the bottom of the mixed layer whose temperature is $\theta_m(t)$; D is the depth to the bottom; and $\theta_q(t,z)$ is the temperature in the quiescent layer below the entrainment layer that is approximated by the zero-order temperature jump.

The temperature in the surface layer increases rapidly with depth from the freezing point $\theta_f \approx 273$ K at the ice-water interface to the mixed-layer temperature θ_m (see Fig. 15 of Malm et al. 1997a). Turbulence in the surface layer is suppressed by the stable density stratification, and the temperature distribution is governed by the temperature transfer equation, $\partial \theta / \partial t = \kappa \partial^2 \theta / \partial z^2 - \partial I / \partial z$, where $\kappa \approx 1.3 \cdot 10^{-7}$ m^2·s^{-1} is the molecular temperature conductivity, and $I(t,z)$ is the kinematic flux of solar radiation (i.e. the radiation heat flux divided by ρ_r and specific heat of water at constant pressure, $c_p \approx 4.2 \cdot 10^3$ J·kg^{-1}·K^{-1}). As only the salient features of the temperature profile are of concern, we ignore the peculiarities of the transition zone between the turbulent mixed layer and non-turbulent layer in the near vicinity of the ice and extend the "molecular" solution down to the mixed layer to match its temperature θ_m. We further assume that the regime of heat transfer in the surface layer may be considered as quasi-stationary. With $\partial \theta / \partial t = 0$, the solution to the above temperature transfer equation reads

$$\theta_s = \theta_f + \frac{z}{\delta}(\theta_m - \theta_f) + \kappa^{-1} \left(\int_0^z I \, dz' - \frac{z}{\delta} \int_0^\delta I \, dz \right). \tag{3}$$

The depth of the surface "conduction" layer, δ, is found from the condition of smooth matching for the temperature profile at the bottom of the surface layer, $\partial \theta / \partial z = 0$ at $z = \delta$.

The temperature in the quiescent layer below the entrainment layer should be found from the temperature transfer equation. To a good approximation, however, the effect of molecular heat transfer can be neglected. Then, the temperature profile in the quiescent layer is given by

$$\theta_q = \theta_{ini} + \int_0^t \left(-\partial I / \partial z \right) dt', \tag{4}$$

where θ_{ini} is the initial temperature profile.

In the mixed layer, the molecular heat flux is identically zero. The temperature transfer equation has the form $\partial \theta / \partial t = -\partial Q / \partial z - \partial I / \partial z$, where Q is the vertical turbulent temperature flux (the heat flux divided by ρ_r and c_p). Integrating this equation with due regard to the parameterisation (2) over the mixed layer, and using boundary condition $Q = 0$ at $z = \delta$, we obtain the following equation of the temperature budget in the mixed layer:

$$(h - \delta) \frac{d\theta_m}{dt} = -Q(h) + I(\delta) - I(h), \tag{5}$$

where $Q(h) = -\Delta\theta \, dh/dt$ is the temperature flux due to entrainment at the bottom of the mixed layer, and $\Delta\theta = \theta_q(h) - \theta_m$ is the zero-order temperature jump across the entrainment layer.

The profile of the vertical turbulent temperature flux in the mixed layer is given by

$$Q(z) = I(\delta)(1 - \zeta) + [I(h) + Q(h)]\zeta - I(z), \tag{6}$$

where $\zeta = (z - \delta)/(h - \delta)$ is the dimensionless vertical co-ordinate. The turbulent flux is zero in the surface conduction layer and in the quiescent layer below the entrainment zone.

The entrainment equation, governing the time-rate-of-change of the mixed layer depth h, should now be derived. To this end, a mixed-layer scaling suitable for the regime of convection considered is required.

3 The mixed layer scaling

The following scales of length, velocity and temperature proposed by Deardorff (1970a, 1970b) are now commonly used in studies of convective flows:

$$h, \qquad w_* = (h\beta Q_s)^{1/3}, \qquad \theta_* = Q_s/w_*, \qquad (7)$$

where h is the depth of the convective layer, $\beta = g\alpha_T$ is the buoyancy parameter (α_T is the thermal expansion coefficient, and g is the acceleration due to gravity), and Q_s is the surface temperature flux. The Deardorff scaling is pertinent to convective flows driven by the surface buoyancy flux. However, it does not apply to the regime of convection considered in the present study. The point is that convection under the ice is driven by the vertically inhomogeneous solar heating. Its energetics has nothing to do with the molecular heat flux at the ice-water interface. A different scaling should be developed.

We utilise the depth of the convectively mixed layer, $(h - \delta)$, as an appropriate length scale. We then propose the following velocity and temperature scales pertinent to convection driven by the vertically distributed heating:

$$w_R = [-(h - \delta)\beta Q_R]^{1/3}, \qquad \theta_R = Q_R/w_R, \qquad Q_R = I(\delta) + I(h) - 2(h - \delta)^{-1}\int_\delta^h Idz, \qquad (8)$$

where the subscript "R" is used instead of the asterisk to avoid confusion with the Deardorff scales. The minus sign in the expression for w_R is introduced to ensure positive velocity scale [according to Eq. (1); the buoyancy parameter is a function of temperature, $\beta(\theta) = g\alpha_T(\theta - \theta_r)$, and is negative at $\theta = \theta_m < \theta_r$].

The physical meaning of the proposed scaling can be elucidated by analogy with the Deardorff scaling. Consider a convective layer driven by the surface buoyancy flux. The quantity $w_*^3 \equiv h\beta Q_s$ is a measure of the generation rate of the turbulence kinetic energy (TKE) in a layer of depth h by the buoyancy forces. This generation rate is the integral of the vertical buoyancy flux, the buoyancy production term in the TKE budget equation, over the convective layer. For the atmospheric convective boundary layer, for example, where the vertical buoyancy flux is to a good approximation linear, this integral is $\frac{1}{2}h\beta Q_s$. Similarly, the quantity $-\frac{1}{2}(h - \delta)\beta Q_R$ is nothing but the TKE generation rate in the layer of depth $h - \delta$ due to vertically distributed heating. This can be easily verified by integrating Eq. (6) over z from δ to h. In doing so, the heat flux due to entrainment should be neglected. Since the entrainment process requires that the TKE be spent, $Q(h)$ cannot be a measure of the TKE generation rate.

The proposed scaling should be verified against empirical and numerical data. Leaving this task for future studies, we use the scaling to derive the entrainment equation whose performance is then verified against empirical data. This provides a rather demanding test for the scaling ideas.

4 The entrainment equation

We employ the budget equation for the turbulence kinetic energy integrated over the mixed layer depth. For the horizontally homogeneous shear-free convective layer considered in the present study, it reads

$$\frac{d}{dt}\left(\int_\delta^h edz\right) = -\int_\delta^h \beta Qdz - F_h - \int_\delta^h \epsilon dz, \qquad (9)$$

where e is the TKE, ϵ is its dissipation rate, and F_h is the vertical flux of energy at the bottom of the mixed layer. In order to parameterise the vertical profiles of e and ϵ, we make use of the scaling developed in the previous section. Following numerous previous researchers (a summary is given by Zilitinkevich 1991), we employ the similarity hypothesis for the convectively mixed layer. It states that the TKE and its dissipation rate, made dimensionless with the appropriate length and velocity scales, i.e. with $(h - \delta)$ and w_R, respectively, are universal functions of dimensionless depth $\zeta = (z - \delta)/(h - \delta)$,

$$e = w_R^2\Phi_e(\zeta), \qquad \epsilon = (h - \delta)^{-1}w_R^3\Phi_\epsilon(\zeta), \qquad (10)$$

where Φ_e and Φ_ϵ are dimensionless functions.

The energy flux at the bottom of the mixed layer, F_h, is due to internal gravity waves that radiate energy into the stably stratified layer below. This flux is proportional to $N^3A^2\lambda$, where $N = (-\beta\partial\theta/\partial z)^{1/2}$ is the buoyancy frequency, and A and λ are the amplitude and length of the waves, respectively (see e.g. Thorpe 1973). Following Zilitinkevich (1991) and Fedorovich and Mironov (1995), we take both A and λ to be proportional to the depth of the entrainment zone, and adopt the following formulation:

$$F_h = \frac{1}{2}C_w\overline{N}^3\Delta h^3, \qquad (11)$$

where $\overline{N}$ is the buoyancy frequency averaged over the quiescent layer $h < z \le D$, $\Delta h = h - h_0$ is the thickness of the layer where the vertical turbulent temperature flux is negative, h_0 is the zero-crossing depth of the vertical turbulent temperature flux, and C_w is a dimensionless constant. Since the buoyancy frequency varies with depth at $z > h$, the layer-averaged N is taken as a characteristic value. The quantity Δh is a crude approximation to the thickness of the entrainment layer. The zero-crossing depth $z = h_0$ is determined from Eq. (6) by setting its r.h.s. to zero and solving for h_0.

Substitution of Eqs. (6), (10) and (11) into Eq. (9) and a little manipulation gives the entrainment equation that can be written in the form

$$(C_e + \mathrm{Ri}_\Delta)\mathrm{E}_h - C_e\mathrm{E}_\delta + C_w\mathrm{Ri}_N^{3/2}\left(\frac{\Delta h}{h-\delta}\right)^3 = C_\epsilon - \frac{2}{5}C_e\mathrm{De}. \tag{12}$$

Here, $\mathrm{E}_h = w_R^{-1}dh/dt$ is the dimensionless time-rate-of-change of the depth to the bottom of the mixed layer, the entrainment rate; $\mathrm{E}_\delta = w_R^{-1}d\delta/dt$ is the dimensionless time-rate-of-change of the depth of the surface layer; $\mathrm{Ri}_\Delta = -w_R^{-2}(h-\delta)\Delta b$ is the Richardson number based on the buoyancy jump across the entrainment layer, $\Delta b = ga_T\left(\theta_m + \frac{1}{2}\Delta\theta - \theta_r\right)\Delta\theta$; $\mathrm{Ri}_N = w_R^{-2}(h-\delta)^2\overline{N}^2$ is the Richardson number based on the buoyancy frequency in the quiescent layer; and $\mathrm{De} = w_R^{-4}(h-\delta)^2d\left(\beta Q_R\right)/dt$ is the non-stationarity parameter termed "the Deardorff number" by Zilitinkevich (1991). Equation (12) contains three dimensionless constants. The estimates of $C_\epsilon = 0.2$, $C_e = 0.8$ and $C_w = 0.01$ were obtained by Zilitinkevich (1991) and Fedorovich and Mironov (1995) using data from measurements in laboratory, atmospheric and oceanic convective boundary layers. We adopt these values.

5 Comparison with empirical data

The vertical temperature profiles computed with the proposed model are compared with data from measurements in Lake Vendyurskoe performed in April 1995. Detailed description of measurements as well as the complete data set are given in Malm et al. (1996, 1997a, 1997b). We adopt the exponential decay law for the flux of solar radiation, $I(t,z) = I_s(t)\sum_{i=1}^n a_i\exp(-\gamma_i z)$, where I_s is the surface value of the radiation flux, n is the number of wavelength bands, a_i are fractions of the total radiation flux for different wavelength bands, and γ_i are attenuation coefficients for different bands. For the two-band approximation, Malm et al. (1996) find that the estimates of $a_1 = a_2 = 0.5$, $\gamma_1 = 2.7$ and $\gamma_2 = 0.7$ are representative of Lake Vendyurskoe. The time-independent value of $I_s = 8\cdot10^{-6}$ K·m·s^{-1} representative of the period of measurements is used for calculations. Using the above estimates and a linear approximation of the initial temperature profile in the quiescent layer, the evolution of the vertical temperature profile in Lake Vendyurskoe over the period of two days is computed. As seen from Fig. 1, the model predictions are in good agreement with the observational data.
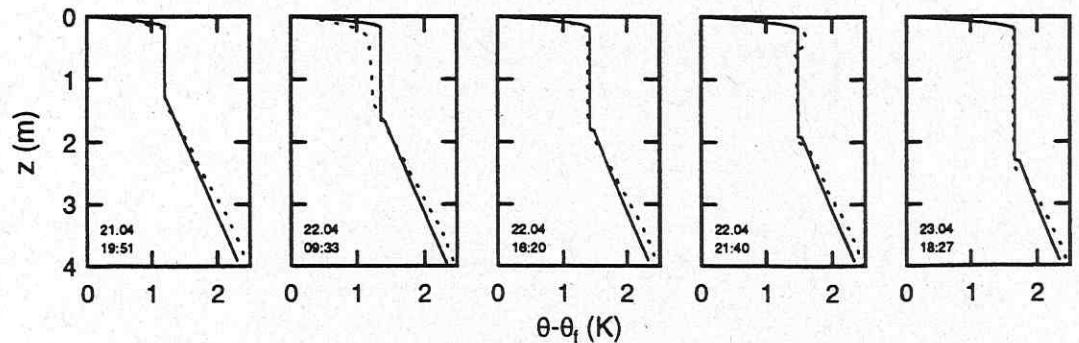

Figure 1. Successive temperature profiles in Lake Vendyurskoe during the period of penetrative convection. Solid curves are the profiles computed with the proposed model. Dashed curves represent measured profiles. The date and the local time of measurements are indicated at the lower left corner at each panel. The depth to the bottom at the point of measurements is $\overline{7}.7$ m.

6 Discussion

The regime of penetrative convection driven by vertically inhomogeneous radiation heating is considered in some detail. Such convection is observed during late spring in ice-covered fresh-water lakes where the water temperature is below the temperature of maximum density. A physically motivated mixed-layer

scaling is proposed for the regime of convection in question. This scaling is used to develop a simple bulk model of the convective layer. The results of model calculation of the vertical temperature structure compare favourably with empirical data.

The proposed scaling should be comprehensively verified. Results of direct measurements of the turbulence quantities, as well as of large-eddy and direct numerical simulations of internal-heating-driven convection, would be appropriate for this purpose. Note that it was, to a great extent, the results from large-eddy simulations of convective planetary boundary layer and Rayleigh convection that led J. W. Deardorff to propose his convective scaling. Direct verification of the proposed scaling will be a subject for future work.

Finally, it should be noted that a regime of convection similar to that in ice-covered fresh-water lakes may be encountered in puddles over melting sea ice. Since the puddle water is nearly fresh and has the temperature below that of maximum density, the vertically inhomogeneous solar heating would drive convective motions just as it does in fresh water lakes. The difference between the two regimes is in boundary conditions. The temperature of the puddle surface changes with time, while in a lake the temperature at the ice-water interface is fixed at the freezing point. Conversely, the lake bottom temperature changes with time, while in the puddle it is fixed at the freezing point. Knowledge of convection in puddles is of practical importance. Convective motions intensify the vertical heat transport towards the ice and thus affect the rate of ice melting.

References

Bengtsson, L., J. Malm, A. Terzhevik, M. Petrov, P. Boyarinov, A. Glinsky, and N. Palshin, 1995: *A Field Study of Thermo- and Hydrodynamics in a Small Karelian Lake during Late Winter 1994.* Report No. 3185, Dept. Water Res. Eng., Inst. of Technology, Univ. of Lund, Sweden, 72 pp.

Deardorff, J. W., 1970a: Preliminary results from numerical integrations of the unstable planetary boundary layer. *J. Atmos. Sci.*, 27, 1209–1211.

Deardorff, J. W., 1970b: Convective velocity and temperature scales for the unstable planetary boundary layer and for Rayleigh convection. *J. Atmos. Sci.*, 27, 1211–1213.

Farmer, D. M., and E. Carmack, 1981: Wind mixing and restratification in a lake near the temperature of maximum density. *J. Phys. Oceanogr.*, 11, 1516–1533.

Fedorovich, E. E., and D. V. Mironov, 1995: A model for shear-free convective boundary layer with parameterized capping inversion structure. *J. Atmos. Sci.*, 52, 83–95.

Imberger, J., 1985: The diurnal mixed layer. *Limnol. Oceanogr.*, 30, 737–770.

Malm, J., A. Terzhevik, L. Bengtsson, P. Boyarinov, A. Glinsky, N. Palshin, and M. Petrov, 1996: *A Field Study of Thermo- and Hydrodynamics in Three Small Karelian Lakes during Winter 1994/1995.* Report No. 3197, Dept. Water Res. Eng., Inst. of Technology, Univ. of Lund, Sweden, 220 pp.

Malm, J., A. Terzhevik, L. Bengtsson, P. Boyarinov, A. Glinsky, N. Palshin, and M. Petrov, 1997a: Temperature and salt content regimes in three shallow ice-covered lakes. 1. Temperature, salt content, and density structure. *Nordic Hydrology*, 28, 99–128.

Malm, J., A. Terzhevik, L. Bengtsson, P. Boyarinov, A. Glinsky, N. Palshin, and M. Petrov, 1997b: Temperature and salt content regimes in three shallow ice-covered lakes. 2. Heat and mass fluxes. *Nordic Hydrology*, 28, 129–152.

Price, J. F., R. A. Weller, and R. Pinkel, 1986: Diurnal cycling: observations and models of the upper ocean response to diurnal heating. *J. Geophys. Res.*, 91, 8411–8427.

Thorpe, S. A., 1973: Turbulence in stably stratified fluids: A review of laboratory experiments. *Boundary-Layer Meteorol.*, 5, 95–119.

Zilitinkevich, S. S., 1991: *Turbulent Penetrative Convection.* Avebury Technical, Aldershot, 179 pp.

Verzeichnis der UFZ-Berichte

Nr. 1/1994
Prognose extremer Umweltereignisse
Sektion Expositionsforschung und Epidemiologie

Nr. 2/1994
Handlungsstrategien für den Leipziger Raum - Visionen, Innovationen, Praktikabilität
Sigrun Kabisch
Sektion Angewandte Landschaftsökologie

Nr. 3/1994
Weiche Standortfaktoren und Flächennutzung
Hans Neumann, Brigitte Usbeck, Hartmut Usbeck

Nr. 4/1994; Band 1 und 2
Modellierung und Kürzestfristvorhersage von Sommersmogsituationen
Sektion Expositionsforschung und Epidemiologie

Nr. 1/1995
Vorkommen und Transfer von Dioxinen und Schwermetallen im Raum Merseburg, Lützen, Naumburg, Zeitz
Bernd Feist, Brigitte Niehus, Gisela Peklo, Peter Popp, Uwe Thuß
Sektion Analytik

Nr. 2/1995
Soziale Brüche und ökologische Konflikte in einer ländlichen Industrieregion: Der Südraum Leipzig
Ursula Bischoff, Sigrun Kabisch, Sabine Linke, Irene Ring, Dieter Rink
Sektion Angewandte Landschaftsökologie

Nr. 3/1995
Modellierung von Bodenprozessen in Agrarlandschaften zur Untersuchung der Auswirkungen möglicher Klimaveränderungen
Uwe Franko, Burkhard Oelschlägel, Stefan Schenk
Sektion Bodenforschung

Nr. 4/1995
Beiträge zum Workshop "Braunkohlebergbaurestseen"
Sektion Hydrogeologie

Nr. 1/1996
Elutionsverhalten und ökotoxisches Potential von Sonderabfällen
Albrecht Paschke, Detlef Lazik, Helmut Segner, Elke Büttner
Sektion Chemische Ökotoxikologie
Sektion Hydrogeologie

Nr. 2/1996
Biologische Indikation in Kleinfließgewässern der Dübener und Dahlener Heide
Claus Orendt
Projektbereich Naturnahe Landschaften

Nr. 3/1996
Potential und Strategien der Wiederbesiedlung am Beispiel des Makrozoobenthons in der mittleren Elbe (Dissertation)
Ute Dreyer
Sektion Gewässerforschung

Nr. 4/1996

Immissionsprognose - Unvariate Modellierung und Kürzestfristvorhersage von Wintersmogsituationen (Dissertation)

Uwe Schlink

Sektion Expositionsforschung und Epidemiologie

Nr. 5/1996

Untersuchungen zur gepflanzten Vegetation und ihrer ökologischen Bedeutung

Michael Winkler

Projektbereich Urbane Landschaften

Nr. 6/1996

Ökologische Charakterisierung von Biotopen im urbanen Raum am Beispiel von Modelltiergruppen

Erik Arndt, Hans Pellmann

Universität Leipzig, Institut für Zoologie

UFZ, Projektberteich Urbane Landschaften

Nr. 7/1996

Ausgewählte Rechtsfragen in bezug auf die Sanierung von Braunkohletagebau-gebieten in den neuen Bundesländern

Reinhard Müller, Birgit Süß

Max-Planck-Arbeitsgruppe Umweltrecht am UFZ

Nr. 8/1996

Hallesche Kleingärten

Nutzung und Schadstoffbelastung als Funktion der sozioökonomischen Stadtstruktur und physisch-geographischer Besonderheiten

Iris Breuste, Jürgen Breuste, Karamba Diaby, Manfred Frühauf, Martin Sauerwein,
Michael Zierdt

Martin-Luther-Universität Halle-Wittenberg

UFZ, Projektbereich Urbane Landschaften

Nr. 9/1996

Die Flächennutzung der Stadt Leipzig im klassifizierten Landsat-TM-Bild

Vera Heinz

Sektion Angewandte Landschaftsökologie

Projektbereich Urbane Landschaften

Nr. 10/1996

Untersuchungen zu Wechselbeziehungen zwischen Immissionen und Flächennutzung auf strukturtypischen Testflächen in Leipzig

K. Freyer, P. Popp, H.C. Treutler, D. Wagler, G. Schuhmann

UFZ, Sektion Analytik, Projektbereich Urbane Landschaften

Universität Leipzig, Interdisziplinäres Institut für Natur- und Umweltschutz

Nr. 11/1996

Stadtböden

Schadstoffbelastung und Schadstoffmobilität

Guido Schulte

Projektbereich Urbane Landschaften

Nr. 12/1996

Erfassung und Bewertung des Versiegelungsgrades befestigter Flächen

J. Breuste, T. Keidel, G. Meinel, B. Münchow, M. Netzband, M. Schramm

UFZ, Projektbereich Urbane Landschaften

Institut für ökologische Raumentwicklung e.V. Dresden

Ingenieurgemeinschaft Wasser-Abfall-Boden, Karlsruhe

Nr. 13/1996
Induktion von CYP1A1 durch Xenobiotica in Leberzellkulturen von Regenbogenforellen
(Dissertation)
Stefan Scholz
Sektion Chemische Ökotoxikologie

Nr. 14/1996
Ökotoxikologische Wirkungen atmogener anorganischer Schadstoffe auf Kiefernforste
Horst Schulz, Gernot Huhn, Siegrid Härtling
Sektion Chemische Ökotoxikologie

Nr. 15/1996
Kinetische Untersuchungen zum Abbau chlorierter und methylierter Benzoesäuren durch Pseudomonas spec. B13 FR 1 (SN45P) (Dissertation)
Roland A. Müller
Sektion Sanierungsforschung/Umweltbiotechnologisches Zentrum (UbZ)

Nr. 16/1996
Untersuchungen zur Situation des Wohnumfeldes ostdeutscher Großsiedlungen am Beispiel von Leipzig-Grünau (Dissertation)
Thomas Keidel
Projektbereich Urbane Landschaften

Nr. 17/1996
Chancen einer Umweltwirtschaft durch §249h-AFG-Projekte untersucht für den Freistaat Sachsen
Helga Horsch
Sektion Ökosystemanalyse, Abteilung Ökologische Ökonomie und Umweltsoziologie

Nr. 18/1996
Modellierung der Ausbreitung kfz-bedingter Schadstoffe in der Stadt Leipzig
Dietrich Wagler
Universität Leipzig, Interdisziplinäres Institut für Natur- und Umweltschutz
UFZ, Projektbereich Urbane Landschaften

Nr. 19/1996
Umweltverhalten und Lebensqualität in urbanen Räumen
Tagungsbericht und wissenschaftliche Beiträge der UFZ-Sommerschule 1996
Sigrun Kabisch (Hrsg.)
Sektion Ökosystemanalyse, Abteilung Ökologische Ökonomie und Umweltsoziologie

Nr. 20/1996
Analytische Untersuchungen zum Schadstoffeintrag durch den Hausbrand - Auswirkungen des gegenwärtigen Strukturwandels auf die urbane Belastungssituation
Werner Engewald, Thomas Knobloch, Arndt Asperger
Universität Leipzig, Inbstitut für Analytische Chemie
UFZ, Projektbereich Urbane Landschaften

Nr. 21/1996
Zusammenstellung der vom UFZ sowie von Partnereinrichtungen durchgeführten Untersuchungen in repräsentativen Kleineinzugsgebieten der Elbe
Ralph Meißner, Helmut Guhr, Rudolf Krönert
Sektion Bodenforschung, Sektion Gewässerforschung
Sektion Angewandte Landschaftsökologie

Nr. 22/1996
Untersuchungen zur atmogenen Stickstoffdeposition und zur Nitratverlagerung
(Dissertation)
Svenje Mehlert
Sektion Bodenforschung

Nr. 23/1996
Untersuchungen zur Freisetzung der gelösten organischen Substanz des Bodens (DOM) und zum Einfluß der DOM auf die Mobilisierung ausgewählter Schadstoffe in Abhängigkeit von Boden- und Standorteigenschaften (Dissertation)
Karsten Kalbitz
Sektion Bodenforschung

Nr. 24/1996
Geschwindigkeitslimitierende Einflußgrößen beim mikrobiellen Schadstoffabbau in phenolischen Deponiewässern (Dissertation)
Frank Eismann
Sektion Sanierungsforschung

Nr. 1/1997
Dynamik von Wasser und Schadstoffen im Boden: Diskrete Simulationsmethoden
Hans Vollmayr
Sektion Chemische Ökotoxikologie

Nr. 2/1997
Beziehungen zwischen Urbanen Flächennutzungsstrukturen und klimatischen Verhältnissen am Beispiel der Stadtregion Leipzig
Ulrich Müller
Sektion Expositionsforschung und Epidemiologie
Projektbereich Urbane Landschaften

Nr. 3/1997
Regionalökologie
Tagungsbericht und wissenschaftliche Beiträge des Deutsch-Argentinischen Workshops Mendoza - Argentinien
Brigitte Großer

Nr. 4/1997
Zur Stickstoffdynamik selbstbegrünter Ackerbrachen im mitteldeutschen Schwarzerdegebiet
(Dissertation)
Gerhard Sauerbeck
Sektion Bodenforschung
Nr. 5/1997
Tern-Tagung
Terrestrische und ökosystemare Forschung in Deutschland
Stand und Ausblick
Heidrun Mühle, Svenne Eichler (Hrsg.)
Projektbereich Naturnahe Landschaften und Ländliche Räume

Nr. 6/1997
Chancen für eine nachhaltige Regionalentwicklung in altindustriellen Regionen unter Berücksichtigung des Konzeptes des regionalen Lebenszyklus - das Beispiel Südraum Leipzig
(Dissertation)
Tillmann Scholbach
Arbeitsgruppe Regionale Zukunftsmodelle

Nr. 7/1997

2. Leipziger Symposium „Ökologische Aspekte der Suburbanisierung"
Tagungsband der Veranstaltung am 13.6. und 14.6.96
J. Breuste
Projektbereich Urbane Landschaften

Nr. 8/1997

Soziologisch-, ökonomisch- und ökologisch lebensfähige Entwicklung
in der Informationsgesellschaft
Wolf Dieter Grossmann, Stefan Fränzle, Karl-Michael Meiß, Thomas Multhaup, Andreas Rösch
Arbeitsgruppe Regionale Zukunftsmodelle

Nr. 9/1997

Untersuchungen in Enclosures und im Freiwasser des Arendsees (Altmark): Mikrobielles
Nahrungsnetz, Zoo- und Phytoplankton in einem cyanophyceen-dominierten eutrophen See
(Dissertation)
Jörg Tittel
Sektion Gewässerforschung

Nr. 10/1997

Einfluß von Standort und Bewirtschaftung auf den N-Austrag aus Agrarökosystemen
U. Franko, S. Schenk, D. Debevc, P. Petersohn, G. Schramm
Sektion Bodenforschung

Nr. 11/1997 (Dissertation)

Der Einfluß von Immissionen auf ausgewählte Insektengruppen
(Homoptera, Auchenorrhyncha; Coleoptera, Carabidae) verschiedener Trophieebenen
(Dissertation)
Sabine Neumann
Sektion Bodenforschung

Nr. 12/1997

Optimierung umweltverträglicher Analysenverfahren für Mineralölkohlen-wasserstoffe im
Boden
H. Borsdorf, J. Flachowsky
Sektion Analytik

Nr. 13/1997

Alternativer Landschaftsplan für eine kleine attraktive Stadt in der Informationsgesellschaft -
Beispiel Visselhövede
Wolf Dieter Grossmann, Karl-Michael Meiß, Stefan Fränzle, Thomas Multhaup
Donald F. Costello, Frank Simon, Michael Sorkin
Arbeitsgruppe Regionale Zukunftsmodelle

Nr. 14/1997

Untersuchungen zum Eintrag von Polycyclischen aromatischen Kohlen-wasserstoffen (PAK)
über den Luftpfad in ländlichen Gebieten des Raumes Halle/Sachsen (Dissertation)
Katja Schäfer[†]
Sektion Bodenforschung

Nr. 15/1997

Schwermetallgehalte der Böden im mitteldeutschen Ballungsraum - ein Überblick
Manfred Altermann, Reinart Feldmann, Michael Steininger
Büro für Bodenökologie, Bodenkartierung, Bodenschutz Halle
UFZ, Projektbereich Naturnahe Landschaften und Ländliche Räume
Martin-Luther-Universität Halle Wittenberg, Institut für Agrartechnik und Landeskultur

Nr. 16/1997

Aspekte der Sozialverträglichkeit der Mobilitätsentwicklung in Leipzig
E. Geisler
Universität Leipzig, Interdisziplinäres Institut für Natur- und Umweltschutz
UFZ, Projektbereich Urbane Landschaften

Nr. 17/1997

^{15}N-Traceruntersuchungen zur Nitrifikation/Denitrifikation, insbesondere zur Bildung von Stickstoffoxiden in Böden und wäßrigen Medien (Dissertation)
Inken Sich
Sektion Bodenforschung

Nr. 18/1997

The influence of soil organic matter (SOM) on the accumulation and transformation of inorganic and organic pollutants
E. Schulz, E.-M. Klimanek, M. Körschens, N.A. Titova, L.S. Travnikova, B.M. Kogut,
V.A. Bol´schakov, Z.N. Kachnovic, S.J. Sorokin, T.N. Avdeeva, S.P. McGrath
UFZ, Department of Soil Sciences
Rothamsted Experimental Station Registered Office, Department Soil Chemistry
Dokutchaev Soil Science Institute, Department Soil Biology, Moscov

Nr. 19/1997

Die Vegetation als Senke und biochemischer Reaktor für luftgetragene Schadstoffe
Judwig Weißflog, Klaus-Dieter Wenzel
Sektion Chemische Ökotoxikologie

Nr. 20/1997

Mobilität und Bioverfügbarkeit luftgetragener Schadstoffe in emittentennahen Agrarböden Sachsen-Anhalts
Michael Manz

Nr. 21/1997

Bestimmung der Deposition von Fremd- und Schadstoffen in Kiefernforste mit Hilfe von Baumborke
Horst Schulz, Gernot Huhn, Uwe Schulz
Sektion Chemische Ökotoxikologie

Nr. 22/1997

Naturschutz in Bergbaufolgelandschaften des Südraumes Leipzig unter besonderer Berücksichtigung spontaner Sukzession
Walter Durka, Michael Altmoos, Klaus Henle
Sektion Biozönoseforschung
Projektbereich Naturnahe Landschaften

Nr. 23/1997

Reststoffe der Kupferschieferverhüttung
Teil 1: Mansfelder Kupferschlacken
Peter Schreck, Walter Gläßer (Hrsg.)
Sektion Hydrogeologie

Nr. 24/1997

Landschaftsstrukturen und Regulationsfunktionen in Intensivagrarlandschaften im Raum Leipzig-Halle.
Regionalisierte Umweltqualitätsziele - Funktionsbewertungen - multikriterielle Landschaftsoptimierung unter Verwendung von GIS (Dissertation)
Burghard Meyer
Sektion Angewandte Landschaftsökologie

Nr. 25/1997

Vorkommen und Verteilung von toxisch relevanten organischen Komponenten und Schwermetallen in ausgewählten Untersuchungsgebieten
Peter Popp, Bernd Feist, Brigitte Niehus, Gisela Peklo, Uwe Thuß
Sektion Analytik

Nr. 26/1997

Mineralölbelastetes Grundwasser - Struktur, Dynamik, biochemisches Abbaupotential sowie Codierung und Verbreitung degradativer Leistungen in mikrobiellen Biozönosen dieses Ökosystems (Dissertation)
Antje Birger
Sektion Hydrogeologie
Sektion Umweltmikrobiologie

Nr. 27/1997

Sanierungsforschung in regional kontaminierten Aquiferen (SAFIRA)
Holger Weiß, Georg Teutsch, Birgit Daus (Hrsg.)
UFZ, Projektbereich Industrie- und Bergbaufolgelandschaften
Eberhard-Karls-Universität, Geologisches Institut

Nr. 1/1998

Experimentelle Tracerstudien und Modellierungen von Austauschprozessen in einem meromiktischen Restsee (Hufeisensee)
Manfred Maiss, Volker Walz, Michael Zimmermann, Johann Ilmberger, Wolfgang Kinzelbach, Walter Gläßer
Sektion Hydrogeologie

Nr. 3/1998

Untersuchungen zur elektrothermischen Verdampfung als Probenzuführungs-technik für die induktiv gekoppelte Plasma-Massenspektrometrie (ETV-ICP-MS) unter besonderer Berücksichtigung der Transportphänomene (Dissertation)
Karsten Grünke
Sektion Analytik

Nr. 4/1998

Sorption von hydrophoben organischen Verbindungen an gelösten Huminstoffen (Dissertation)
Anett Georgi
Sektion Sanierungsforschung

Nr. 5/1998

Rice Terraces of Ifugao (Northern-Luzon, Philippines)
- Conflicts of Landuse and Environmental Conservation
Josef Settele, Harald Plachter, Joachim Sauerborn, Doris Vetterlein
UFZ, Interdisciplinary Department of Conservation Biology and Natural Resources
Philipps-University Marburg
Justus-Liebig-University Giessen
Brandenburg-Technical-University Cottbus

Nr. 6/1998

Landschaftsbewertung unter Verwendung analytischer Verfahren und Fuzzy-Logic
Ergebnisse des Workshops "Einsatzmöglichkeiten von Fuzzy Sets in der Landschaftsbewertung" vom 26. bis 28. Februar 1997 am UFZ-Umweltforschungszentrum Leipzig-Halle GmbH
Ralf Grabaum und Uta Steinhard (Hrsg.)
Projektbereich Naturnahe Landschaften und Ländliche Räume
Sektion Angewandte Landschaftsökologie

Nr. 7/1998

Wassergewinnung in Talgrundwasserleitern im Einzugsgebiet der Elbe

W. Nestler, W. Walther, F. Jacobs, R. Trettin, K. Freyer

Hochschule für Technik und Wirtschaft Dresden (FH), LB Geotechnik und Wasserwesen

Technische Universität Dresden, Institut für Grundwasserwirtschaft

Universität Leipzig, Institut für Geophysik und Geologie

UFZ, Sektion Hydrogeologie, Sektion Analytik

Nr. 8/1998

Diversität und regionale Nachhaltigkeit: Entwicklungsperspektiven des Industriestandortes Böhlen

Irene Ring, Helga Horsch

Abteilung Ökologische Ökonomie und Umweltsoziologie an der Sektion Ökosystemanalyse

Nr. 9/1998

Interdependenzen von gebauter, sozialer und natürlicher Umwelt
und deren Einfluß auf Wohnzufriedenheit und Seßhaftigkeit

Quartiersbezogene stadtsoziologische Untersuchungen in Leipzig-Stötteritz im Rahmen des Themenschwerpunktes "Sozialräumliche Differenzierung und stadtökologischer Strukturwandel"

Abteilung Ökologische Ökonomie und Umweltsoziologie an der Sektion Ökosystemanalyse

Nr. 10/1998

Microbiology of Polluted Aquatic Ecosystems

Proceedings of the Workshop held on the 4th and 5th December 1997 at the UFZ Centre for Environmental Research Leipzig-Halle

Petra Maria Becker (Editor)

Department of Remediation Research

Nr. 11/1998

Untersuchungen zum Boden/Pflanze - Transfer ausgewählter organischer Umweltschadstoffe in Abhängigkeit von Bodeneigenschaften (Dissertation)

Kathrin Heinrich

Sektion Bodenforschung

Nr. 12/1998

Isotopenbiogeochemische Untersuchungen über Umsetzungsprozesse des Schwefels in Agrarökosystemen mittels der stabilen Isotope ^{34}S und ^{18}O (Dissertation)

Katrin Knief

Sektion Hydrogeologie

Nr. 13/1998

Leistungssteigerung bei der biologischen Bodenreinigung in Perkolationssystemen

Christian Löser, Andreas Zehnsdorf, Petra Hoffmann, Heinz Seidel

Sektion Sanierungsforschung

Nr. 14/1998

Qualitätszielkonzept für Stadtstrukturtypen am Beispiel der Stadt Leipzig
- Entwicklung einer Methodik zur Operationalisierung einer nachhaltigen Stadtentwicklung auf der Ebene von Stadtstrukturen -

Evelyne Wickop, Peter Böhm, Katrin Eitner, Jürgen Breuste

Projektbereich Urbane Landschaften

Nr. 15/1998

Bewertung von Maßnahmenotwendigkeiten des Umwelt- und Ressourcenschutzes im Raum Leipzig-Halle-Bitterfeld

Burghard C. Meyer, Rudolf Krönert

Sektion Angewandte Landschaftsökologie